# THE ROLE OF HUMAN SOMATOSENSORY CORTEX IN TACTILE STIMULUS PROCESSING: FMRI RESPONSES TO MICROSTIMULATION OF INDIVIDUAL TACTILE AFFERENTS.

Sharlini Sankaran

A dissertation submitted to the faculty of the University of North Carolina at Chapel Hill in partial fulfillment of the requirements for the degree of Doctor of Philosophy in the Department of Biomedical Engineering.

Chapel Hill
2007

Approved by:

Mark A. Tommerdahl, Ph.D.

Jeffrey MacDonald, Ph.D.

Sean Gomez, Ph.D.

Oleg Favorov, Ph.D.

Gregory K. Essick, Ph.D.

ABSTRACT

Sharlini Sankaran: The role of human somatosensory cortex in tactile stimulus processing: fMRI responses to microstimulation of individual tactile afferents.

(Under the direction of Mark A. Tommerdahl)

Mounting evidence shows that primary somatosensory cortex, particularly SI, is actively engaged in dynamic processing of sensory information evoked by skin stimulation. SI plays both active and modulating roles in amplitude and frequency discrimination as well as in the processing of noxious mechanical and thermal stimuli. SI is one cortical region in which interactions between cortical activity evoked by low frequency flutter and high frequency vibration are spatially and temporally integrated. In this dissertation, functional magnetic resonance imaging was used to image cortical responses to microstimulation of individual, functionally identified skin mechanoreceptive afferents which are, under natural stimulus conditions, effectively activated by very selective ranges of stimulation frequency. Microstimulation of mechanoreceptive and nociceptive afferents evoked significant activation in multiple cortical areas. Peak magnitudes of hemodynamic responses in SI and SII did not differ significantly when rapidly adapting afferent microstimulation frequency was increased from 30 to 200Hz. Thus, rapidly adapting afferent activation alone cannot account for the suppression of SI cortical activity that is observed when high frequency vibrotactile stimuli are applied to the skin; this leads to the hypothesis that PC microstimulation causes suppression of SI cortical activity regardless of stimulus frequency. Images of activity evoked by microstimulation of PC afferents support this hypothesis.

Additionally, microstimulation of nociceptive afferents evoked significant activation in multiple cortical areas consistent with animal studies utilizing invasive data collection methods. Future studies of hemodynamic responses to vibrotactile stimulation and noxious stimulation will clarify human cortical mechanisms responsible for the spatial-temporal integration evoked by different modalities of skin stimulation. The construction and utilization of an MRI-compatible vibrotactile stimulator that can be used in such future studies is also described in this manuscript.

To Amma and Daddy – who inspired me to begin
Will – who encouraged me to persist
and Nisha – who gave me a reason to finish.

ACKNOWLEDGMENTS

I am very grateful to my dissertation committee, in particular Dr. Mark Tommerdahl who rescued me from the pit of despair and set me back on the road to graduation with his support, encouragement, and practical advice.

This work was made possible with the support of Dr. Francis McGlone and a student research fellowship (PS000232) from Unilever Research, U.K. I am thankful to Dr. Edward Kelly for serving as my dissertation advisor before his retirement. Drs. Susan Francis and members of the Sir Peter Mansfield Magnetic Resonance Centre at the University of Nottingham were patient in teaching me fMRI analysis methods. Thank you to Drs. Mats Trulsson at Karolinska Institute and Goran Westling at the University of Umea, Sweden, who performed the microstimulation procedures in the work described here. Drs. Mark Howard and Chris Dancer from Unilever Research were instrumental in helping resolve technical issues. I also wish to thank Dr. Weili Lin and Ms. Kathy Wilber at UNC for assistance with MRI imaging protocols. I am grateful to Dr. Greg Essick and other faculty members at the Dental Research Center at UNC for providing me with the space and equipment necessary to complete the data analysis.

And finally, "it takes a village to finish a dissertation…" I owe a great deal of my success to the unwavering support of my family – my husband Will Polk, my parents Sankaran Ramanathan and Parvathi Devaraj, my in-laws William and Iris Polk, and my sisters Chandini and Sumanna, who led by example. Thank you to the many friends, colleagues, and neighbors who listened patiently whenever I needed support.

TABLE OF CONTENTS

LIST OF TABLES

Table

LIST OF FIGURES

Figure

## 1. Introduction: The role of primary somatosensory cortex in integration and processing of tactile stimuli

Primary somatosensory cortex comprises functional areas SI and SII cortices and in the human brain is anatomically located on the postcentral gyrus on the parietal lobe. SI cortex is the main functional cortical area responsible for localization of tactile stimuli (Kandel et al 2000). Somatosensory information from the limbs and trunk is conveyed to the ventral posterior lateral nucleus of the thalamus via the dorsal column-medial lemniscal ascending pathway, and thermal and noxious stimuli are conveyed to the thalamus via the anterolateral pathway. Thalamocortical connections convey the information from the thalamus to SI and SII (Kandel et al 2000).

In addition to stimulus localization, SI is engaged in dynamic processing of sensory information evoked by both noxious and innocuous skin stimuli. For example, previous studies have shown that SI plays active and modulating roles in amplitude and frequency discrimination (Mountcastle et al 1969, Tommerdahl et al 1999, Whitsel et al 2001). SI is also involved in the processing of noxious mechanical and thermal stimuli (Tommerdahl et al 1996).

The role of human SI in tactile stimulus processing is investigated using functional magnetic resonance imaging (fMRI) in this manuscript. FMRI is a non-invasive imaging technique that measures neuronal activity-related changes in cerebral blood oxygenation levels (see Appendix). In Chapter 2, the role of primary somatosensory cortex in frequency discrimination is investigated by examining fMRI responses to microstimulation of

individual mechanoreceptive afferents. In Chapter 3, fMRI is used to investigate primary somatosensory cortical responses to microstimulation of individual nociceptive afferents. Chapter 4 describes the construction and use of an fMRI-compatible vibrotactile stimulator that can be used to further study the role of SI in the processing of sensory stimuli.

***References***

Kandel ER, Schwartz JH, and Jessell TM (2000) Principles of Neural Sciences, Fourth Edition. New York, NY: McGraw-Hill.

Mountcastle VB, Talbot WH, Sakata H, and Hyvarinen J (1969) Cortical neuronal mechanisms in flutter-vibration studied in unanesthetized monkeys. Neuronal periodicity and frequency discrimination. J Neurophysiol 32: 452-484.

Tommerdahl M, Delemos KA, Vierck CJ, Favorov OV, and Whitsel BL (1996) Anterior parietal cortical response to tactile and skin-heating stimuli applied to the same site. J Neurophysiol 75: 2662-2669.

Tommerdahl M, Delemos KA, Whitsel BL, Favorov OV, and Metz CB (1999) Response of anterior parietal cortex to cutaneous flutter versus vibration. J Neurophysiol 82: 16-33.

Whitsel BL, Kelly EF, Xu M, Tommerdahl M, Quibrera M (2001) Frequency-dependent response of SI RA-class neurons to vibrotactile stimulation of the receptive field. Somatosens Mot Res 18: 263-285.

## 2. Cortical responses to microstimulation of single mechanoreceptive afferents.

### *Background*

One of the intriguing questions in the field of somatosensory neurophysiology is how a subject perceives and discriminates between different frequencies presented at the skin, particularly at frequencies above 50Hz. Neurophysiological studies have shown that the SI response is very different to "flutter" and "vibration" skin stimuli (Whitsel et al 2001, Tommerdahl et al 1999a). The term "flutter" refers to skin stimuli with frequencies less than 50Hz, and "vibration" refers to skin stimuli with frequencies greater than 50Hz. Flutter stimuli preferentially engage more Rapidly-Adapting Type 1 (RA1) and Slowly-Adapting Type 1 (SA1) afferents (Mountcastle et al, 1969). In contrast, vibration stimuli preferentially engage more Pacinian (PC) afferents than RA1 afferents (Mountcastle et al 1969, Mountcastle et al 1990).

While a number of theories exist about how humans discriminate between different frequencies of vibrotactile stimulation, the most persistent is the "periodicity hypothesis" originally proposed by Mountcastle and colleagues (Mountcastle et al 1969). This hypothesis states that the capacity to discriminate stimulus frequency over the range of 5 – 50Hz is largely attributable to the ability of SI rapidly-adapting (RA) pyramidal neurons to discharge action potentials in a consistent temporal relationship to stimulus motion. Whitsel and colleagues subsequently proposed that perceptual frequency discriminative capacity at frequencies between 50 and 200Hz could be accounted for by the firing rate of the SI RA

neurons (Whitsel et al, 2001). This hypothesis was based on data demonstrating that RA afferents could, in fact, be entrained to the stimulus frequency very well in this higher frequency range (Whitsel et al., 2001).

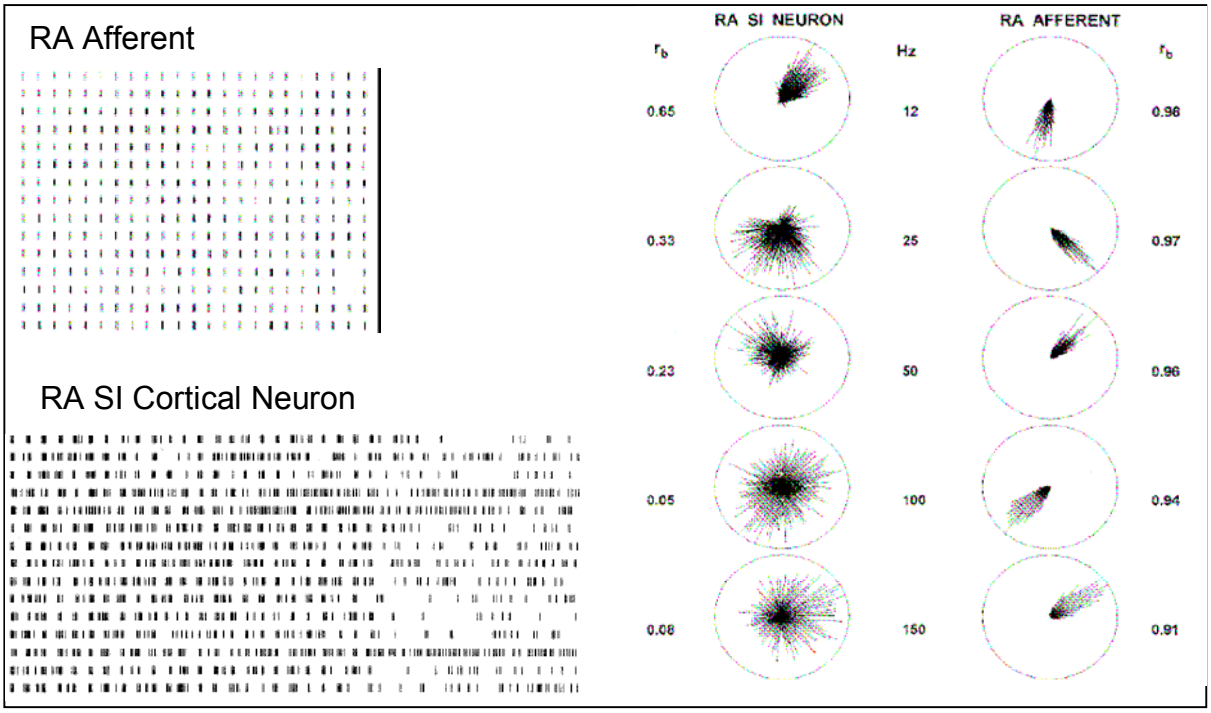


**Figure 1 (modified from Whitsel et al, 2001): Spike raster trains and circular histograms recorded from RA afferents and RA neurons. Spiking activity in RA afferents remains tightly entrained to the stimulus (exemplary afferent activity on top right), but this is not always the case for RA SI cortical neurons (activity from an exemplary neuron shown on the bottom right) . The right two columns show circular histograms for spiking activity for 5 different RA afferents and 5 different RA SI neurons. The RA afferents were tightly entrained to the stimulus (rightmost column), but the 5 RA SI neurons shown here exhibited different degrees of entrainment.**

Electrode recordings from RA afferents show that the afferent response is tightly entrained to the stimulus, regardless of stimulus frequency. The top left column of Figure 1 shows that spiking activity from an exemplary RA afferent remained well-entrained to the 200Hz stimulus that was applied to the forelimb (Whitsel et al 2001). In contrast, not all SI RA neurons respond vigorously to high frequency (50-200Hz) stimulation (see bottom right raster plot on Figure 2), but those SI RA neurons that do respond well to 200Hz stimulation are entrained very well to that stimulus. The circular plot in the top row of the column labelled "SI RA neuron" in Figure 2 shows an example of an SI RA neuron that was well-entrained to a high-frequency stimulus. In fact, Whitsel et al found that only neurons whose RF center was coincident with the stimulus site were entrained, while other SI RA neurons – though close in proximity in the cortex – were not (Whitsel et al., 2001). One of the difficulties in such a study is the identification of which SI RA neurons to record from, and in that particular report, a combined method of optical intrinsic signal (OIS) imaging and electrophysiological recording was used to identify and characterize the SI response to different frequencies of vibrotactile stimulation.

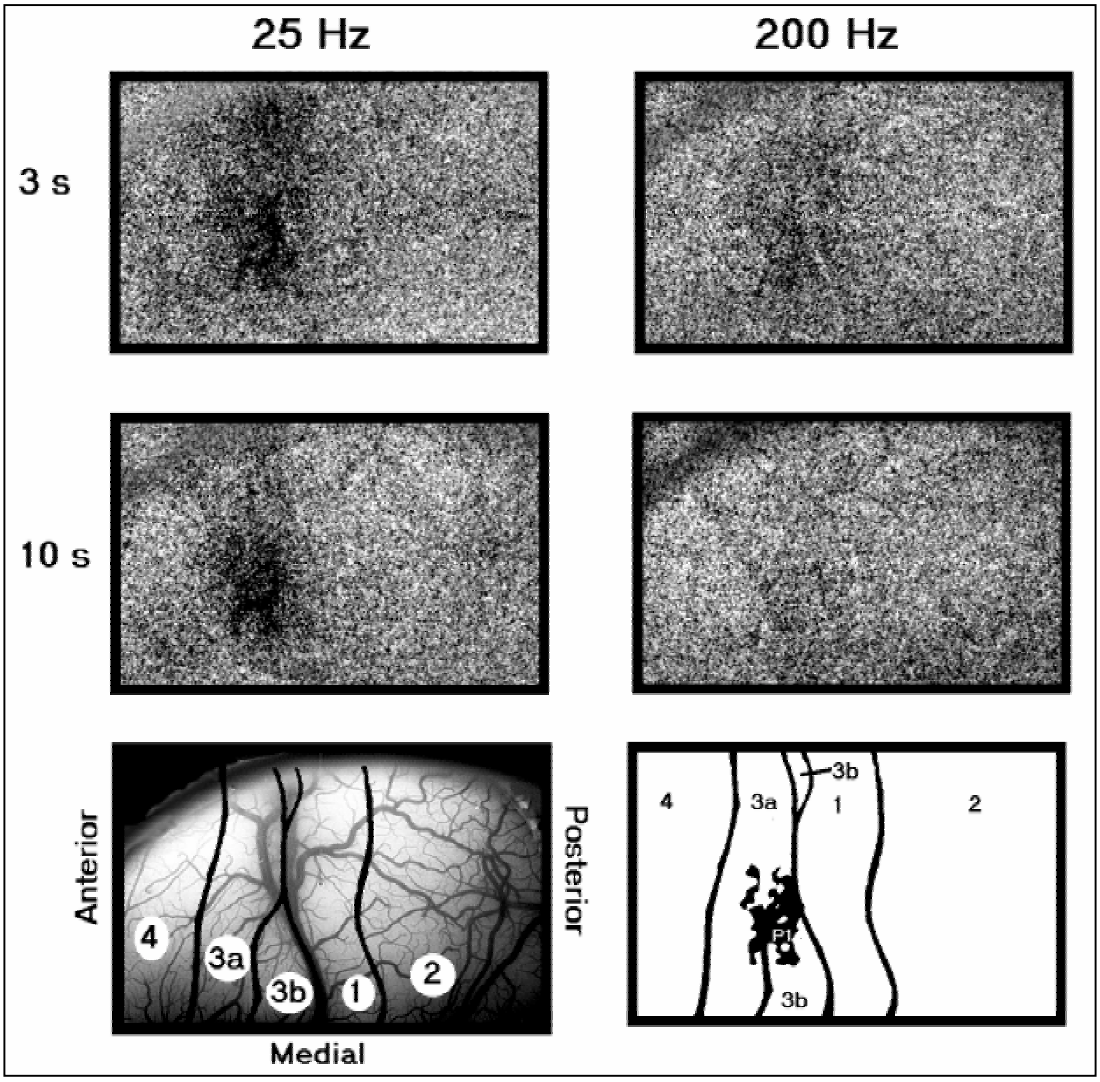


**Figure 2 (modified from Tommerdahl et al 1999a): OIS recordings of the responses to 25Hz and 200Hz stimuli. 25Hz stimuli are more effective in evoking a sustained SI response than 200Hz stimuli. Top: responses to a 25- (left) and 200-Hz (right) stimulus to the same skin site at 3 s after stimulus onset. Middle: responses to the same stimuli 10 s after stimulus onset. Bottom: image of surface vasculature (left); thresholded image of the response to 25 Hz at 10 s after stimulus onset (right) shows locations of cytoarchitectonic boundaries within SI.**

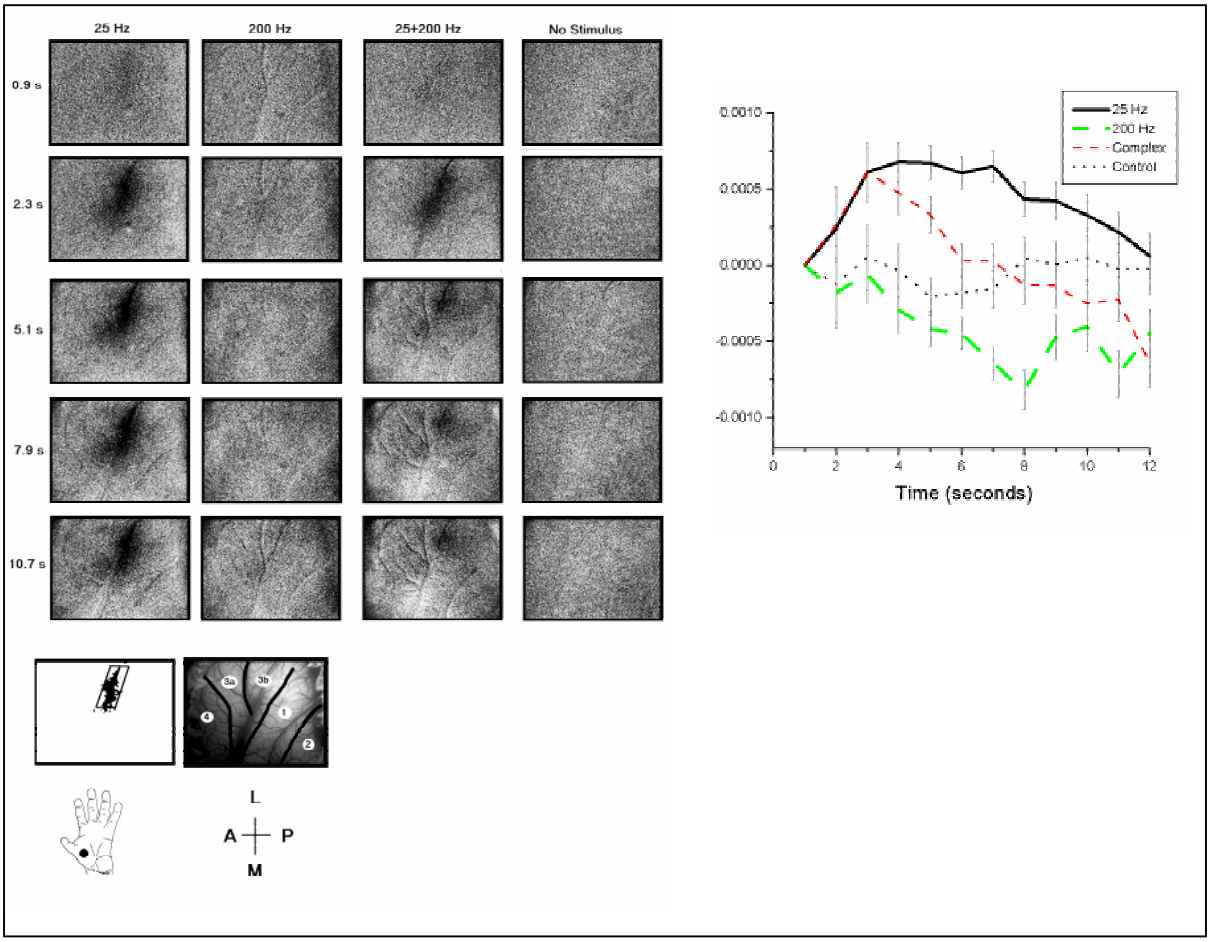


**Figure 3 (modified from Tommerdahl et al 1999a): OIS responses to different modes of vibrotactile stimulation. Left: Comparison of the time course of the responses of the contralateral SI forelimb region to 25- , 200-, and combined 25 Hz + 200 Hz stimulation of a skin site on the thenar eminence. Rightmost column: pattern of absorbance change (no organized pattern is apparent) in the absence of skin stimulation. The response to 25-Hz stimulation is well maintained over the total period of skin stimulation, whereas the increase in absorbance evoked by the combined 25 Hz + 200 Hz stimulus to the same skin site approximates that obtained with the 25-Hz stimulus only during the 1st 1-3 s of stimulation and becomes increasingly weaker with time. Plot at bottom right**

**shows average absorbance vs. time after stimulus onset. Flags indicate ±1 SE. Bottom left: cortical map and inset drawing of the forelimb showing the site of stimulation.**

The difference map of the OIS response to two different frequencies of stimulation is shown in Figure 2 (From Tommerdahl et al 1999a). Darker regions indicate increased OIS response, which correlates with increased neuronal activity. The SI response to a flutter stimulus is strong, and remains strong for the duration of a sustained stimulus (Figure 2, left column, compare 3s and 10s OIS responses). In contrast, the OIS response to a sustained 200Hz stimulus diminishes with time (right column of Figure 2).

Longer duration (>1sec) vibratory stimuli have been demonstrated to evoke an SI response that is below-background, although the initial response to the stimulus is above-background (Tommerdahl et al 1999a, b, 2005). For example, in Figure 3, the OIS response to a sustained 200Hz stimulus becomes weakened over time compared to the response to a 25Hz stimulus (compare the first and second columns of Figure 3). Stimulation with simultaneous 25Hz and 200Hz results in a response that is **less** than that evoked by the 25Hz stimulus alone, indicating that there is a mechanism responsible for active suppression of the SI response. (Figure 3, Tommerdahl et al 1999b).

One reason that it has been difficult to study the SI response to high frequencies is because of the increasing recruitment of PC afferent drive that occurs with stimulus frequencies above 50Hz (Whitsel et al, 2003). Although PC afferents project thalamocortically to SI, they do not project to cortical layer IV, but rather to the upper layers; thus their effect is quite different than that of RA or slowly-adapting (SA) afferent excitatory projections, which do project to layer IV. Additionally, PC afferents project directly

(thalamocortically) to Layer IV of SII, a cortical region which is highly interconnected with SI (Jones 1998, Rausell and Jones 1991a, b, Rausell et al 1992).

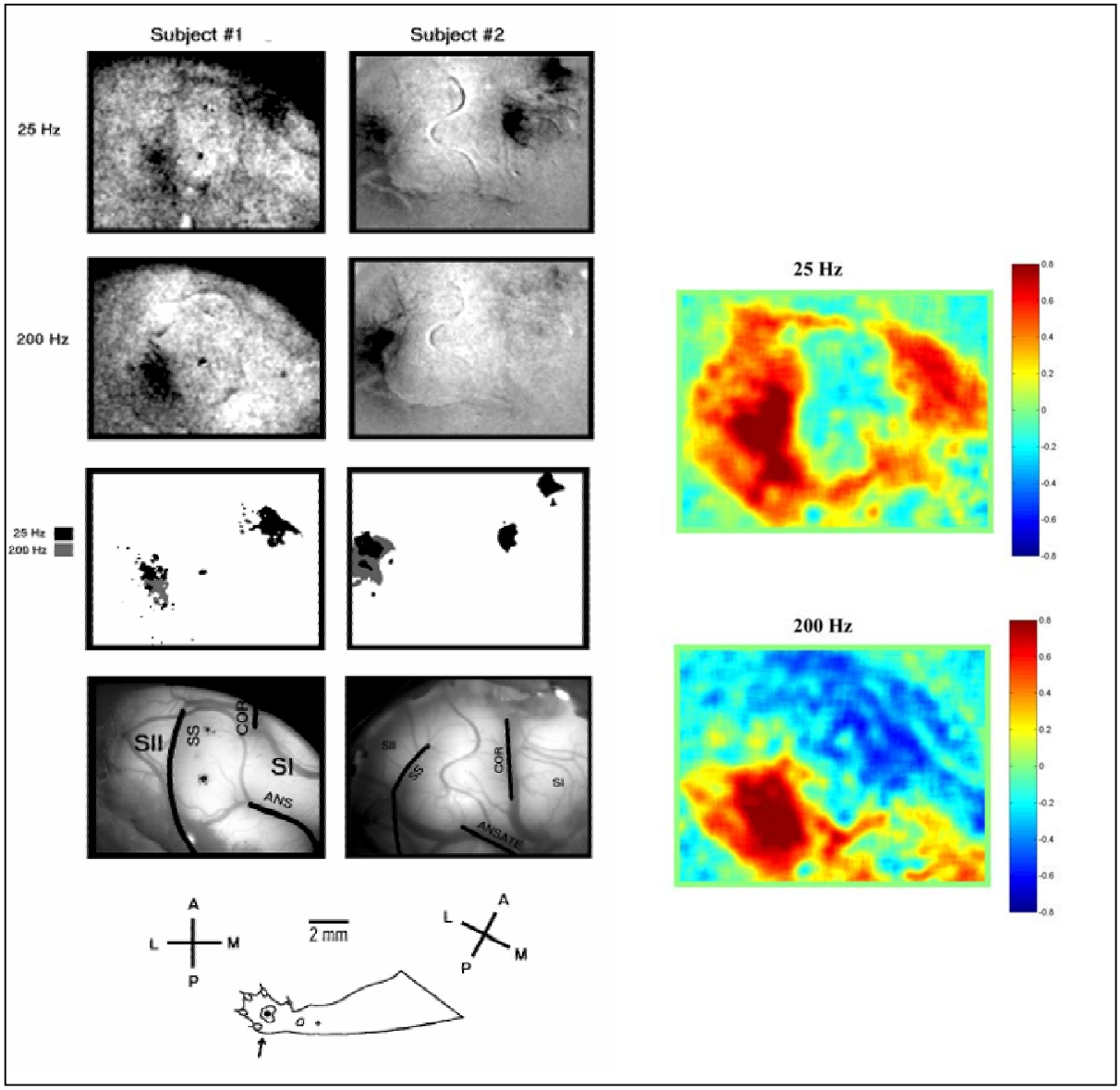


**Figure 4 (modified from Tommerdahl et al 199b): OIS-imaging results obtained from 2 subjects. Locations of the 2 × 2mm boxels within which a measurement of average absorbance was obtained at multiple time points after onset of skin stimulation indicated by rectangles (right column, 3rd row). *Top*: difference images from 2 subjects showing the responses of SI and SII in the hemisphere contralateral to 25-Hz central-**

**pad stimulation. The responding region of SI is located at *top right* of each image; and responding region of SII is located at *bottom left. Middle*: difference images from the same 2 subjects showing the responses of SI and SII in the hemisphere contralateral to 200-Hz central-pad stimulation. *Bottom*: each panel shows the superimposed thresholded responses of a subject to 25-Hz (black) and to 200-Hz (gray) stimulation. Diagram *below* panels shows surface vascular patterns with locations of sulci enhanced by bold lines. COR, coronal sulcus; SS, suprasylvian sulcus; ANS, ansate sulcus. Right column, top: correlation map obtained from the data acquired under 25-Hz stimulation; bottom: obtained from the data acquired under 200-Hz stimulation. Color scale (right) indicates the value of the correlation coefficient. Under the 200-Hz stimulus condition, the activity in most locations in the SI forelimb region is anticorrelated with the time course of the absorbance change that the 200-Hz stimulus evokes in the maximally activated boxel within SII---see bottom; whereas under the 25-Hz condition, the activity at most sites in both SI and SII is positively correlated with the time course of the absorbance change that the 25-Hz stimulus evokes within the maximally activated SII boxel (top).**

A number of reports have indicated that high frequency mechanical stimulation evokes a response in SI that is relatively weaker than that evoked in SII. Harrington and colleagues found a more frequent occurrence of activation in SI cortex for a 35Hz vibrotactile stimulus than for a 150Hz stimulus, but the reverse was found for SII cortex (Harrington and Downs, 2001). Sleigh et al found that increasing vibrotactile stimulus frequency from 20 to 200Hz led to a corresponding reduction in the number of activated

pixels in SI, while conversely increasing the number of activated pixels in SII (Sleigh et al, 2001). The left half of Figure 4 shows the OIS response to forepaw stimulation in SI and SII of 2 different subjects (Tommerdahl et al, 1999b). In both subjects, a 25Hz flutter stimulus evokes strong, sustained activity in both SI and SII. In contrast, although 200Hz vibration does evoke activity in SII very effectively, SI activity is relatively weak. In fact, the increase in SII activity appears to be correlated with the decrease in activity in SI. (Rightmost column Figure 4, Tommerdahl et al 1999b).

A recent report by Tommerdahl and colleagues showed that one of the mitigating factors in the population response to 200Hz stimulation is the proportion of RA/SA to PC innervation at the stimulus site (Tommerdahl et al, 2005). At stimulus sites that have a higher RA to PC innervation density (such as the tips of the digits), SI responds more vigorously to high frequency stimulation than it does to the same stimulus at a site with lower RA to PC innervation (such as the forearm). Data obtained with and without an annulus ring, as well as data obtained in the presence and absence of topical anesthetic, further confirmed the relationship between the ratio of RA to PC innervation density and the degree to which the SI response was impacted by the activation of the PC afferent population (Tommerdahl et al., 2005).

Integration of the cortical activity arising from the activation of both PC and RA afferents in response to high-frequency vibrotactile stimulation leads to a view that is somewhat mixed. On one hand, SI RA neurons are capable of responding periodically (in an entrained manner) to 200Hz stimulation (Whitsel et al 2001, 2003). On the other hand, the output of the SI RA neurons could be modified by the cortical activity initiated by the drive from the PC system (Tommerdahl et al, 2005). Thus, although there is a growing body of

evidence that SI RA neurons play a major role in frequency discrimination in the above 50Hz range via periodic response, it is difficult to selectively study the effects of increasing the frequency of stimulation of RA afferents without also engaging the PC afferent population. One question that arises from the previously cited literature is: would direct stimulation of isolated RA afferents lead to a vigorous response in SI and SII, or alternatively, would higher frequency stimulation of RA afferents lead to a weak response in SI, as high frequency mechanical stimulation has been shown to do? In other words, is the mechanism responsible for the SI suppression of activity due to the frequency of stimulation, or due to the contributions of the different afferent types stimulated by a skin vibrotactile stimulus?

One way to answer the question is by studying the response to stimulation of individual afferents. In this work, the method of peripheral microneurography was used to isolate and stimulate single mechanoreceptive afferents (MRA) in conscious humans (Knibestol and Vallbo 1970, Ochoa and Torebjork 1983, Vallbo and Johansson, 1984, Vallbo et al 1984). Previous human studies have successfully used noninvasive imaging methods to study the cortical responses to microstimulation of single MRAs (Kelly et al, 1997, Trulsson et al, 2001, McGlone et al 2002). In this chapter, fMRI is used to address the question of whether or not high frequency microstimulation of individual RA or SA afferents can account for the suppression of activation in SI that is observed when a high frequency vibrotactile stimulus is applied to the RF center. Whole brain fMRI is used to obtain cortical activation maps evoked by microstimulation of single afferents at 30Hz and 200Hz, and the evoked hemodynamic responses in SI and SII are compared.

***Methods***

Informed consent was obtained from all subjects in compliance with the University of North Carolina's Institutional Review Board. All microneurography and microstimulation equipment was tested to ensure subject safety and minimize interaction with the imaging instrumentation (Trulsson et al 2001, McGlone et al 2002). Subjects remained in a supine position on a movable bed; the left or right arm was immobilized. Figure 6 shows a schematic of the experimental setup which is described below.

A coated tungsten needle microelectrode was inserted into the median nerve 1-2 inches medial to the wrist. The nerve bundle was then impaled and electrode position carefully adjusted until single afferent impulses from an MRA were detected. The RF for each isolated MRA was defined with von Frey hairs and its boundary marked on the skin. Afferents were classified using the standard criteria defined by Knibestol and Johansson (Knibestol and Vallbo 1970, Johansson and Vallbo 1979). Subjects were asked to report the location and extent of the stimulus-evoked sensation and correspondence between the projected RF and the RF of the stimulated afferent was verified (Vallbo and Johansson 1984). Subjects were also asked to report the perceived quality of the sensation, and to monitor any change in sensation throughout the session.

The electrode was connected to a constant-current stimulator delivering positive square-wave electrical pulses (Vallbo et al 1984). Stimulus current was adjusted to just above the threshold at which a sensation was evoked to minimize the risk of exciting multiple afferents. The magnitude of the stimulating current never exceeded 10μA. If the location, shape, and size of the projected RF did not match the mapped RF, or if multiple

projected RFs were reported, no imaging was carried out and the position of the microstimulating electrode was shifted to a new location in the nerve.[1]

Twenty repetitions of 30Hz stimulus were delivered during 2s stimulation and 14s or 18s rest. Subjects were instructed to attend to the stimuli. Echoplanar imaging (Siemens Allegra 3T) was used concurrently with afferent microstimulation to acquire whole brain fMRI images with TR=2s, TE=30ms, Flip angle = 90°. Sixteen contiguous 3mm-thick transverse slices were acquired with an in-plane resolution of 3mm x 3mm. Anatomical localization was achieved for each subject by coregistration of echoplanar image data to high-resolution $0.9mm^3$ isotropic T1-weighted images.

If at any time during a scan the subject no longer felt the stimulus, or if the quality of stimulus or RF changed, the scanning session was stopped. Each isolated afferent was checked at the end of scanning to ensure that the size and shape of the RF agreed with the RF of the initially isolated afferent. Selected afferents whose isolation remained stable and whose response remained constant throughout the 30Hz scanning session were also microstimulated using the same paradigm at 200Hz and 3Hz.

Images were motion-corrected and globally normalized. The images were then spatially smoothed using a Gaussian filter of 5mm full width half maximum. Statistical Parametric Mapping (SPM; Friston et al 1995) was used to generate activation maps of the hemodynamic response to the stimulus at a statistically significant level of $p<0.001$ (uncorrected). This *t* threshold was chosen in order to best evaluate the hemodynamic

[1] The procedure of isolating, characterizing, and stimulating a single MRA is described in detail in Kelly et al, 1997.

response function in contralateral SI and SII, areas which are *a priori* known to be activated in response to microstimulation (Gelnar et al 1998, Trulsson et al 2001, McGlone et al 2002).

To allow anatomical localization and to aid in identification of activated areas, the echoplanar images were registered to the high-resolution anatomical images for each subject, using Analyze (Mayo Foundation, Rochester, MN), MEDx (Sensor Systems, Inc.), and FSL (Smith 2002). In the high-resolution anatomical images, SI was defined as the territory bounded anteriorly by the central sulcus, posteriorly by the post-central sulcus, medially by the knob region and laterally by the lateral margin of the post-central gyrus. SII was defined inferiorly by the lateral sulcus, anteriorly by the central sulcus, and medially by insular cortex (Nelson et al 2004).

To verify localization of activated areas, FSL's FLIRT algorithm (Jenkinson and Smith 2001, Jenkinson et al 2002) was used to register each subject's anatomical and EPI images to a standardized template, the MNI brain (Evans et al 1992), and statistical parametric analysis was repeated for the normalized images. A Matlab script was used to convert the resultant MNI coordinates for each activated cluster to Talairach coordinates (Brett 1999). An interactive Talairach atlas was used to identify the functional areas corresponding to these locations for each subject (Kochunov and Uecker 2003).

The time course of pixel intensity values for activated regions of interest was obtained from the statistical maps of the motion-corrected (but not spatially normalized) EPI images using volume-of-interest (VOI) data extraction in SPM with a radius of 0mm. From ;each cluster, the time-course intensity values for the most highly statistically significant voxel were extracted into a database. The arrays of data values extracted in this manner were averaged over the 20 stimulus cycles and the average response was plotted against time.

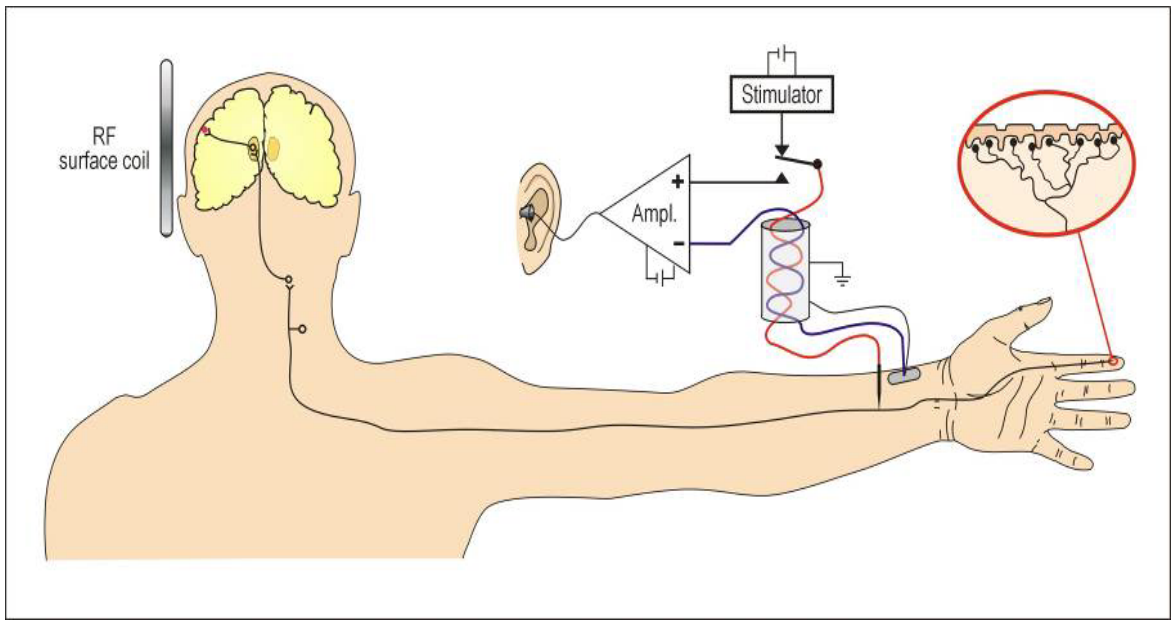


**Figure 5 (modified from Kelly et al, 1997): Experimental setup used in Chapters 2 and 3. The subject is positioned in the scanner (indicated by the RF surface coil) while the microelectrode is inserted into the nerve bundle. The microelectrode is connected to an amplifier through which the neurographer can identify the afferent type. Once the afferent is identified, its receptive field (shown in the red oval inset) is mapped. The stimulator is used to deliver frequency and amplitude controlled stimuli through the microelectrode.**

***Results***

A total of 20 afferents were successfully isolated and microstimulated on six healthy right-handed subjects (4 male, 2 female). These consisted of 20 MRAs: 13 RA afferents, 5 SA afferents, and 2 PC afferents. All afferents were microstimulated at 30Hz; selected MRAs that remained stable after the 30Hz scanning session were also microstimulated at 200Hz and/ or 3Hz. A total of 28 runs were carried out during afferent microstimulation at frequencies of 3, 30, and 200Hz.

RF maps and perceptual reports

In all cases, mapped RFs corresponded closely in size and location with subjects' perceived RFs; typically the discrepancy in position and size was less than 1mm. The locations of the mapped RFs for all 20 afferents are shown in Figure 6. Nineteen of the 20 RFs were located on the glabrous skin of the hand; one SA afferent (Subject 5, see Figure 6 for RF location) had an RF located on the dorsal side of the hand.

Table 1 summarizes the RF properties of the isolated and stimulated afferents, as well as subjects' description of the sensory experience evoked by stimulation at 30Hz. All RA and SA afferents had RFs that were oval or circular, with diameters less than 10mm and sharply defined boundaries. Microneurography revealed that the spike activity was evoked in the RA and SA afferents in response to light stroking across the RF, and the quality of the perceived sensation in all cases was reported by subjects to be uniform throughout the RF. Subjects consistently described the sensation evoked by RA microstimulation at 30Hz as "buzzing" or "flutter," and the sensation evoked by 200Hz microstimulation as feeling the same as the sensation at 30Hz but "faster" or "higher pitched." When RAs were

microstimulated at 3Hz, subjects reported "six distinct taps" during each 2s stimulus period. The sensation evoked by 30Hz microstimulation of SA afferents was described as a slow or constant indentation or pulling of the skin. The sensation at 200Hz SA microstimulation was described as feeling the same as 30Hz but faster. Subjects reported feeling 6 weak but clear taps at 3Hz. None of the subjects described the microstimulation of RAs and SAs as painful at any frequency.

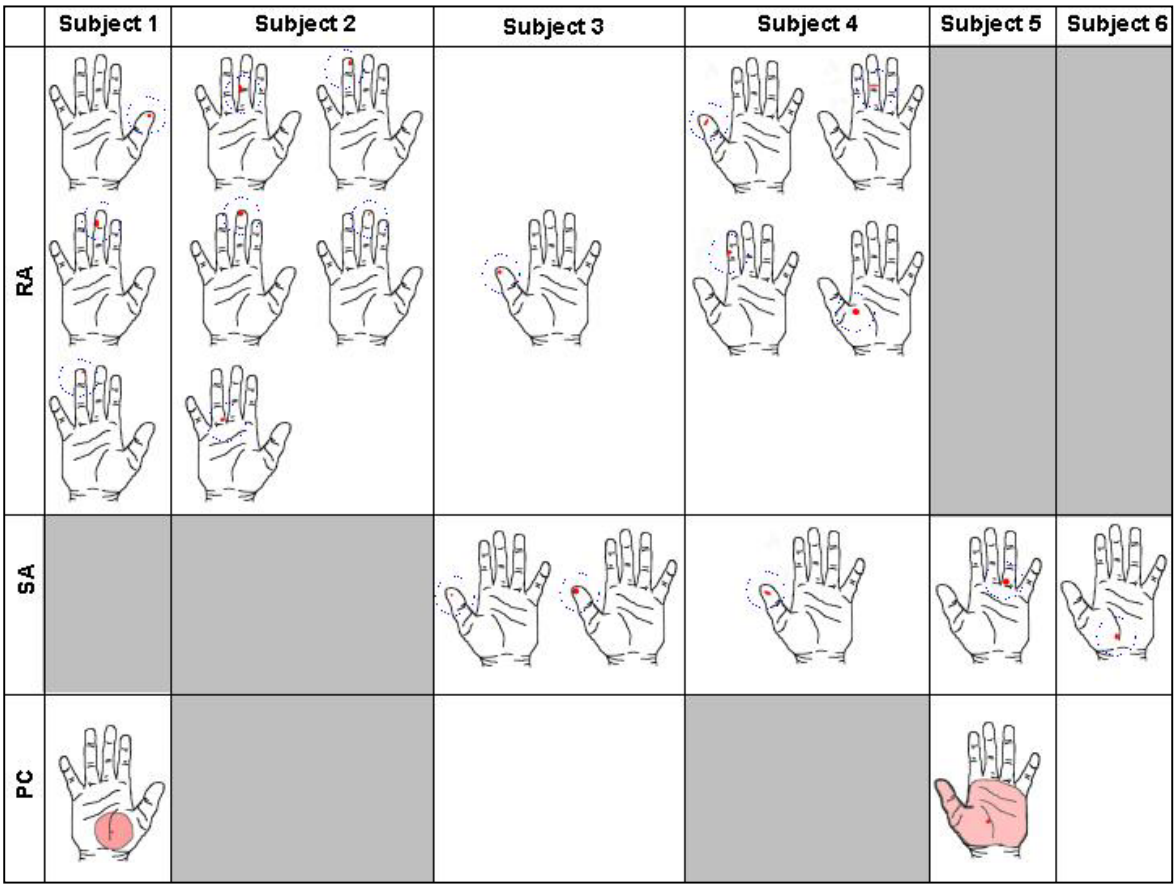


**Figure 6: Locations of RFs of microstimulated afferents. Table is grouped by subject (columns) and afferent types (rows). Red filled circles indicate RF location, and blue dotted lines clarify RF location in the case of smaller RFs.**

| Afferent type | Number | Typical RF size/shape | Description of sensation evoked by 30Hz microstimulation |
|---|---|---|---|
| RAI | 13 | Oval or circular, 2-6mm diameter (long axis) | Buzzing sensation |
| SAI | 5 | oval, 2-8mm diameter (long axis) | Slow indentation, inward pulling |
| PC | 2 | large, irregular (on the order of cm) | Diffuse vibration with 'hotspot' of stronger vibration in approximate center of RF |

**Table 1: Table of isolated afferents by type. The number of isolated afferents of each type is indicated in the 2nd column, and the RF size/shape is described in the 3rd column. The rightmost column contains subjects' descriptions of the sensations to microstimulation of that particular afferent type.**

The RFs of both isolated PC afferents were much larger than those of RA and SA afferents, with ill-defined borders and a central "hotspot" where the stimulus-evoked sensation was most intense (see Figure 6 and Table 1, Subjects 1 and 5). On Subject 1, the RF was an irregular oval at the base of the thumb measuring approximately 3 x 2cm, with a small central hotspot that could be activated by tapping. This subject described the sensation evoked by microstimulation of the PC afferent at 30Hz as a "vibratory sensation, diffuse over the base of the thumb with a clear hot spot in the center", and the sensation at 200Hz as "same as 30Hz but stronger, with no clear pitch difference." The RF of the PC afferent isolated on Subject 5 covered the entire palm and thumb, and included a centrally located

hotspot. Subject 5 described the sensation evoked by microstimulation of the PC afferent at 30Hz as "a buzzing sensation with a hotspot equidistant between the base of the fingers and the wrist." At 200Hz, Subject 5 reported experiencing "the same as the 30Hz, a little more intense but with the same sensation." No sensation was reported by either subject in response to 3Hz microstimulation of the PC afferent. After the 3Hz MR scanning session the frequency of microstimulation was increased and both subjects verified the sensations and perceived RFs reported previously at 30Hz and 200Hz, indicating that the stimulating electrode was still in its original location and was activating the same afferent.

Functional imaging and hemodynamic responses

In this chapter, whole-brain cortical activation maps evoked by microstimulation of MRAs are presented for the first time. Previous studies used a surface coil positioned over the subject's parietal cortex to show that microstimulation of RA and SA afferents evokes a statistically significant fMRI response in SI and SII cortices contralateral to the site of stimulation (Trulsson et al, 2001; McGlone et al 2002). The results presented in this chapter show that, in addition to SI and SII, other cortical areas that are known to be involved in higher order processing of sensory stimuli – such as the posterior parietal, supplementary motor, frontal, and insular cortices – demonstrate a measurable fMRI response even when only a single MRA is stimulated (Tables 2 and 3, Figures 7a, b and 12).

The first documented fMRI responses to microstimulation of PC afferents are also presented (Table 4, Figures 15 a, b and 16). In one of the two subjects for whom a PC afferent was successfully microstimulated, a significant level of fMRI activation was observed in contralateral SI cortex. In both subjects, Subjects 1 and 5, for whom PC

afferents were microstimulated, multiple areas of fMRI activation were observed in other cortical regions known to be responsible for the processing of somatosensory stimuli: namely bilateral SII, posterior parietal, cingulate, supplementary motor, motor, insula, and frontal cortices.

The number of afferents for which a significant response was evoked in SI and SII is shown in Table 2 (t-test, $p<0.001$ uncorrected). At this level of statistical significance, contralateral SI activation was observed in response to microstimulation of all afferents except for 30Hz microstimulation of 1 RA afferent. Microstimulation of the same RA afferent at 200Hz evoked a statistically significant response in SI. Contralateral SII activation was observed in 8 of the 13 RA afferents microstimulated at 30Hz, all 8 RA afferents microstimulated at 200Hz, 4 out of 5 SA afferents, and both PC afferents. Ipsilateral SII activation was observed in 10 of the 13 RA afferents microstimulated at 200Hz, 6 of 8 RA afferents microstimulated at 200Hz, 3 of 5 SA afferents, and both PC afferents.

An *F*-test modeling both the hemodynamic response function and its temporal derivative was used to further visualize overall activation pattern since single afferent microstimulation produces such a small focal area of activation, and also to account for differences in subjects' hemodynamic response properties. When the *F*-test was performed at a level of $p<0.001$ (uncorrected), statistically significant areas of activation were observed in contralateral SI and bilateral SII areas for all of the afferents that were microstimulated.

| Afferent type | Contralateral SI | Ipsilateral SI | Contralateral SII | Ipsilateral SII |
|---|---|---|---|---|
| RA: 30Hz (n=13) | 12 | 4 | 8 | 10 |
| RA: 200Hz (n=8) | 8 | - | 8 | 6 |
| SA: 30Hz (n=5) | 5 | 1 | 4 | 3 |
| SA: 200Hz (n=1) | 1 | - | 1 | 1 |
| PC: 30Hz (n=2) | 1 | - | 2 | 2 |
| PC: 200Hz (n=1) | - | - | 1 | 1 |

**Table 2: Number of afferents showing significant fMRI activation in SI and SII in response to microstimulation. The threshold for significance was set at $p<0.001$.**

Other areas of activation that were frequently activated in response to microstimulation of MRAs are the supplementary motor area (12 of 13 RAs, 4 of 5 SAs, 2 PCs), primary motor cortex (10 of 13 RAs; 4 of 5 SAs, 1 PC), cingulate gyrus (10 of 13 RAs; no SAs, 1 PC), insular cortex (11 of 13 RAs, 4 of 5 SAs, 1 PC), the posterior parietal area (11 of 13 RAs, 4 of 5 SAs, 2 PCs), and the orbitofrontal cortex (10 of 13 RAs, 2 of 5 SAs, 2 PCs). These areas of activation are consistent with those found in whole brain fMRI studies of the responses to vibrotactile stimulation (Francis et al 2000, Gelnar et al 1998, Harrington and Downs 2001).

For the purposes of verifying the Talairach coordinates of each cluster of activated pixels, all data was registered to the standardized Montreal Neurological Institute (MNI) brain template (Evans et al 1992). The MNI coordinates were converted to Talairach coordinates using a Matlab script (Brett 1999). Table 3 lists the peak *t* value of each

activated cluster greater than 3 pixels (k>3) for three exemplary RA afferents, two of them microstimulated at 30 and 200Hz, and 1 exemplary SA1 afferent. Since no multiple comparison corrections were performed, clusters less than 3 pixels were regarded as statistically insignificant. The corresponding stereotaxic coordinates are listed below the peak value. Table 4 contains a list of peak *t* values and corresponding Talairach coordinates for the PC afferents. The more liberal threshold of $t$=3.33, corresponding to $p<0.001$ on an uncorrected t-test, is used for statistical thresholding since a more stringent threshold might reduce activation in areas considered to be functionally significant (Loring et al 2002).

The *t*-maps generated by statistical analysis were registered to and displayed on the subject's own high-resolution anatomical MR image for accurate visualization of the areas of activation. Figures 7a and 7b show the fMRI activation maps ($p<0.001$ uncorrected) for an exemplary RA microstimulated at 30 and 200Hz (Subject 1).

| Subjects / Regions | Subj. 1 RA right hand | Subj. 4 RA left hand | | Subj. 4 RA left hand | | Subj. 3 SAI left hand |
|---|---|---|---|---|---|---|
| | 30Hz | 30Hz | 200 Hz | 30Hz | 200 Hz | 30Hz |
| Contralateral SI (B.A. 1, 2, 3) | **3.60** -55 -18 28 | **3.44** 51 -24 32 | **3.48** 50 -21 50 | **3.40** 47 -26 40 | **4.03** 56 -22 40 | **3.47** 66 -18 24 |
| Contralateral SII (B.A. 40) | ***3.28*** -53 -33 50 | **3.49** 64 -26 32 | **5.66** 65 -21 50 | **4.90** 47 -33 35 | **6.24** 65 -23 24 | **5.33** 9 -32 28 |
| Ipsilateral SII (B.A. 40) | ***2.83*** 56 -22 24 | **6.26** -58 -33 28 | **n.s.** | **3.73** -54 -46 24 | **5.04** -54 -30 24 | **3.47** -61 -25 32 |
| SMA (B.A. 6) | ***3.26*** 4 -4 50 | **3.44** 49 1 28 | **3.59** -51 -1 20 | **n.s.** | **6.08** -63 -7 35 | **3.92** 52 10 45 |
| Motor Cortex (B.A. 4) | **n.s.** | **n.s.** | **n.s.** | **n.s.** | **n.s.** | **n.s.** |
| Cingulate (B.A. 24) | **3.98** 2 2 40 | **n.s.** | **3.95** 5 6 35 | **3.45** 11 8 35 **3.72** 3 3 45 **4.42** -6 46 1 | **3.40** -3 -2 28 | **3.59** -2 23 35 |
| Insular cortex (B.A. 13) | **n.s.** | **n.s.** | **3.79** 33 23 12 **5.77** -34 -5 20 | **n.s.** | **3.38** 36 -5 20 **3.38** -37 -7 20 | **3.56** 17 -35 50 |
| Posterior Parietal (B.A. 5, 7) | **3.67** 4 -30 50 **4.13** 15 -45 55 | **n.s.** | **3.78** 19 -38 50 | **n.s.** | **n.s.** | **3.80** 28 42 35 |
| Frontal (B.A. 8,9) | **3.61** -46 20 24 | **5.62** 24 17 45 **5.21** -19 46 45 | **3.43** 24 19 45 **3.99** -24 41 40 | **4.05** 6 45 45 | **n.s.** | **n.s.** |
| Other | **n.s.** | **B.A. 19: 4.56** 13 -73 24 **B.A. 44: 4.71** 57 13 20 | **n.s.** | **B.A. 19**: **3.39** 27 –71 40 | **B.A. 19: 5.84** 41 -71 8 **3.96** -41 -73 8 | |

**Table 3: Peak *t*-values of areas of activation in response to microstimulation of RA and SA afferents, with corresponding stereotaxic coordinates. $t \geq 3.33$ represents significant activity in a global search corresponding to $p<0.001$. Values in italics indicate lower**

**p<0.05 corresponding to $t \geq 2.67$. Coordinates are expressed in millimeters and refer to the medial-lateral (relative to the midline; positive=right hemisphere), anterior-posterior (relative to anterior commissure; positive=anterior), and superior-inferior (relative to commissural line; positive=superior) stereotaxic planes (Talairach and Tournoux, 1988). B.A., Brodmann Area, n.s., non significant.**

| Subjects / Regions | Subject 1 PC afferent | | Subject 5 PC afferent |
|---|---|---|---|
| | 30 Hz (right hand) | 200 Hz (right hand) | 30 Hz (left hand) |
| Contralateral SI (B.A. 1, 2, 3) | **n.s.** | **n.s.** | **5.01** 66 -20 24 |
| Contralateral SII (B.A. 40) | **3.81** -54 -30 35 | **5.55** -59 -29 24 | **6.92** 50 -24 50 |
| Ipsilateral SII (B.A. 40) | **5.88** 58 -39 24 | **3.47** 60 -33 28 | **6.62** -60 -30 28 |
| SMA (B.A. 6) | **3.91** -29 -19 60 | **4.12** 30 -18 60 | **6.19** 52 -10 45 |
| Motor Cortex (B.A. 4) | **3.43** -33 -20 60 | **4.78** 4 -30 60 | **n.s.** |
| Cingulate (B.A. 24) | **3.67** -8 14 32 | **3.33** -4 -5 32 | **3.39** -2 20 30 |
| Insular cortex (B.A. 13) | ***2.94*** -33 –13 20 | **4.41** -36 -20 20 | **n.s.** |
| Posterior Parietal (B.A. 5,7) | ***3.10*** 5 -41 55 | **3.41** 15 -47 50; ipsi | **3.61** 8 -44 60 **4.58** -15 -75 35 |
| Frontal (B.A. 8, 9, 10) | **n.s.** | **4.83** 6 37 50 **4.02** 47 18 24 | **3.45** 21 39 45 |
| Other activated cortical areas | **n.s.** | **B.A. 18: 3.46** 21 -93 20 | **B.A. 44: 3.78** 60 10 8 |

**Table 4: Peak *t*-values of areas of activation in response to microstimulation of PC afferents, with corresponding stereotaxic coordinates. $t \geq 3.33$ represents significant**

**activity in a global search corresponding to p<0.001. $t \geq 2.67$ corresponds to p<0.05 and is indicated in italics. B.A., Brodmann Area; n.s., non significant.**

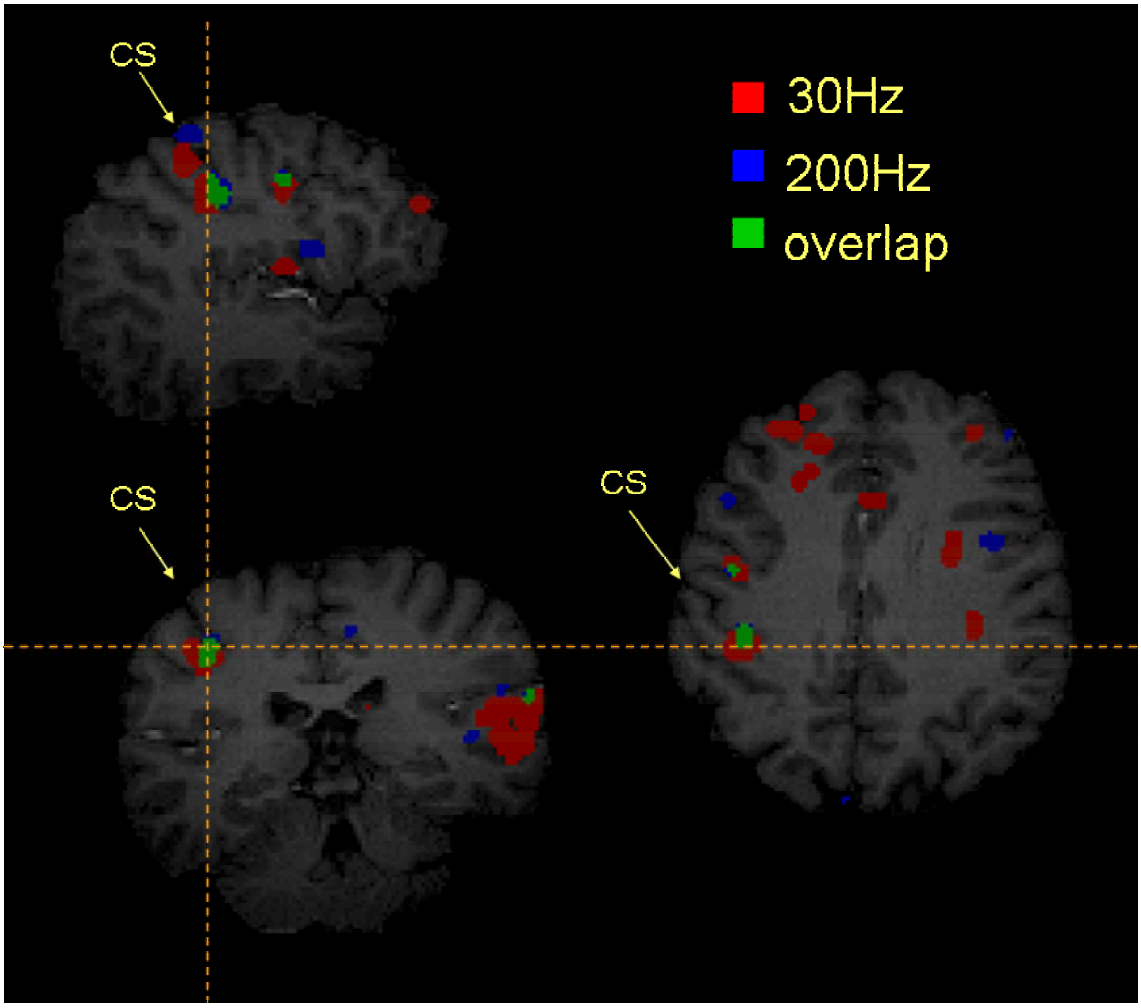


**Figure 7a: Contralateral SI and ipsilateral SII activation in response to 30 (red) and 200Hz (blue) microstimulation of an RA afferent. Areas of overlap are shown in green. Top: Sagittal view, bottom left: coronal view, bottom right: transverse view. Other observed areas of activation include contralateral premotor area, frontal cortex, and supplementary motor cortex. CS = Central Sulcus, LF = Lateral Fissure.**

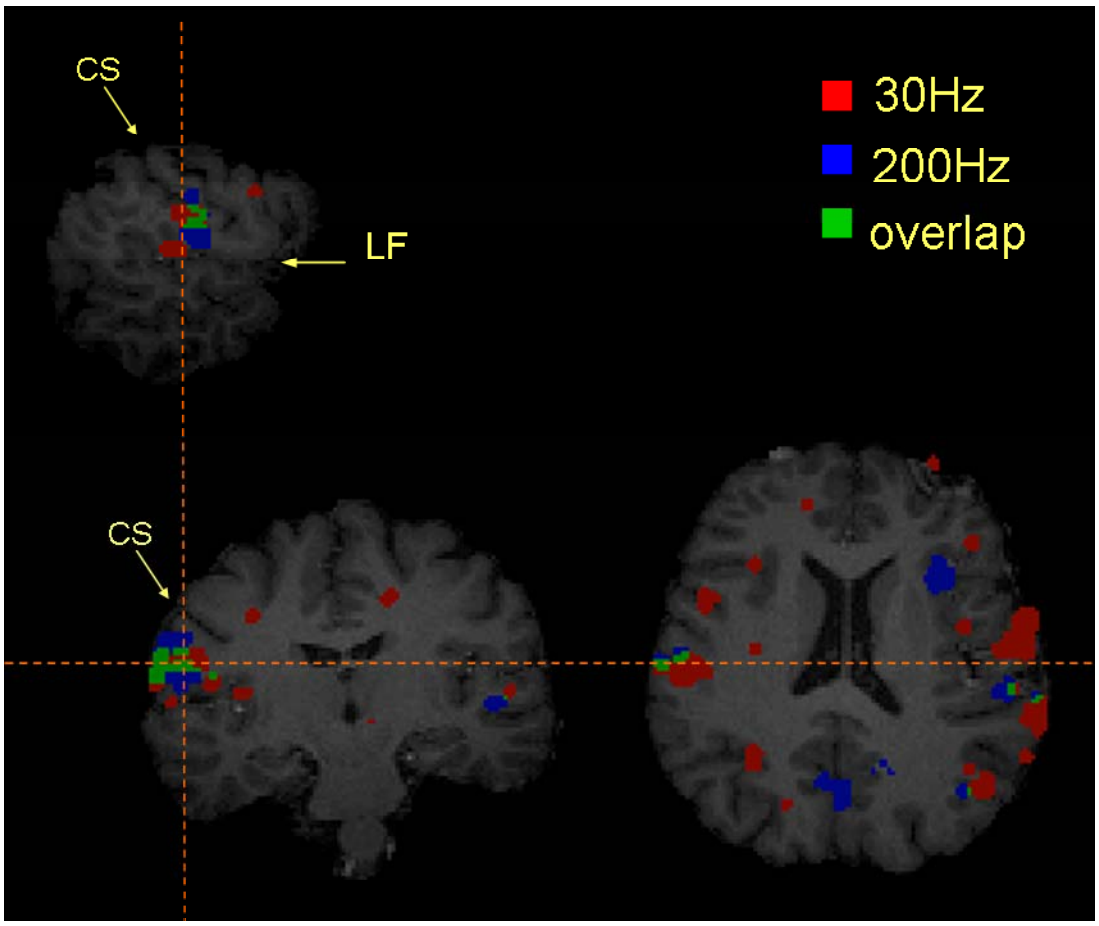


**Figure 7b: Bilateral SII activation in response to 30 (red) and 200Hz (blue) microstimulation of an RA afferent. Areas of overlap are shown in green. Top: Sagittal view, bottom left: coronal view, bottom right: transverse view. Other areas of activation that are observed include posterior parietal area, insular cortex, and frontal cortex. CS = Central Sulcus, LF = Lateral Fissure.**

Areas of fMRI activation for this particular RA at $p<0.001$ included SI and SII cortices contralateral to the site of stimulation, with extensive overlap as would be expected from microstimulation of the same afferent. Other cortical areas of activation included

frontal cortex, ipsilateral SII, and supplementary motor area. The spatial pattern of activation shown in Figure 2 is typical of all RA afferents that were microstimulated in this study.

The time course data for the most significantly activated pixel (highest correlation to the stimulus) in SI and SII is shown in Figure 8 for the same exemplary RA whose fMRI activation map is shown in Figures 7a and 7b. Vertical dotted lines on Figure 9 show the beginning of each 2s stimulus cycle. This "raw" data has not been smoothed or averaged, only adjusted for motion correction and global intensity normalization. Three Hz data was obtained by selecting a progressively more lenient threshold ($p<0.05$) and plotting the time course of the most highly significantly correlated pixel in SI. In all cases, a cyclical response can be observed that is consistent with the stimulus cycle. This data was averaged over all 20 stimulus cycles to generate an average hemodynamic response plot for each activated area.

The average hemodynamic response plot for the raw data shown in Figure 8 is shown in Figure 9. For this particular RA, the peak SI response microstimulation at 200Hz is greater than the response to microstimulation at 30Hz. In both SI and SII, the response to 3Hz microstimulation is comparatively weak, possibly explaining why the fMRI activation maps thresholded at $p<0.001$ did not show a significant response.

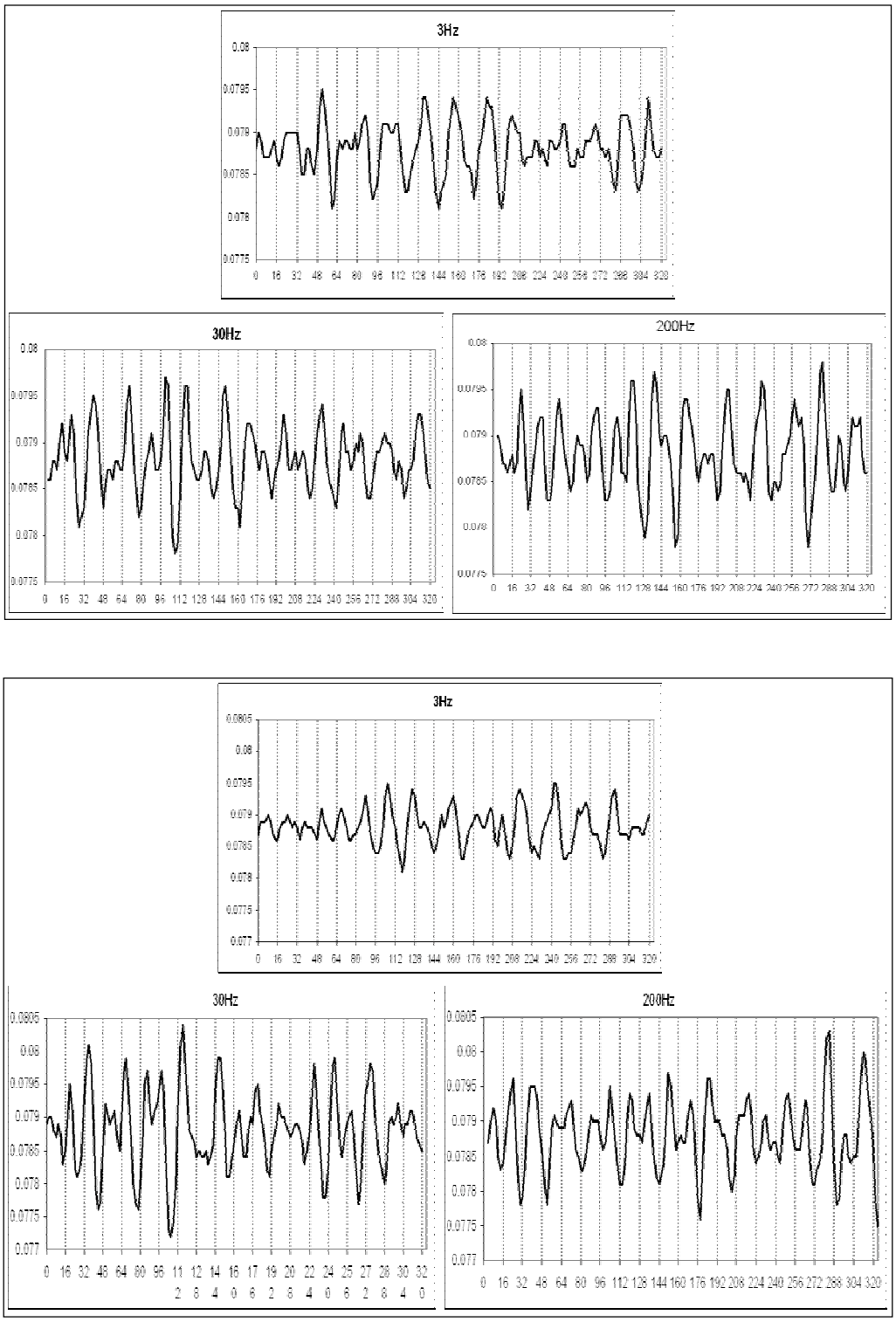


**Figure 8: Time course of hemodynamic responses to 3, 30, and 200Hz microstimulation of the RA shown in Figure 7. Time course data plotted for most significantly activated pixel in SI (top) and SII (bottom). X-axis: time (s); y-axis: intensity (arbitrary units).**

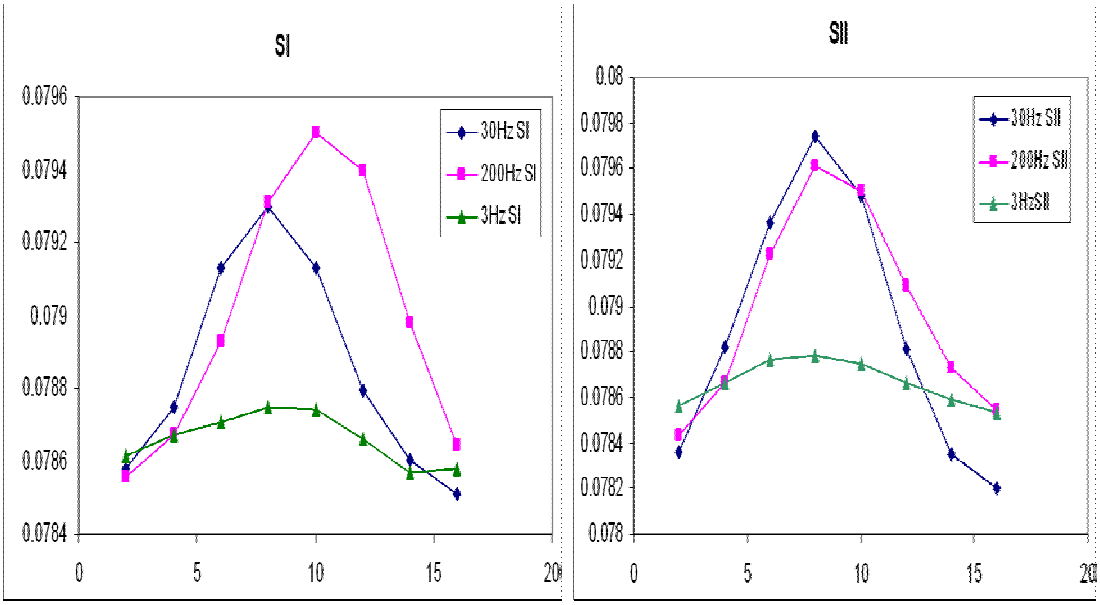


**Figure 9: Average time course of signal change over 1 stimulus cycle. The average time course of most significantly activated pixel in SI (left) and SII (right) in response to 3 (green), 30 (blue), and 200Hz (pink) microstimulation of the same RA whose time course is shown in Figure 8. x-axis: time (s); y-axis: pixel intensity (arbitrary units).**

Similar analyses were performed for all 8 RA afferents for which 30 and 200Hz microstimulation protocols were successfully completed. The average hemodynamic responses in contralateral SI and SII for both stimulus conditions (30 and 200Hz) are shown in Figure 11. When the data is averaged for all 8 RA afferents, the responses to 30Hz and 200Hz microstimulation are not significantly different from each other. The average signal change from baseline to peak was also computed for each of the 8 RA afferents and is shown in Figure 10. Again, the responses to 30Hz and 200Hz microstimulation are similar in magnitude.

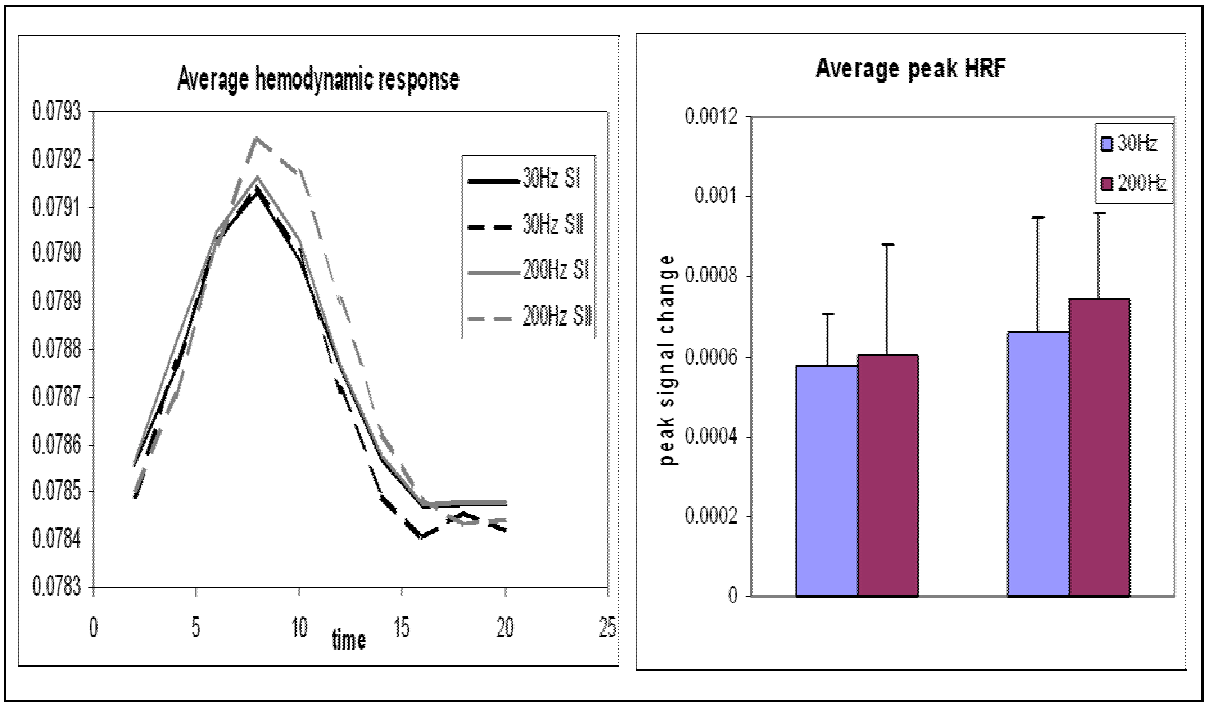


**Figure 10: Average time course responses of most significantly activated pixels in SI and SII in response to microstimulation of 8 RA afferents. Left: average time course of the signal change in the most activated pixel in SI (solid line) and SII (dashed line) in response to 30 (black) and 200Hz (gray) microstimulation. Right: average peak change in signal intensity for 30Hz (blue) and 200Hz (magenta) stimulation in SI and SII. Error bars indicate +/- 1 SE.**

Similar spatial patterns of activation were observed in the fMRI response to microstimulation of SA afferents. Figure 11 shows fMRI activation maps ($p<0.001$ uncorrected) for an exemplary SA microstimulated at 30 and 200Hz (subject 3).

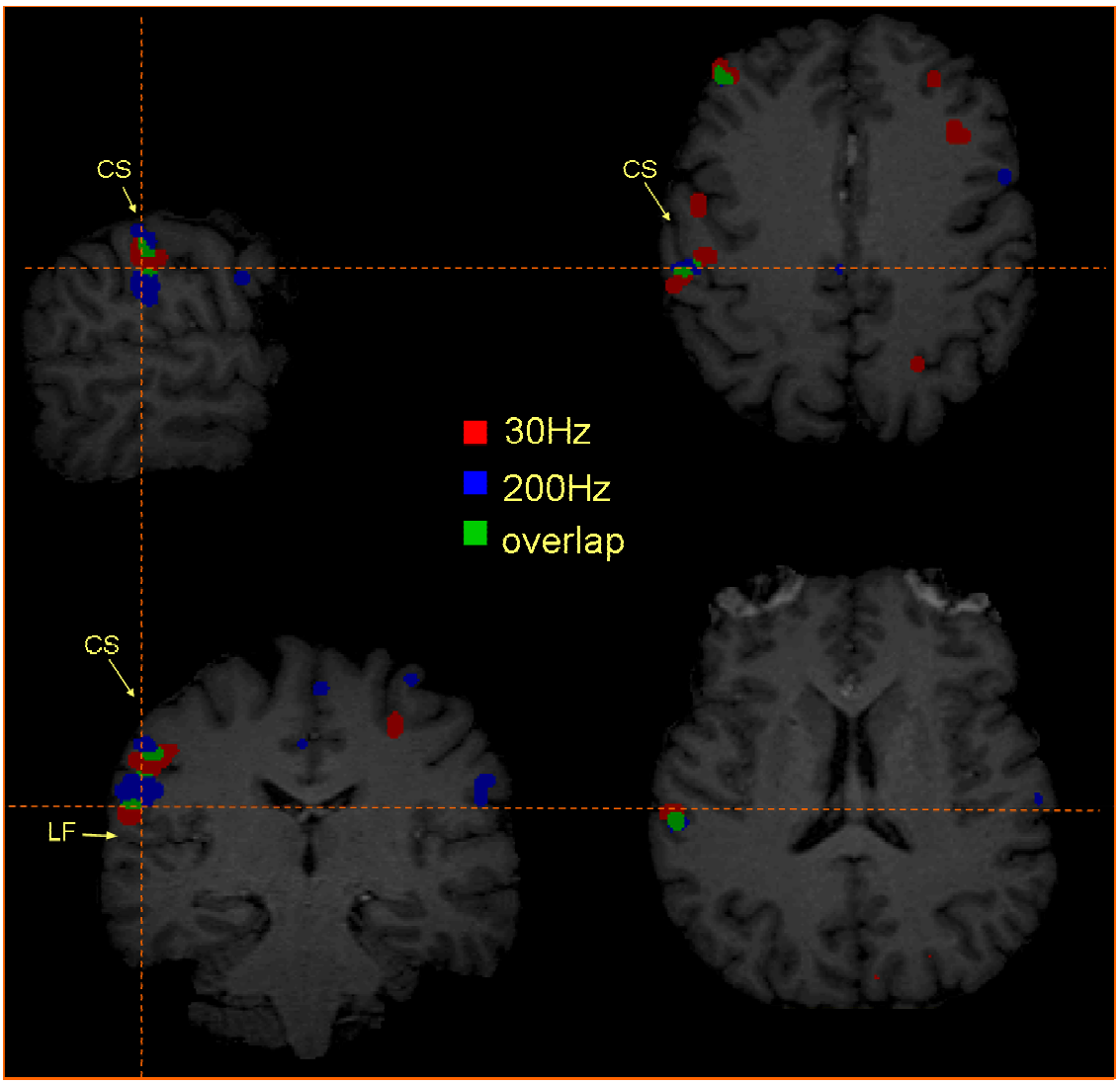


**Figure 11: Contralateral SI and SII activation in response to 30 (red) and 200Hz (blue) microstimulation of an SA afferent. Areas of overlap are shown in green. Top left: sagittal view, bottom left: coronal view, right column: transverse view. Crosshairs indicate slicing planes. Other areas of activation that are observed include ipsilateral SII, contralateral motor area, and frontal cortex. CS = Central Sulcus, LF = Lateral Fissure.**

As in the case of the exemplary RA afferent shown in Figure 7, extensive overlap in the activated area can be seen in the contralateral SI and SII regions. Areas of activation are also observed in the supplementary motor area and contralateral middle frontal cortices. In response to 30Hz microstimulation, primary motor, pre-motor, and ipsilateral frontal cortex activation can be observed. Ipsilateral SII activation is seen in response to 200Hz microstimulation. As in the case of the RA afferents, 3Hz microstimulation did not evoke a statistically significant hemodynamic response in this or any other SA afferent.

Time course data for the most significantly activated pixels in SI and SII contralateral to the site of stimulation were extracted from each dataset in the manner described above. Figure 12 shows time course data of the most highly significantly activated pixels in SI and SII in response to microstimulation of an exemplary SA afferent. The time course data obtained in this manner was averaged over all 20 cycles and the average for all 5 SA afferents was taken. The average hemodynamic responses of the most significantly activated pixels in SI and SII are plotted in Figure 13. Both responses follow similar time courses and are very similar in magnitude.

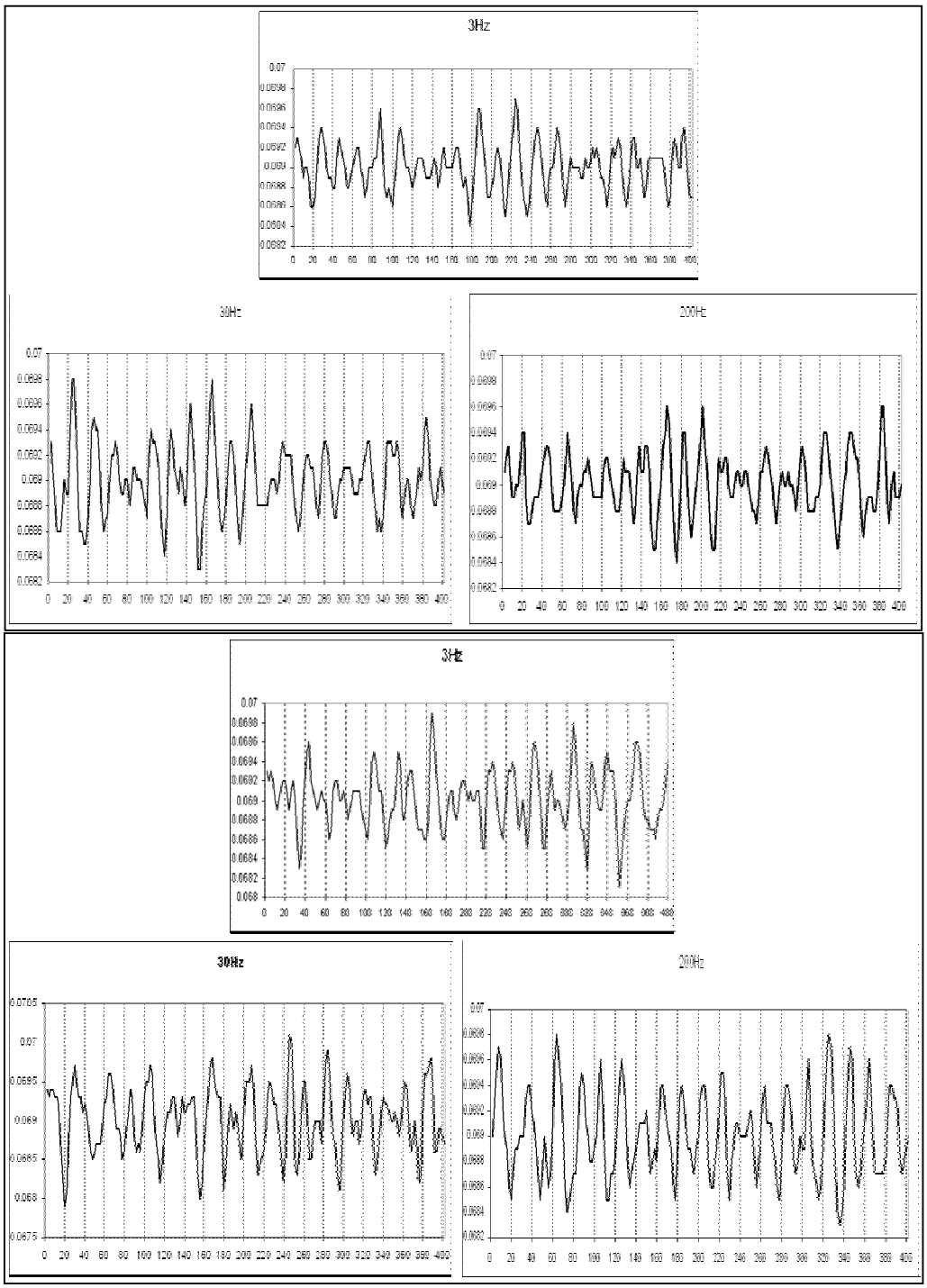


**Figure 12: Time course of hemodynamic responses to 3, 30 and 200Hz microstimulation of the exemplary SA shown in Figure 11. Time courses of most significantly activated pixel in SI (top) and SII (bottom). x-axis = time (s); y-axis = pixel intensity (arbitrary units).**

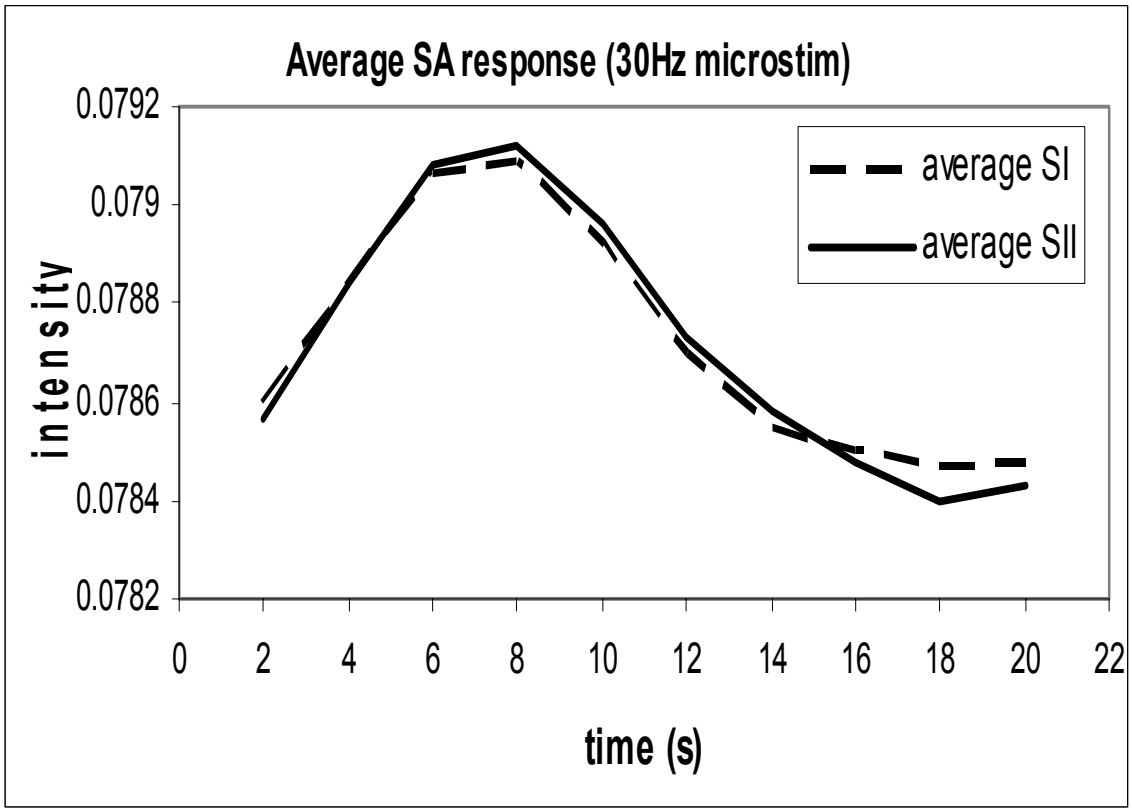


**Figure 13: Average SI (solid line) and SII (dashed line) time course responses to 30Hz microstimulation of all 5 SA afferents at 30Hz. x-axis: time (seconds), y-axis: intensity (arbitrary units).**

Microstimulation of one of the PC afferents (Subject 5) at 30Hz led to an observed fMRI response in contralateral SI and bilateral SII. In subject 1, no statistically significant SI activation was observed in response to microstimulation of a PC afferent either at 30 or 200Hz. A complete list of activated areas in response to microstimulation of both PC afferents is given in Table 4. Figures 14a and 14b show fMRI responses to microstimulation of a PC afferent (Subject 5) at 30 and 200Hz.

The hemodynamic responses in SI and SII for both PC afferents (Subjects 1 and 5) are shown in Figure 15. The SI and SII responses from Subject 1 were obtained by lowering the statistical threshold to a level at which activation was observed in SI ($p<0.1$).

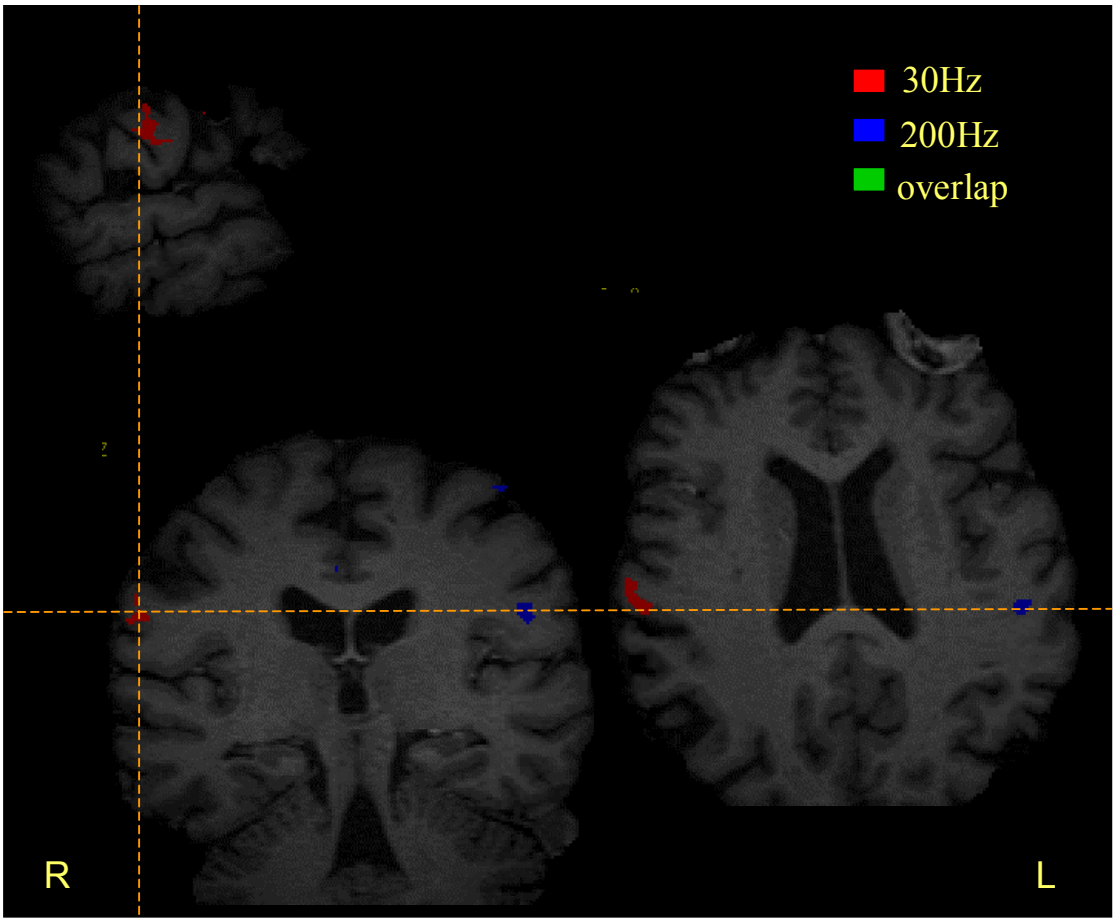


**Figure 14a: fMRI activation in contralateral motor cortex and bilateral SII in response to microstimulation of a PC afferent. Cingulate cortical activation in response to the 200Hz stimulus (in blue) was also observed in the coronal slice. Top left: sagittal view, bottom left: coronal view, right column: transverse view. Crosshairs indicate slicing planes.**

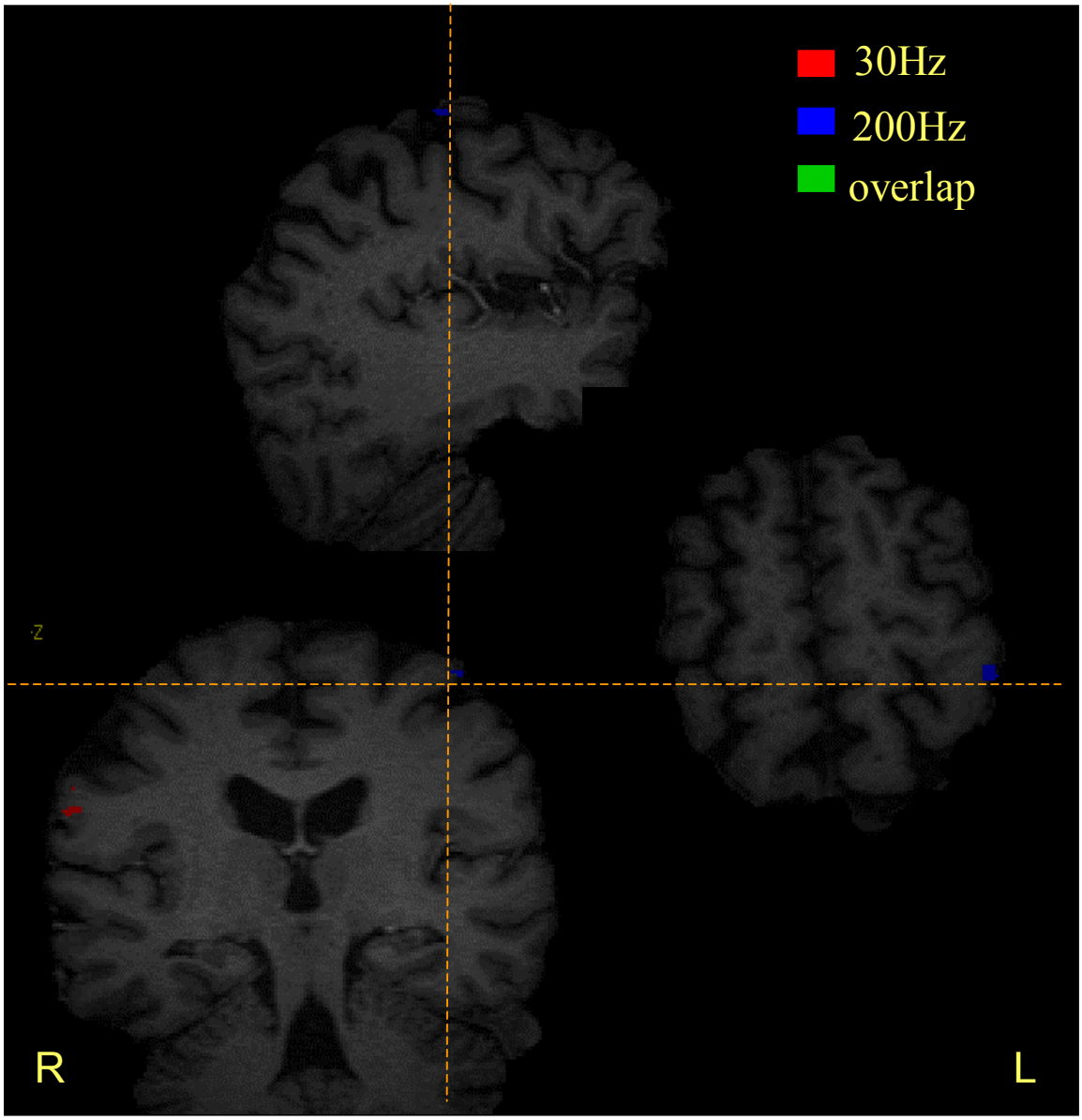


**Figure 14b: fMRI activation in motor cortex contralateral to the site of microstimulation of a PC afferent. SI activation was not observed at p<0.001 uncorrected. CS = Central Sulcus.**

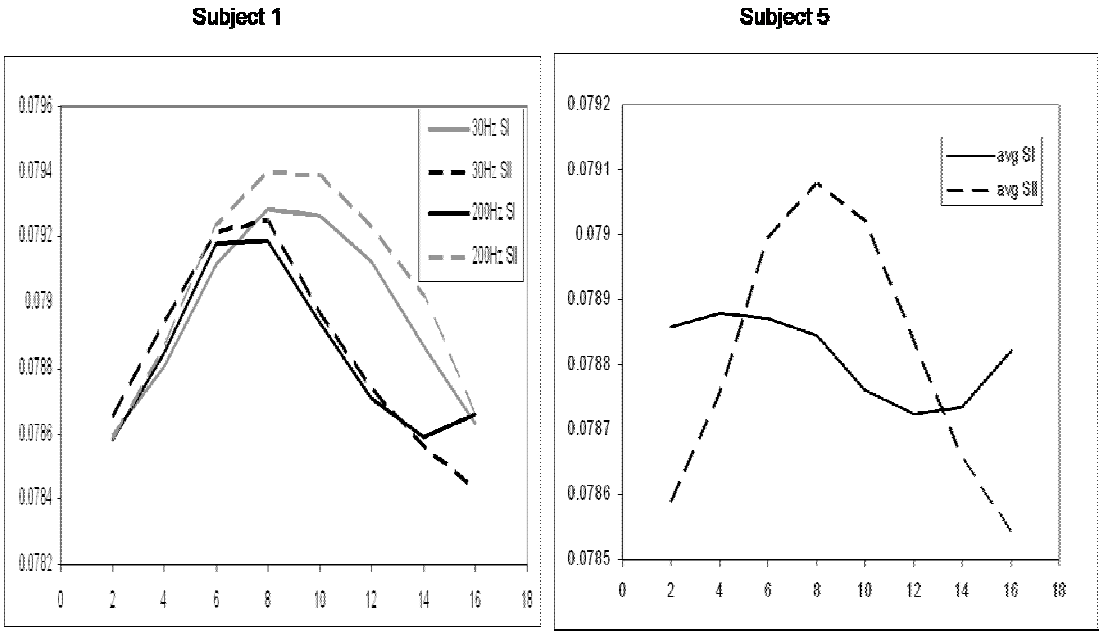


**Figure 15: Average hemodynamic responses to microstimulation of 2 PC afferents. The average time courses of the most significantly active pixels in SI (solid line) and SII (dashed line) are shown for the two subjects. Only 30Hz data was obtained for Subject 5 (right). X-axis = time (s), Y-axis = pixel intensity (arbitrary units).**

***Discussion***

The main purpose of this study was to determine whether high-frequency microstimulation of RA afferents can account for the suppression of SI activation that is seen when a high-frequency stimulus is applied to the skin. Perceptual reports from previous studies indicate that microstimulation of RA afferents using stimulus frequencies in the flutter range (20-40Hz) evokes a clearly-defined sensation of a cyclical flutter or wobble, but microstimulation of RA afferents using stimulus frequencies in the vibration range (100-120Hz) evokes a sensation of buzzing or a constant indentation (Ochoa and Torebjork 1983, Vallbo and Johansson 1984, Vallbo et al 1984). Similarly, subjects in our study reported that microstimulation of RA afferents elicited a sensation of weak tapping at 3Hz, a flutter sensation at 30Hz, and a sensation of a higher-pitched buzzing at 200Hz. Subjects' ability to detect pitch differences between 30 and 200Hz microstimulation supports the evidence that RA neurons play a major role in frequency discrimination regardless of whether the stimulus is in the flutter or vibration frequency range.

The most likely explanation for the lack of observed fMRI response to 3Hz microstimulation is that the change in hemodynamic response evoked by a 3Hz stimulus of a single MRA is too weak to be detected with the fMRI technology (both hardware and signal processing techniques) used in this study. Our results confirm those of Whitsel et al (2001, 2003): that microstimulation of RA afferents evokes a robust hemodynamic response in contralateral SI regardless of whether the frequency of microstimulation is in the flutter or vibration ranges. Hemodynamic cortical responses to SA and PC afferent stimulation also remain the same at different frequencies of microstimulation (30Hz and 200Hz), further indicating that the fMRI response depends on the type of afferent stimulated, and not frequency of microstimulation. Thus, RA afferent drive does not appear to be the mechanism

responsible for the suppression of SI activity observed when a prolonged, high-frequency stimulus is applied to the skin.

Tommerdahl et al have shown in animal studies that the PC afferent drive is the mechanism responsible for funnelling the SI response to high frequency stimuli over time (Tommerdahl et al, 2005). To answer the question of whether a similar mechanism exists for frequency discrimination in humans, further studies must be conducted that 1) use stimuli that engage both RA and PC afferents, and 2) use a stimulus protocol more suited to the study of cortical dynamics. Such further studies using fMRI to explore the cortical mechanisms underlying frequency discrimination in humans are proposed in Chapter 5 (future work).

***Conclusions***

Whole brain fMRI images of the response to microstimulation show that multiple cortical areas are involved in the processing of sensory stimuli even when only one MRA is microstimulated. These results are in agreement with studies showing that skin sensory stimulation evokes activation in multiple cortical areas, including primary sensory cortices and secondary sensory areas such as the posterior parietal cortex, insular cortex, and supplementary motor area.

High frequency microstimulation of RA afferents does not account for the suppression of SI activation that is seen in response to a prolonged high frequency vibrotactile stimulus applied on the skin. Further studies are needed to confirm the hypothesis that PC afferent drive is responsible for 'funneling' the SI response to high frequency skin stimulation in humans, as has been shown in animal studies.

***References***


Brett, M. (1999) The MNI brain and the Talairach atlas. Cambridge, MA: Cambridge Imagers.

Evans AC, Collins DL, Milner B (1992) An MRI-based stereotactic atlas from 250 young normal subjects. Soc Neurosci Abstr, Anaheim.

Francis ST, Kelly EF, Botwell R, Dunseath WJR., Folger SE (2000) fMRI of the responses to vibratory stimulation of digit tips. Neuroimage 11: 188-202.

Friston KJ, Holmes AP, Worsley KJ, Poline JB, Frith C, and Frackowiak RSJ (1995) Statistical Parametric Maps in Functional Imaging: A General Linear Approach. Hum Brain Mapp 2:189-210.

Gelnar PA, Krauss BR, et al. (1998). Fingertip representation in the human somatosensory cortex: an fMRI study. Neuroimage 7: 261-283.

Harrington GS and Downs III JH (2001) FMRI mapping of the somatosensory cortex with vibratory stimuli: Is there a dependency on stimulus frequency? Brain Res 897: 188-192.

Jenkinson M and Smith SM (2001) A global optimization method for robust affine registration of brain images. Med Image Anal 5: 143-156.

Johansson RS and Vallbo AB (1979) Tactile sensibility in the human hand: Relative and absolute density of four types of mechanoreceptive units in the glabrous skin. J Physiol (Lond) 286: 283-300.

Jones EG (1998) Viewpoint: The core and matrix of thalamic organization. Neurosci 85: 331-345.

Kelly EF, Trulsson M, and Folger SE. (1997) Periodic microstimulation of single mechanoreceptive afferents produces frequency-following responses in human EEG. J Neurophysiol 77: 137-144.

Knibestol M and Vallbo AB (1970) Single unit analysis of mechanoreceptor activity from the human glabrous skin. Acta Physiol Scand 80: 178-195.

Kochunov P and Uecker A (2003). Talairach Daemon Client. San Antonio, TX, The Research Imaging Center - UTHSCSA.

Loring, DW Meador, KJ Allison JD, Pillai JJ, Lavin T, Lee GP, Balan A, and Dave V (2002) Now you see it, now you don't: statistical and methodological considerations in fMRI. Epilepsy Behav 3: 539-547.

McGlone F, Kelly EF, Trulsson M, Francis ST, Westling G, and Bowtell R (2002). Functional neuroimaging studies of human somatosensory cortex. Behav Brain Res 135: 147-158.

Mountcastle VB, Steinmetz MA, and Romo R (1990) Frequency discrimination in the sense of flutter: psychophysical measurements correlated with postcentral events in behaving monkeys. J Neurosci 10: 3032- 3044.

Mountcastle VB, Talbot WH, Sakata H and Hyvarinen J (1969). Cortical neuronal mechanisms in flutter vibration studied in unanesthetized monkeys. Neuronal periodicity and frequency discrimination. J Neurophysiol 32: 452-484.

Nelson AJ, Staines WR, Graham SJ, and McIlroy WE (2004) Activation in SI and SII: The influence of vibrotactile amplitude during passive and task-relevant stimulation. Cog Brain Res 19:174-184.

Ochoa J and Torebjork E (1983) Sensations evoked by intraneural microstimulation of single mechanoreceptor units innervating the human hand. J Physiol (Lond) 342: 633-654.

Rausell E, Bae CS, Vinuela A, Huntley GW, and Jones EG (1992) Calbindin and parvalbumin cells in monkey VPL thalamic nucleus: Distribution, laminar cortical projections, and relations to spinothalamic terminations. J Neurosci 12: 4088 - 4111.

Rausell E, and Jones EG (1991a) Histochemical and immunocytochemical compartments of the thalamic VPM nucleus in monkeys and their relationship to the representational map. J Neurosci 11: 210-225.

Rausell E, and Jones EG (1991b) Chemically distinct compartments of the thalamic VPM nucleus in monkeys relay principal and spinal trigeminal pathways to different layers of the somatosensory cortex. J Neurosci 11: 226-237.

Sleigh A, Francis S, McGlone F, Kelly E, Gowland P, and Bowtell R (2001) Effect of frequency of vibrotactile stimulation on the brain response measured using fMRI. Proc Intl Soc Mag Reson Med 9: 661.

Smith SM (2002) Fast robust automated brain extraction. Hum Brain Mapp 17: 143-155.

Talairach J, Tournoux P (1988) Co-planar stereotactic atlas of the human brain. New York: Thieme Medical.

Tommerdahl M, Delemos KA, Whitsel BL, Favorov OV, and Metz CB (1999a) Response of anterior parietal cortex to cutaneous flutter versus vibration. J Neurophysiol 82: 16-33.

Tommerdahl, M., Whitsel BL, Favorov OV, and Metz CB (1999b) Responses of contralateral SI and SII in cat to same-site cutaneous flutter vs. vibration. J. Neurophysiol. 82: 1982-1992.

Tommerdahl M, Favorov, OV, and Whitsel BL (2005). Effects of high-frequency skin stimulation on SI cortex: Mechanisms and functional implications. Somatosens Motor Res 22: 151-169.

Trulsson M, Francis ST, Kelly EF, Westling G, Bowtell R, and McGlone F (2001) Cortical responses to single mechanoreceptive afferent microstimulation revealed with fMRI. Neuroimage 13: 613-622.

Vallbo AB and Johansson RS (1984) Properties of Cutaneous mechanoreceptors in the human hand related to touch sensation. Hum Neurobiol 3: 3-14.

Vallbo AB, Olsson KA, Westberg KG, and Clark FJ (1984) Microstimulation of single tactile afferents from the human hand: Sensory attributes related to unit type and properties of receptive fields. Brain 107: 727-749.

Whitsel BL, Kelly EF, Xu M, Tommerdahl M, and Quibrera M (2001) Frequency-dependent response of SI RA-class neurons to vibrotactile stimulation of the receptive field." Somatosens Mot Res 18: 263-285.

Whitsel BL, Kelly EF, Quibrera M, Tommerdahl M, Li Y, Favorov OV, Xu M, and Metz CB (2003) Time-dependence of SI RA neuron response to cutaneous flutter stimulation. Somatosens Mot Res 20: 45-69.

## 3. Nociceptive afferent microstimulation evokes fMRI activation in multiple cortical areas.

### *Background*

Nociception is defined as the physiological response to perceived or actual tissue damage. A noxious stimulus may or may not result in actual perception of pain (Kandel et al 2000). Noxious skin stimuli typically engage multiple types of receptors – these receptors are called nociceptors. The type of pain experienced depends on the nociceptor type being stimulated: myelinated afferents such as A-delta mediate the sharp pricking sensation that is sometimes called "first pain". Unmyelinated afferents such as C-fibers mediate the slower, burning sensation sometimes known as "second pain" (Kandel et al 2000, Ochoa and Torebjork 1989).

Until the advent of noninvasive brain imaging technologies, the cortical role in pain perception remained unclear (Apkarian et al 2005). Early researchers proposed that the brain stem and middle brain were responsible for detection and processing of painful stimuli and that cortical involvement in perception of pain was minimal (Head and Holmes, 1911; Penfield and Boldrey, 1937). However, later studies have confirmed that SI and SII receive noxious cutaneous input from somatosensory thalamus (Kenshalo et al 1980, Rausell and Jones 1991a, b, Shi and Apkarian 1995).

Functional imaging methods such MEG, multi-channel EEG, PET, and fMRI have made it possible to noninvasively record cortical responses to noxious stimuli. Studies conducted using these methods have shown that multiple cortical areas, including

SI and SII, are involved in pain processing (Apkarian et al 2005). In fact, different regions of SI appear to be involved in the processing of noxious and mechanical stimuli. Tommerdahl et al demonstrated that the SI cortical response to mechanical stimulation and thermal stimulation is regionally different (Tommerdahl et al 1996). For example, in Figure 16 below, the SI response to mechanical stimulation is localized more towards the area 3b/ area 1 border whereas the SI response to noxious thermal stimulation is localized more towards the area 3b/ area 3a border.

Mechanical stimulation has been shown to modify the level of perceived pain (i.e. touch gate, Melzack and Wall, 1965). The cortical SI response is also modified when mechanical and thermal stimuli are applied simultaneously. Simultaneous mechanical and thermal stimulation in the form of heated taps resulted in a topographic shift in the evoked cortical response – even though the site of stimulation was the same (Figure 17, Tommerdahl et al 1996).

The SI effects of mechanical and noxious stimuli cannot easily be separated when skin stimuli are used. As in the previous chapter, in this chapter single afferent microstimulation was used to study the cortical responses to noxious stimuli alone by selectively stimulating A-delta and C-fiber afferents. The SI responses to nociceptive afferent and mechanoreceptive afferents microstimulation were compared using fMRI.

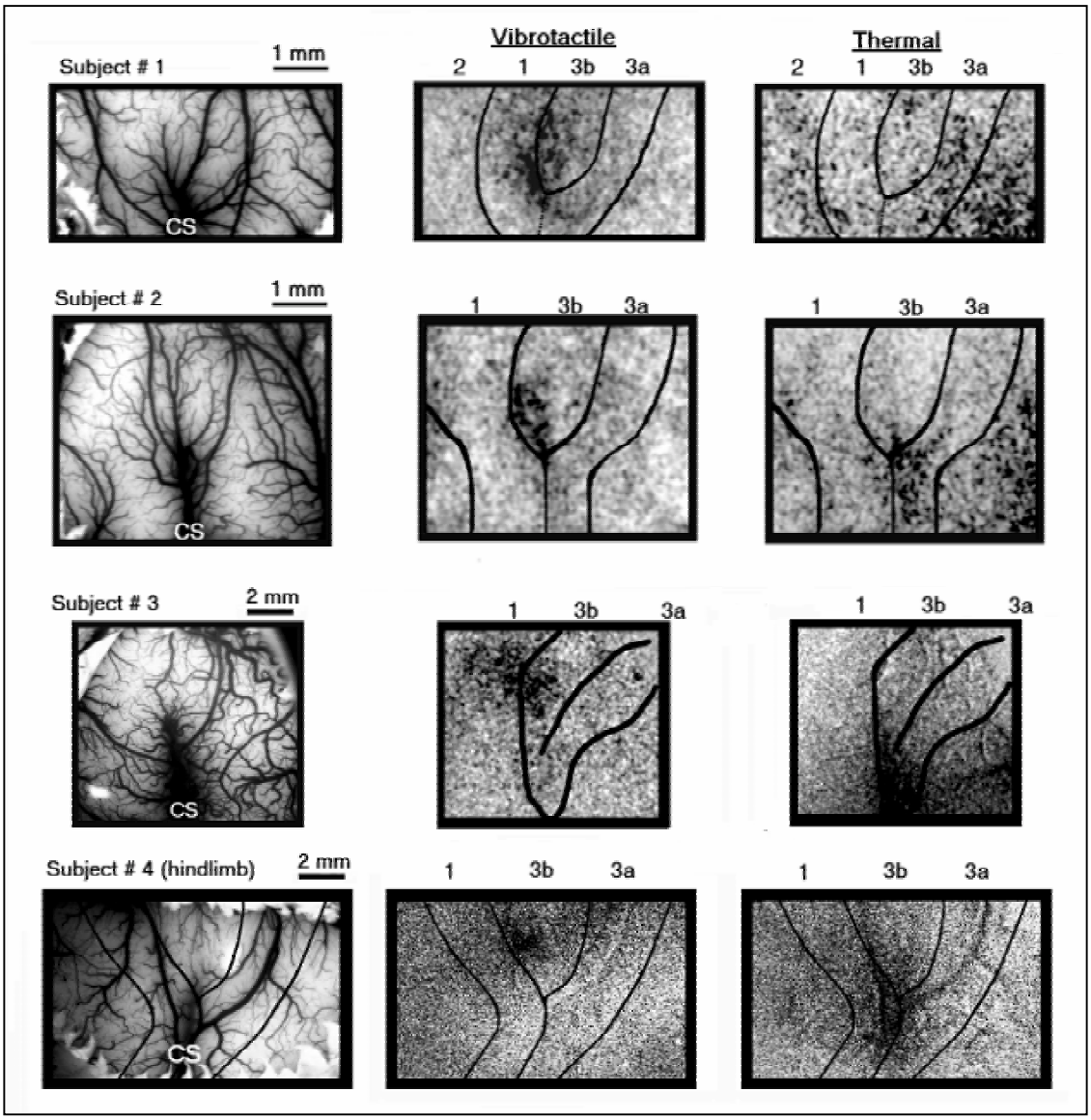


**Figure 16 (modified from Tommerdahl et al 1996): Cortical OIS response to mechanical stimulation (center column) and noxious thermal stimulation (right column) in four subjects. Lines on images: cytoarchitectonic boundaries. Leftmost column: vascular patterns, CS: central sulcus.**

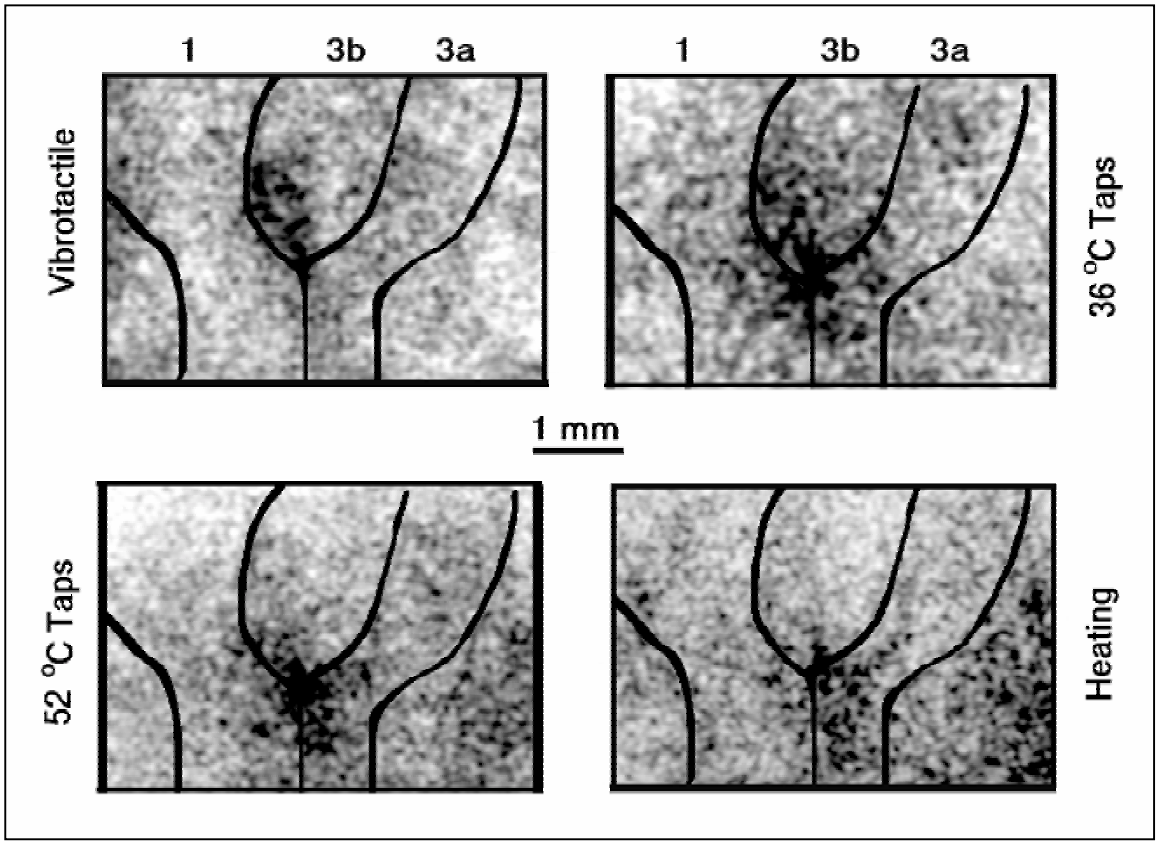


**Figure 17 (modified from Tommerdahl et al, 1996): Anterior parietal OIS responses to different modes of stimulation in the same subject. All stimuli were delivered to the same site on the contralateral interdigital pad. Top left: response to 25Hz vibrotactile stimulation at room temperature. Top right: response to 1.2s skin taps at 36°C. Bottom left: response to 1.2s skin taps at 52°C. Bottom right: response to skin heating ramps applied with probe in stationary contact with the skin.**

***Methods***

Informed consent was obtained from all subjects in compliance with the University of North Carolina's Institutional Review Board. All microneurography and microstimulation equipment was tested to ensure subject safety and minimize interaction with the imaging instrumentation (Trulsson et al., 2001; McGlone et al., 2002). Subjects remained in a supine position on a movable bed; the left or right arm was immobilized (see Figure 6 for a schematic of the experimental setup). A coated tungsten needle microelectrode was inserted into the median nerve 1-2 inches medial to the wrist. The nerve bundle was then impaled and electrode position carefully adjusted until single afferent impulses were detected. Afferents were classified using standard criteria (Knibestol and Vallbo, 1970; Johansson and Vallbo, 1979). Subjects were asked to report the location and extent of the stimulus-evoked sensation and correspondence between the projected RF and the RF of the stimulated afferent was verified (Vallbo and Johansson, 1984). Subjects were also asked to report the perceived quality of the sensation, rate any painful sensation, and to monitor any change in sensation throughout the session.

The electrode was connected to a constant-current stimulator delivering positive square-wave electrical pulses (Vallbo et al., 1984). Stimulus current was adjusted to just above the threshold at which a sensation was evoked to minimize the risk of exciting multiple afferents. The magnitude of the stimulating current never exceeded 10μA. If the location, shape, and size of the projected RF did not match the mapped RF, or if multiple projected RFs were reported, no imaging was carried out and the position of the

microstimulating electrode was shifted to a new location in the nerve.[2] If at any time during a scan the subject no longer felt the stimulus, or if the quality of stimulus or RF changed, the scanning session was ended. Each isolated afferent was checked at the end of scanning to ensure that the size and shape of the RF agreed with the RF of the initially isolated afferent.

Twenty repetitions of 30Hz stimulus were delivered during 2s stimulation and 14s or 18s rest. Subjects were instructed to attend to the stimuli. Echoplanar imaging (Siemens Allegra 3T) was used concurrently with afferent microstimulation to acquire whole brain fMRI images with TR=2s, TE=30ms, Flip angle = 90°. Sixteen contiguous 3mm-thick transverse slices were acquired with an in-plane resolution of 3mm x 3mm. Anatomical localization was achieved for each subject by coregistration of echoplanar image data to high-resolution $0.9mm^3$ isotropic T1-weighted images.

Images were motion-corrected and globally normalized. The images were then spatially smoothed using a Gaussian filter of 5mm full width half maximum. Statistical parametric mapping (SPM; Friston et al 1995) was used to generate activation maps of the hemodynamic response to the stimulus at a statistically significant level of $p<0.001$ (uncorrected). This low *t* threshold was chosen in order to best evaluate the hemodynamic response function in contralateral SI and SII, areas which are *a priori* known to be activated in response to microstimulation (Gelnar et al., 1998; Trulsson et al., 2001; McGlone et al., 2002).

[2] The procedure of isolating, characterizing, and stimulating a single MRA is described in detail in Kelly et al, 1996.

To allow anatomical localization and to aid in identification of activated areas, the echoplanar images were registered to the high-resolution anatomical images for each subject, using Analyze (Mayo Foundation, Rochester, MN), MEDx (Sensor Systems, Inc.), and FSL (Smith, 2002). In the high-resolution anatomical images, SI was defined as the territory bounded anteriorly by the central sulcus, posteriorly by the post-central sulcus, medially by the knob region and laterally by the lateral margin of the post-central gyrus. SII was defined inferiorly by the lateral sulcus, anteriorly by the central sulcus, and medially by insular cortex (Nelson et al., 2004).

To verify localization of activated areas, FSL's FLIRT algorithm (Jenkinson and Smith, 2001; Jenkinson et al., 2002) was used to register each subject's anatomical and EPI images to a standardized template, the MNI brain (Evans et al., 1992), and statistical parametric analysis was repeated for the normalized images. A Matlab script was used to convert the resultant MNI coordinates for each activated cluster to Talairach coordinates (Brett, 1999). An interactive Talairach atlas was used to identify the functional areas corresponding to these locations for each subject (Kochunov and Uecker, 2003).

The time course of pixel intensity values for activated regions of interest was obtained from the statistical maps of the motion-corrected (but not spatially normalized) EPI images using volume-of-interest (VOI) data extraction in SPM with a radius of 0mm. From each cluster, the time-course intensity values for the most highly statistically significant voxel were extracted into a database. The arrays of data values extracted in this manner were averaged over the 20 stimulus cycles and the average response was plotted against time.

***Results***:

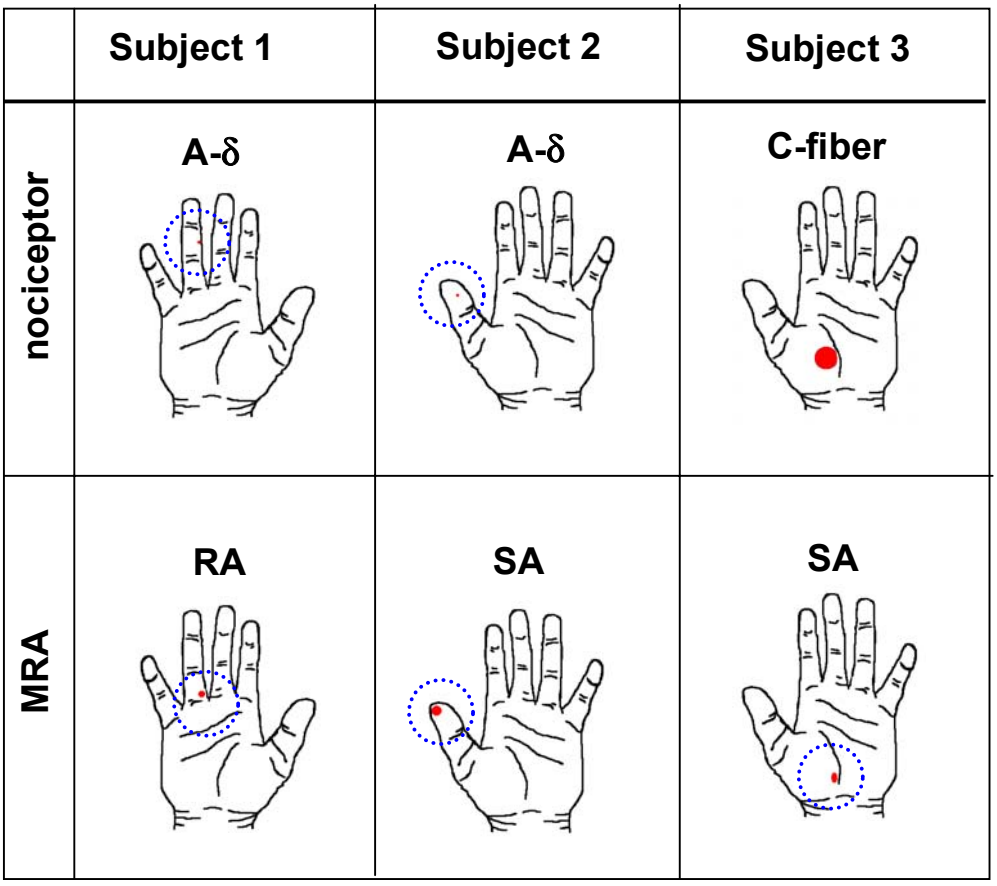


**Figure 18: Receptive field locations of 3 nociceptive afferents (top row) and 3 MRAs (bottom row) with adjacent RFs. Red filled circles indicate location and size of RFs, blue dotted circles clarify the location in the case of afferents with small RFs.**

Three nociceptive afferents, two A-delta and 1 C-fiber small bundle, were successfully isolated and microstimulated during concurrent fMRI imaging. Figure 18 shows the mapped RF locations for the three nociceptive afferents and for three MRAs with RFs adjacent to each of the nociceptive afferents. Table 5 summarizes the sensations evoked by microstimulation of the nociceptive afferents. Sensations evoked

by microstimulation of the three MRAs whose RFs are shown in Figure 18 are also tabulated for comparison.

The RFs of the two A-delta afferents occupied a small circular point about 1mm in diameter (See subjects 1 and 2, Figure 18 and Table 5). The RF of the A-delta afferent isolated on Subject 1 was located on the second joint of digit 4. This subject described the sensation evoked by microstimulation of the A-delta afferent at 30Hz as "a short bee sting or a very localized pinprick", and assigned the pain a rating of 4 on a scale of 1-10, with 1 being no pain and 10 the worst pain imaginable. The RF of the A-delta afferent isolated on Subject 2 was located on the left thumb tip. Subject 2 described the sensation evoked by microstimulation as "a sharp needle prick similar to an actual pinprick" and rated the pain as 3-4 on a scale of 1-10.

The RF of the C-fiber small bundle occupied a 10mm-diameter circle located at the base of the left palm (Figure 18 and Table 5, Subject 3). No spiking activity could be detected in the afferent when the RF was stimulated by brushing or touch stimuli – forceful scratching on the skin was required to elicit a spike response in the afferent. Subject 3 noted that the sensation "felt like sharp pinpricks at positive polarity current, and was a single burning sensation throughout the entire RF at the negative polarity current." Both pain sensations were rated 4-5 on a scale of 1-10. FMRI imaging was conducted using positive current pulses; the negative current was used for confirmation of the afferent type, following the protocol used by Ochoa and Torebjork (Ochoa and Torebjork 1989).

Multiple cortical areas of fMRI activation were observed in response to microstimulation of all three nociceptive afferents. Table 6 lists the cortical areas in

which significant fMRI activation was evoked in response to microstimulation of each nociceptive afferent, along with corresponding Talairach coordinates. No areas of activation were found that were unique to the microstimulation of nociceptive afferents. Microstimulation of both A-delta afferents evoked significant ($p<0.001$ uncorrected) areas of fMRI activations in areas SI and SII contralateral to the site of stimulation. Other areas of activation that were observed in response to microstimulation of A-delta afferents included ipsilateral SII, SMA, and insular cortex. Areas of activation not normally associated with pain processing including frontal cortex and Brodmann Areas 44 and 45 (Broca's area) were also observed; these are likely to reflect the subject paying attention to the stimulus. Figure 19 shows fMRI areas of activation evoked by microstimulation of the A-delta and SA afferents that were isolated on Subject 2. The areas of fMRI activation evoked by microstimulation of the A-delta are adjacent to or overlap with fMRI areas of activation evoked by microstimulation of the SA afferent.

Microstimulation of the C-fiber evoked significant areas of fMRI activation ($p<0.001$ uncorrected) bilaterally in SI and SII. Other significant areas of activation were observed in the insula, posterior parietal, frontal cortex, and supplementary motor area. Figure 20 shows fMRI areas of activation evoked by microstimulation of the C-fiber and SA afferents that were isolated on Subject 3. As in the case of Subjects 1 (not shown) and 2, the areas of fMRI activation evoked by microstimulation of the C-fiber and of the SA afferent overlap, especially in SII.

| Afferent | RF location | FAS Rating* | Subject's description | Microneurography observations |
|---|---|---|---|---|
| A-delta (Subject 1) | D4 – second phalanx | 4 | Like a very short bee sting or localized pinprick. | Could hear small spikes when RF was stimulated with von Frey hair; RF was a pinpoint. |
| Control RA1 | D4 base | N/A | "flutter" | N/A |
| A-delta (Subject 2) | Thumb tip | 3 to 4 | Like a sharp needle on skin, but not penetrating the skin. Was similar to a needle prick in only one spot. | RF was a pinpoint. |
| Control SA1 | Thumb tip | N/A | Slow indentation, constant amplitude | N/A |
| C-fiber (Subject 3) | Base of palm | 4 to 5 for both polarities | Sharp pinpricks at positive polarity, single burning pain over the RF at negative polarity+. | Needed forceful scratching on skin to evoke spike activity. Did not respond with 1.6g von Frey hair. |
| Control SA1 | Base of palm | N/A | Felt like flutter, not painful. | N/A |

**Table 5: Descriptions of sensations evoked by microstimulation of nociceptive afferents and MRAs with adjacent or overlapping receptive fields in the same subject.**

* On a scale of 1-10, with 1 being no pain and 10 being the most painful

+ fMRI imaging was performed concurrent with microstimulation using 7.5μA positive polarity pulses.

| Subject / Regions | Subject 1<br>A-delta<br>30 Hz<br>(right hand) | Subject 2<br>A-delta<br>30Hz<br>(left hand) | Subject 3<br>C-fiber<br>30Hz<br>(left hand) |
|---|---|---|---|
| Contralateral SI<br>(B.A. 1, 2, 3) | 3.69<br>(53 -16 50) | n.s. | 5.92<br>(65 -20 35) |
| Contralateral SII<br>(B.A. 40) | 4.94<br>(53 23 –16) | n.s. | 5.26<br>(63 –29 24) |
| Ipsilateral SII<br>(B.A. 40) | n.s. | 3.03<br>(62 30 24) | 4.00<br>(-51 –26 20) |
| SMA<br>B.A. 6) | 3.39<br>(-25 2 60) | n.s. | 3.75<br>(-20 4 58) |
| Motor Cortex<br>(B.A. 4) | 4.23<br>(33 -15 50) | 3.94<br>(62 –9 28) | n.s. |
| Cingulate<br>(B.A. 24) | n.s. | *3.19*<br>(-4 4 40) | n.s. |
| Insular cortex<br>(B.A. 13) | 3.60<br>(33 17 12) | 4.31<br>(37 –8 20) | 3.80<br>(-35 -8 20) |
| Posterior Parietal<br>(B.A. 5,7) | n.s. | 3.45<br>(43, -64 45; ipsi) | 3.97<br>(35 -49 55; contra)<br>3.98<br>(-40 -50 55; ipsi) |
| Frontal<br>(B.A. 8, 9, 10) | 3.74<br>(37 42 32) | 4.86<br>(48 12 40) | 4.11 (34 58 16)<br>3.98 (57, 4, 24) |
| Other activated cortical areas | **B.A. 45**: 3.46<br>(57 27 16) | **B.A. 44:** 3.35<br>(-58 9 20) | **B.A. 44**: 4.06 (48 18 24) |

**Table 6: Peak *t*-values of areas of activation in response to microstimulation of nociceptive afferents, with corresponding stereotaxic coordinates. $t \geq 3.33$ represents significant activity in a global search corresponding to $p<0.001$. $t \geq 2.67$ corresponds to $p<0.005$ and is indicated in italics. B.A., Brodmann Area; n.s., non-significant; contra, contralateral; ipsi, ipsilateral to the stimulated arm.**

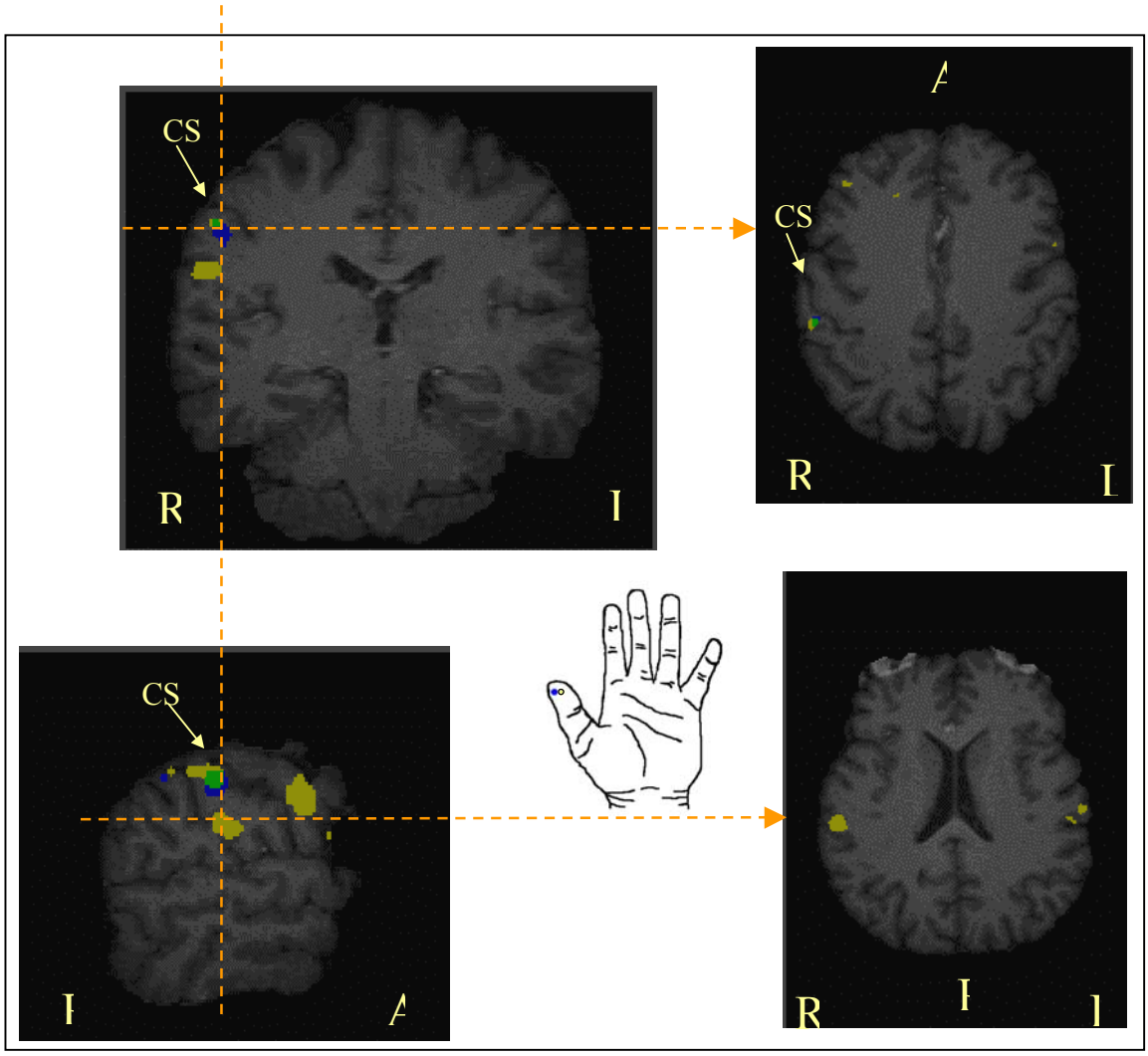


**Figure 19: fMRI areas of activation evoked by microstimulation of an A-delta afferent (yellow), and an RA1 afferent with an adjacent RF (in blue). Activation thresholded at at p<0.001 uncorrected. Inset drawing of hand indicates RF locations of the afferents that were microstimulated. A=anterior, P=posterior, R= right, L=left, CS=central sulcus.**

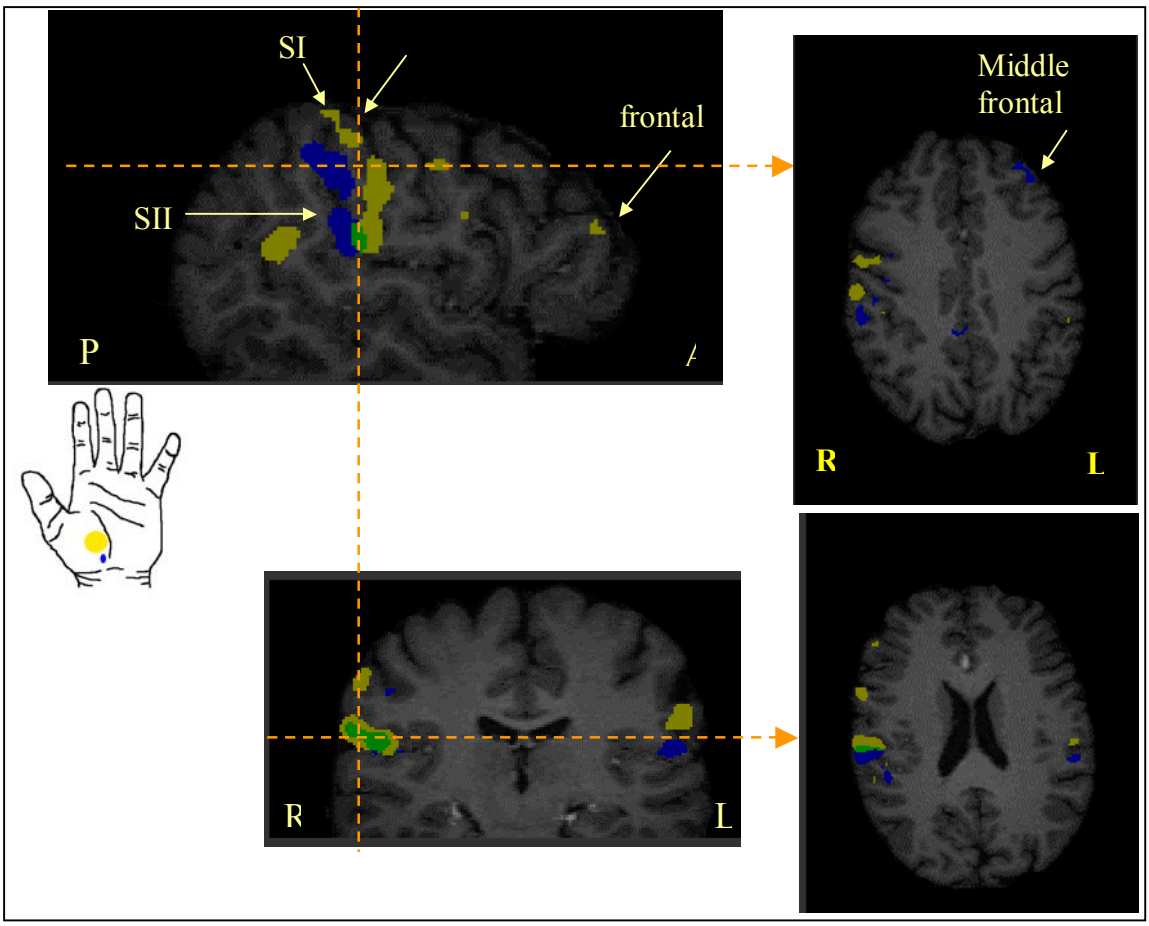


**Figure 20: fMRI areas of activation evoked by microstimulation of a C-fiber small bundle (yellow), and an SA1 afferent with an adjacent RF (blue). Activation thresholded at p<0.001 uncorrected. Inset drawing of hand indicates RF locations of the afferents that were microstimulated. A=anterior, P=posterior, R= right, L=left, CS=central sulcus.**

The time course of the most significantly activated pixel in SI and SII was averaged for all twenty stimulus cycles in the manner described in Chapter 2. The resultant average hemodynamic response is shown in Figure 21 for the two A-delta afferents, and in Figure 22 for the C-fiber small bundle. In all cases, hemodynamic response reached a peak about 4-6 seconds after stimulus onset, and declined rapidly to near-baseline levels when the stimulus was turned off. Time courses for the most significantly activated pixels in other cortical areas followed similar time courses as those in SI and SII.

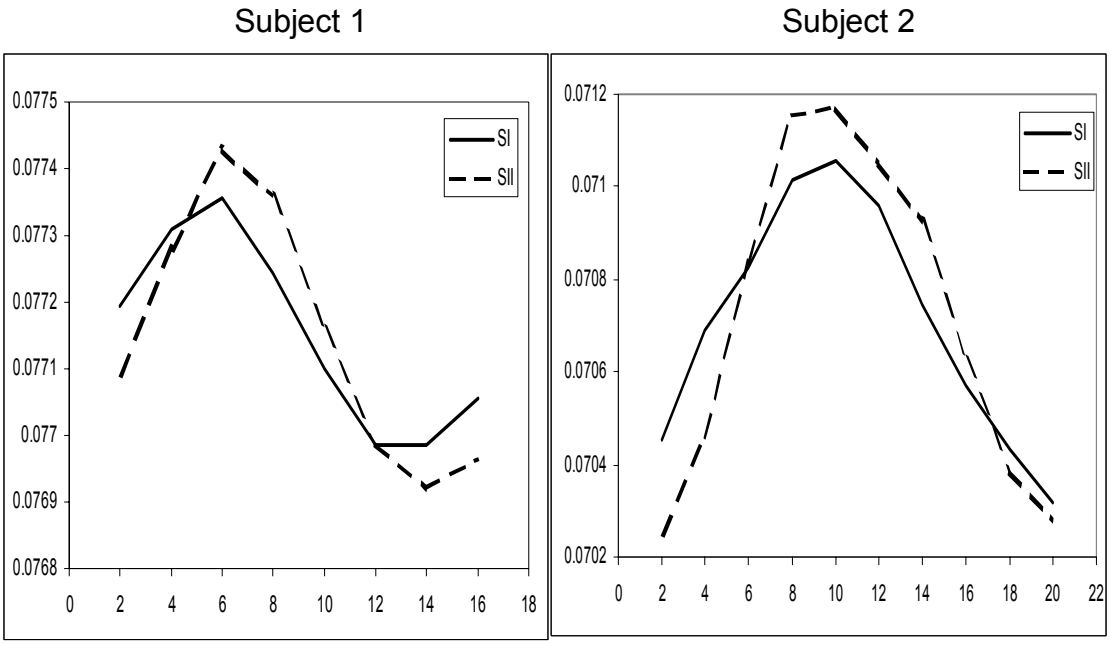


**Figure 21: Hemodynamic responses in SI (solid line) and SII (dashed line) evoked by microstimulation of two A-delta afferents. Responses are averaged over 20 stimulus cycles. X-axis = time (seconds); Y-axis = pixel intensity.**

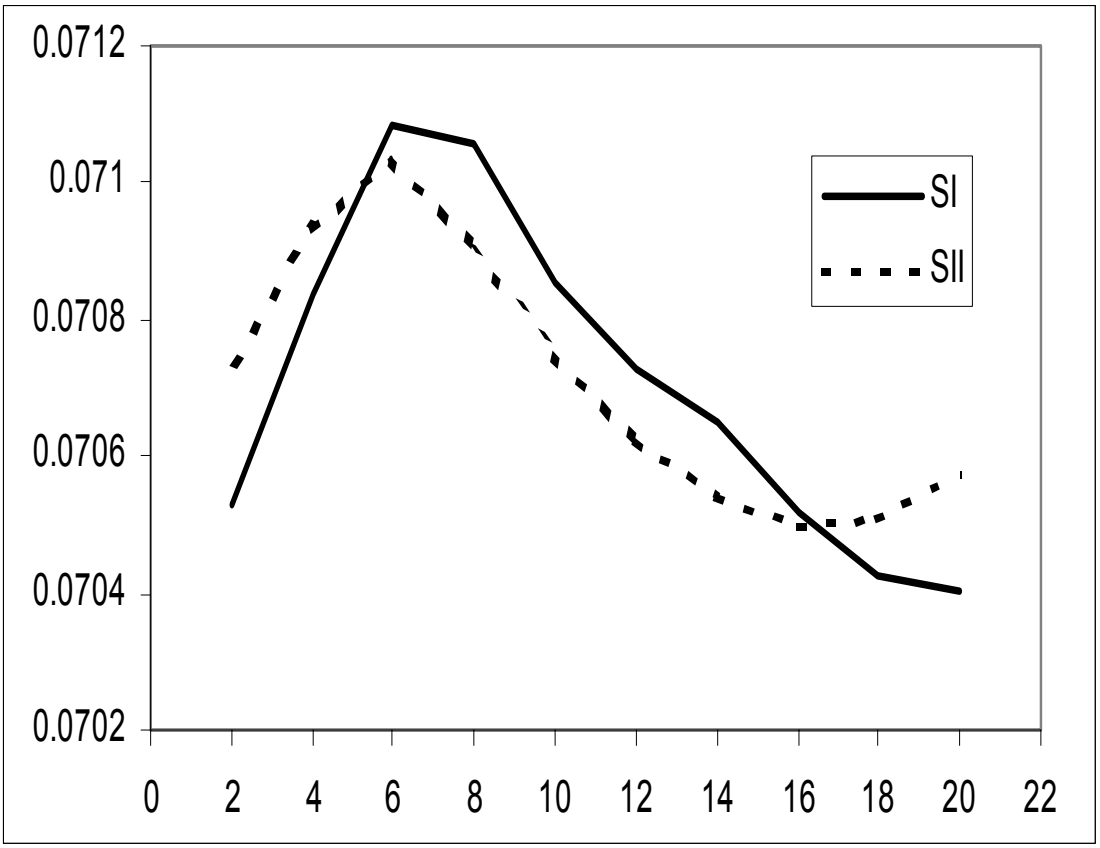


**Figure 22: Hemodynamic responses in SI (solid line) and SII (dashed line) evoked by microstimulation of a C-fiber small bundle. Responses are averaged over 20 stimulus cycles. X-axis = time (seconds); Y-axis = pixel intensity.**

***Discussion***

Although only three nociceptive afferents were microstimulated in this study, this is the first time that fMRI of the responses to microstimulation have been successfully imaged and documented. In all three cases, the characteristics of the microstimulated nociceptive afferents such as RF field size/ shape, spiking characteristics, and sensations evoked by microstimulation were in agreement with the criteria established by Ochoa et al (1989). Subjects' perceived sensations were also in agreement with previous studies of the responses to microstimulation of nociceptive afferents (Ochoa et al 1989).

The results of this study confirm that multiple cortical areas are involved in the processing of painful stimuli. Microstimulation of nociceptive afferents evoked statistically significant hemodynamic responses in cortical areas known to be involved in the sensory aspect of the processing of painful stimuli, specifically SI, SII, supplementary motor area, posterior parietal and insula (see Apkarian et al 2005 for review). Significant fMRI activation was also observed in Brodmann areas 44 and 45 and in frontal cortex but this is probably due to suppression of movement and/ or attentional effects. The field of view of our fMRI images did not include thalamus and cerebellum, two areas known to be activated in response to noxious stimuli (Apkarian et al 2005).

The ACC is thought by many researchers to play an integral role in the perception of painful stimuli. Several fMRI and PET studies have documented significant ACC activation in response to noxious stimulation (See Apkarian et al, 2005 for review). In this study, a statistically significant fMRI response was not detected in the ACC of any of the three subjects for whom nociceptive afferents were microstimulated. The most probable explanation for the lack of observed ACC response is that microstimulation of a

single or small bundle nociceptive afferents did not produce a stimulus that was strong enough to evoke an fMRI response in the ACC. Noxious skin stimuli tend to recruit multiple nociceptive afferents, and the resultant spatial summation causes a stronger painful sensation than that caused by microstimulation. This suggestion is supported by the findings of Apkarian et al (2000), who found that the cortical responses to painful stimuli were larger in spatial extent when stimulus conditions favored activation of larger numbers of nociceptive afferents. In addition, the stimulus in our study was only applied for brief periods of time; no "wind-up" protocol was used that would produce temporal summation of the signal.

The hemodynamic responses to microstimulation of nociceptive and mechanoreceptive afferents were similar, exhibiting a single peak and returning to baseline when the stimulus was turned off. Chen et al observed a two-peak hemodynamic response in SI when a noxious heat stimulus was applied to the skin (Chen et al 2002). The discrepancy in the results of the two studies can be attributed either to differences in the stimulus protocol or due to the fact that stimulation of only one afferent does not recruit the additional mechanisms necessary for modulation of pain perception. Further studies are needed with a larger sample size and a stimulus protocol similar to that used by Chen et al. A stimulus protocol with a longer off time and interstimulus interval will allow time for the hemodynamic response to recover to baseline. Under those stimulus circumstances, the question of whether the "two peak" hemodynamic response is a result of nociceptive afferent input or of other cortical mechanisms can be determined.

### *Conclusions*

FMR imaging of the responses to single afferent microstimulation confirms that areas traditionally labeled as somatosensory areas, namely SI and SII cortices, are in fact activated in response to a pure noxious stimuli, corresponding to the ability to precisely localize the RFs of the afferents being microstimulated. Time courses of the somatosensory cortical hemodynamic responses to microstimulation of nociceptive afferents did not differ significantly from the responses to microstimulation of MRAs.

***References***

Apkarian AV, Bushnell MC, Treede R-D, and Zubieta J-K (2005) Human brain mechanisms of pain perception and regulation in health and disease. Pain 9: 463-484.

Apkarian AV, Gelnar PA, Krauss BR, and Szeverenyi NM (2000) Cortical responses to thermal pain depend on stimulus size: a functional MRI study. J Neurophysiol 83: 3113- 3122.

Brett M (1999) The MNI brain and the Talairach atlas. Cambridge, MA: Cambridge Imagers.

Chen J-I, Ha B, Bushnell MC, Pike B, and Duncan GH (2002) Differentiating noxious- and innocuous-related activation of human somatosensory cortices using temporal analysis of fMRI. J Neurophysiol 88: 464-474.

Evans AC, Collins DL, Milner B (1992) An MRI-based stereotactic atlas from 250 young normal subjects. Soc Neurosci Abstr, Anaheim.

Friston KJ, Holmes AP, Worsley KJ, Poline JB, Frith C, and Frackowiak RSJ (1995) Statistical Parametric Maps in Functional Imaging: A General Linear Approach. Hum Brain Mapp 2:189-210.

Head H and Holmes G (1911) Sensory disturbances from cerebral lesions Brain 34: 102-254.

Jenkinson M, Bannister PR, Brady M, and Smith S (2002) Improved optimisation for the robust and accurate linear registration and motion correction of brain images. Neuroimage 17: 825-841.

Jenkinson M and Smith SM (2001) A global optimization method for robust affine registration of brain images. Med Image Anal 5: 143-156.

Johansson, R. S. and Vallbo, A. B. (1979) Tactile sensibility in the human hand: Relative and absolute density of four types of mechanoreceptive units in the glabrous skin. J Physiol (Lond) 286: 283-300.

Kandel ER, Schwartz JH, and Jessell TM (2000) Principles of Neural Sciences, Fourth Edition. New York, NY: McGraw-Hill.

Kochunov P and Uecker A (2003) Talairach Daemon Client. San Antonio, TX, The Research Imaging Center - UTHSCSA.

McGlone F, Kelly EF, Trulsson M, Francis ST, Westling G, and Bowtell R (2002). Functional neuroimaging studies of human somatosensory cortex. Behav Brain Res 135: 147-158.

Melzack R and Wall PD (1965) Pain mechanisms: a new theory. Science 150: 971-979.

Nelson AJ, Staines WR, Graham SJ, and McIlroy WE (2004) Activation in SI and SII: The influence of vibrotactile amplitude during passive and task-relevant stimulation. Cog Brain Res 19:174-184.

Ochoa JL and Torebjork HE (1989) Sensations evoked by intraneural microstimulation of C-nociceptor fibres in human skin nerves. J Physiol 415: 583-599.

Penfield W and Boldrey E (1937) Somatic motor and sensory representation in the cerebral cortex of man as studied by electrical stimulation. Brain 60:389–443.

Kenshalo Jr DR, Giesler Jr GR, Leonard RB, and Willis WD (1980) Responses of neurons in primate ventral posterior lateral nucleus to noxious stimuli. J Neurophysiol 43: 1594-1614.

Knibestol M and Vallbo AB (1970) Single unit analysis of mechanoreceptor activity from the human glabrous skin. Acta Physiol Scand 80: 178-195.

Kochunov P and Uecker A (2003). Talairach Daemon Client. San Antonio, TX, The Research Imaging Center - UTHSCSA.

Rausell E, Jones EG (1991a) Histochemical and immunocytochemical compartments of the thalamic VPM nucleus in monkeys and their relationship to the representational map. J Neurosci 11: 210-225.

Rausell E, Jones EG (1991b) Chemically distinct compartments of the thalamic VPM nucleus in monkeys relay principal and spinal trigeminal pathways to different layers of the somatosensory cortex. J Neurosci 11: 226-237.

Shi T, Apkarian AV (1995) Morphology of thalamocortical neurons projecting to the primary somatosensory cortex and their relationship to spinothalamic terminals in the squirrel monkey J Comp Neurol 361: 1-24.

Smith SM (2002) Fast robust automated brain extraction. Hum Brain Mapp 17: 143-155.

Tommerdahl M, Delemos KA, Vierck CJ, Favorov OV, and Whitsel BL (1996) Anterior parietal cortical response to tactile and skin-heating stimuli applied to the same site. J Neurophysiol 75: 2662 - 2669.

Trulsson M, Francis ST, Kelly EF, Westling G, Bowtell R, and McGlone F (2001) Cortical responses to single mechanoreceptive afferent microstimulation revealed with fMRI. Neuroimage 13: 613-622.

Vallbo AB and Johansson RS (1984) Properties of Cutaneous mechanoreceptors in the human hand related to touch sensation. Hum Neurobiol 3: 3-14.

Vallbo AB, Olsson KA, Westberg KG, and Clark FJ (1984) Microstimulation of single tactile afferents from the human hand: Sensory attributes related to unit type and properties of receptive fields. Brain 107: 727-749.

## 4. An MRI-compatible vibrotactile stimulator

### *Introduction*

In order to expand current understanding of cortical somatosensory information processing available from animal (Mountcastle et al 1969, Nelson et al 2004, Tommerdahl et al 1999a, b, 2005, Whitsel et al 2001, 2003), human psychophysical (Goble and Hollins 1993; Goble and Hollins 1994) and human functional neuroimaging studies (Francis et al 2000, Kelly et al 1999, Logothetis et al 2000), an fMRI-compatible vibrotactile stimulator is needed that is stable, has good dynamic range, and has little detectable electrical noise. In addition, the stimulator used must be capable of delivering a precise, controlled, and stable stimulus. The stimulator should be capable of delivering triggered stimuli matching the timing of boxcar-design and single-trial experimental methods used in fMRI studies (Lin et al 1996, Sakai et al 1995).

Most existing human and animal studies of somatosensory information processing have used electromagnetic, servo-controlled devices, similar to those first introduced by Chubbuck (Chubbuck, 1970), to deliver a pure sinusoidal stimulus of adjustable amplitude and frequency. However, these electromechanical devices are not compatible with the high static magnetic fields that are present in MR environments. Additionally, the amount of displacement delivered to the subject's skin must be readily and precisely measurable. This measurement has been done in previous studies using a linear variable displacement transducer (DT); however, linear variable DTs are essentially electromagnetic devices with iron cores and thus unsuitable for use in MR environments.

To address the generation and delivery of a well-controlled, pure sinusoidal stimulus to the skin, we used a piezoelectric bender element connected to a plastic probe. The displacement of the skin was measured using an optical DT, which does not experience intereference from nor interfere with magnetic fields. The bender and DT are contained in a non-magnetic metal casing (the "bender box"), and the power and processing electronics contained in a separate metal enclosure (the "amplifier box"), which is connected to the bender box by a shielded cable. The stimulator has been successfully used in several fMRI experiments to explore human cortical responses to vibrotactile stimulation (Francis et al, 2000; McGlone et al 2002).

***Methods***

The stimulator is physically contained in two separate boxes, connected by a 15m long shielded cable wire. Figure 23 shows the overall schematic of the amplifier box and bender box.

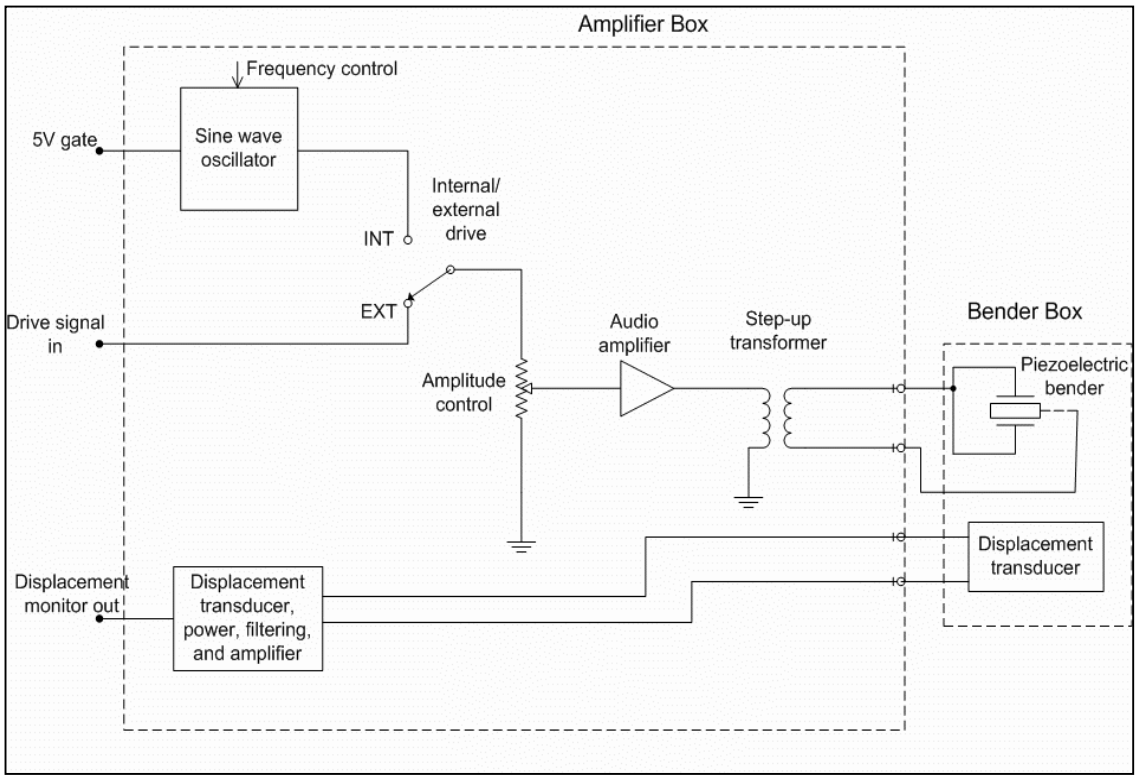


**Figure 23: Overall block diagram of the vibrotactile stimulator. The stimulator is physically contained in two boxes, the amplifier box and the bender box.**

The bender box contains the piezoelectric bender (T223-H4CL-503Y Composite Shim Bending Element, Piezo Systems, Inc., Cambridge MA) and optical DT, mounted in an aluminum enclosure. The amplifier box contains the signal generation and amplifier electronics. Within the amplifier box is a sine wave oscillator with an external

frequency control. The drive signal for the bender can be derived either from this internal sine wave oscillator or from an external drive signal, selectable by a simple internal/external switch. Amplitude of the internal or external signal may be controlled manually. An integrated circuit audio amplifier and a step-up transformer amplify the signal and deliver it to the bender.

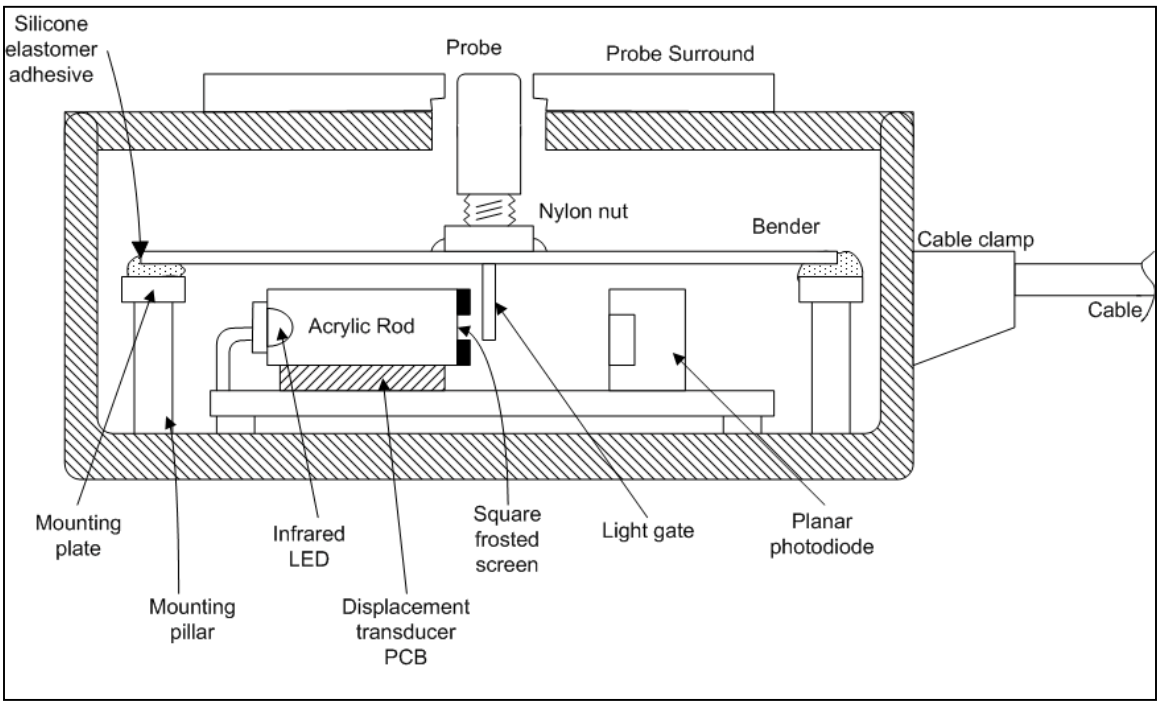


**Figure 24: Details of the bender box construction. The piezoelectric bender crystal is attached to a plastic probe. Motion of the probe causes modulation of the light signal, which is then measured by the photodiode.**

The construction of the bender box is shown in Figure 24. The piezoelectric bender is mounted on both ends to fiberglass plates, using a silicone elastomer adhesive. A beam mounting configuration is used to provide greater force to the bender elements, with a tradeoff of less displacement compared to a cantilever mounting. This particular

bender part has a composite conductive shim in its center and is used parallel poled to lessen the drive voltage necessary for a given force. A stiff plastic probe is attached to the center of the bender using a nylon nut, and this probe then moves with the bender. The probe surround helps limit the area of tactile stimulation to that region directly in contact with the probe (Bolanowski et al 1988). A light gate, or shutter mechanism, is attached to the center of the bender, directly opposite the probe (Figure 24). Thus, when the probe is in contact with the skin, the movement of the light gate corresponds to the skin displacement experienced by the subject.

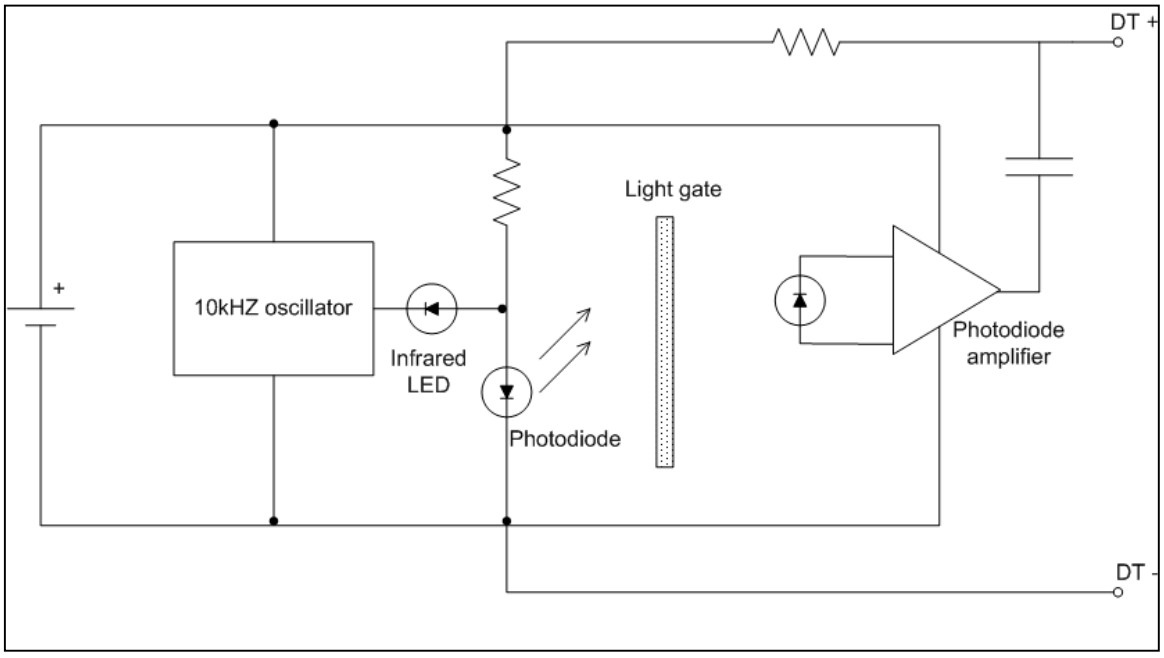


**Figure 25a: Circuit diagram of the displacement transducer shown schematically in Figure 24. Optical DT schematic.The displacement transducer consists of an infrared LED and a photodiode which emit light onto the light gate. Movement of the bender (shown in Figure 24) causes modulation of the light signal. The signal is**

**recorded by the photodiode amplifier, and fed to the positive and negative displacement transducer terminals, DT + and DT -.**

The optical DT schematic is shown in greater detail in Figure 25a. The infrared light-emitting diode (LED) is switched at 10kHz by a square wave signal from a CMOS (complementary metal-oxide semiconductor) oscillator. The modulated infrared light emitted by the LED causes pulses of current to flow in the planar photodiode. The LED, light gate, and photodiode are arranged in such a way that when the light gate is displaced, the degree of optical coupling between the LED and photodiode varies in a manner approximately linearly proportional to the displacement of the light gate. The change in the optical coupling in turn leads to a change in the amplitude of the photodiode current signal. The photodiode amplifier converts the current signal to a voltage signal. The voltage signal is capacitatively coupled to the positive supply terminal of the transducer circuit, DT+. Because the power supply to the transducer is a high-impedance current source rather than a voltage source, the 10kHz displacement signal appears as a differential signal superimposed upon the DC voltage across supply terminals DT+ and DT-.

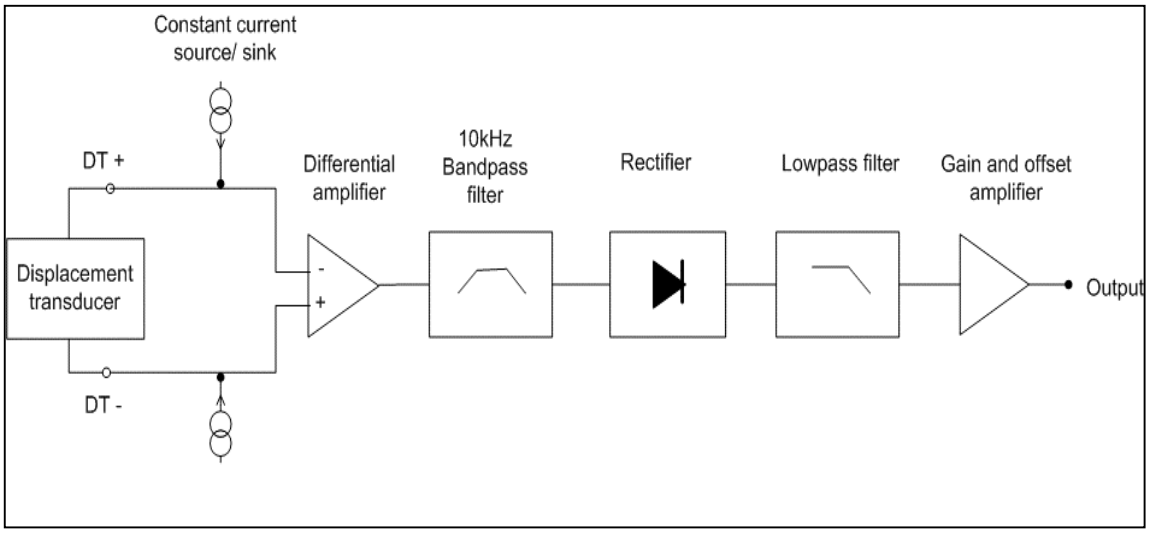


**Figure 25b: Displacement transducer power and processing electronics. The displacement signal is fed through a differential amplifier, and the difference signal is then filtered and rectified, and finally amplified again to produce the output displacement signal.**

The DT power and processing electronics referred to in Figure 24 are shown in greater detail in Figure 25b. A complementary current source and sink supply the 20mA current to power the transducer. This symmetrical arrangement reduces the circuit's susceptibility to electrical noise picked up by the cable. An AC-coupled differential amplifier extracts the AC displacement signal and converts it to a single-ended voltage signal. This signal is fed into a bandpass filter, which passes the 10kHz signal while filtering out high- and low-frequency noise. The mean amplitude of the signal is then obtained by full-wave rectification and lowpass filtering. The last amplifier stage consists of a DC-coupled amplifier with DC offset and gain, both of which are adjustable

by preset potentiometers. This amplifier removes the DC offset from the signal and sets the gain of the transducer to some convenient and known value (typically 10mV/μm). The output from this amplifier is a voltage signal which varies linearly with the position of the probe.

***Results***

The stimulator has been in operation for more than six years without showing any degradation in performance. During initial testing, some radiofrequency (RF) noise was experienced, probably due to mains-borne noise being carried along the bender cable. This RF noise was eliminated by placing a simple ferrite core filter on the cable. The DT has proven to be stable and has shown no measurable drift in mV/μm ratio over a 12-month period. The DT has a good dynamic range, with the ratios of input to output signals remaining constant in a range of frequencies from 3Hz to 250Hz. Figure 26 shows the input/output curves for the DT at several sample frequencies, demonstrating that the ratio of input/ output signals is not diminished with higher stimulus frequencies.

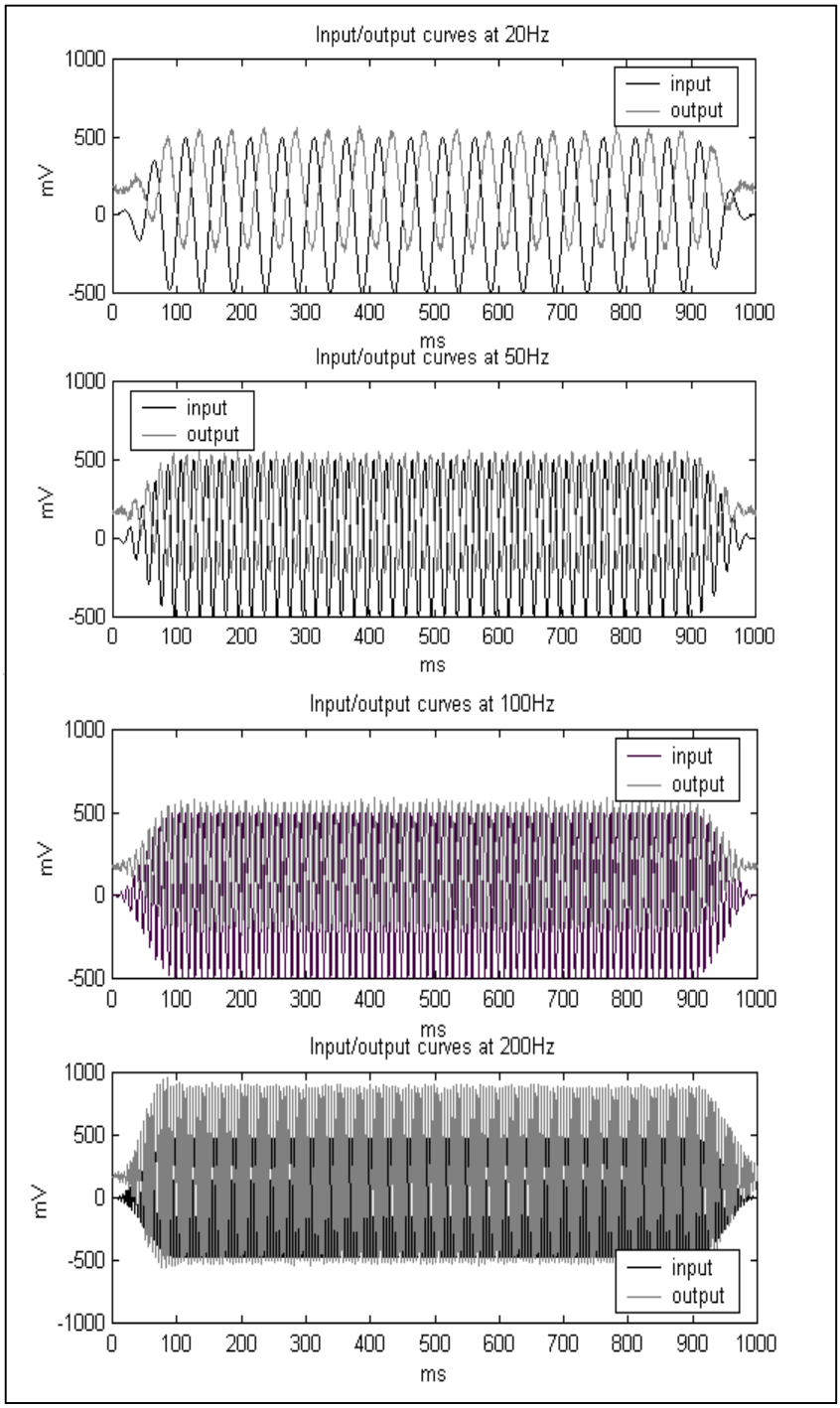


**Figure 26: Input/Output curves for the displacement transducer signal at 20, 50, 100 and 200 Hz. The input/output amplitude ratio remains the same over the range of frequencies tested. The output signal has a DC offset of ~100mV.**

The vibrotactile stimulator system has successfully been tested in two different MR scanners, and in both cases the resultant images were noise- and artifact-free. The average percentage difference between the phantom MRI signal-to-noise ratio (SNR) with the bender on and off is 0.402 +/- 0.001 %, demonstrating that the presence of the bender did not cause a significant change in MR image quality. The difference map of the SNR, scaled to 100%, is shown in Figure 27, and shows no spatial patterns indicating interference. The values in each pixel were calculated by the formula $((SNR_{ON} - SNR_{OFF})/SNR_{ON})$ X 100%. The image in Figure 27 was acquired using a spherical phantom with the bender placed about 1m from the head coil, approximately where a patient's hand would rest.

The random pattern of Figure 27 indicates that no interference or distortion is present in the MR image. The stimulator has proven consistently reliable in providing a noise-free sinusoidal stimulus, and has been used in several fMRI studies mapping cortical representation of the digits of the human hand (Francis et al, 2000; McGlone et al, 2002). The bender was used to apply a 30Hz flutter stimulus to a subject's right index fingertip. The stimulus was applied for 20s, with an interstimulus interval of 60s. Significant fMRI activation can be observed in the subject's left SI cortex and right SII cortex (see Figures 28a and b).

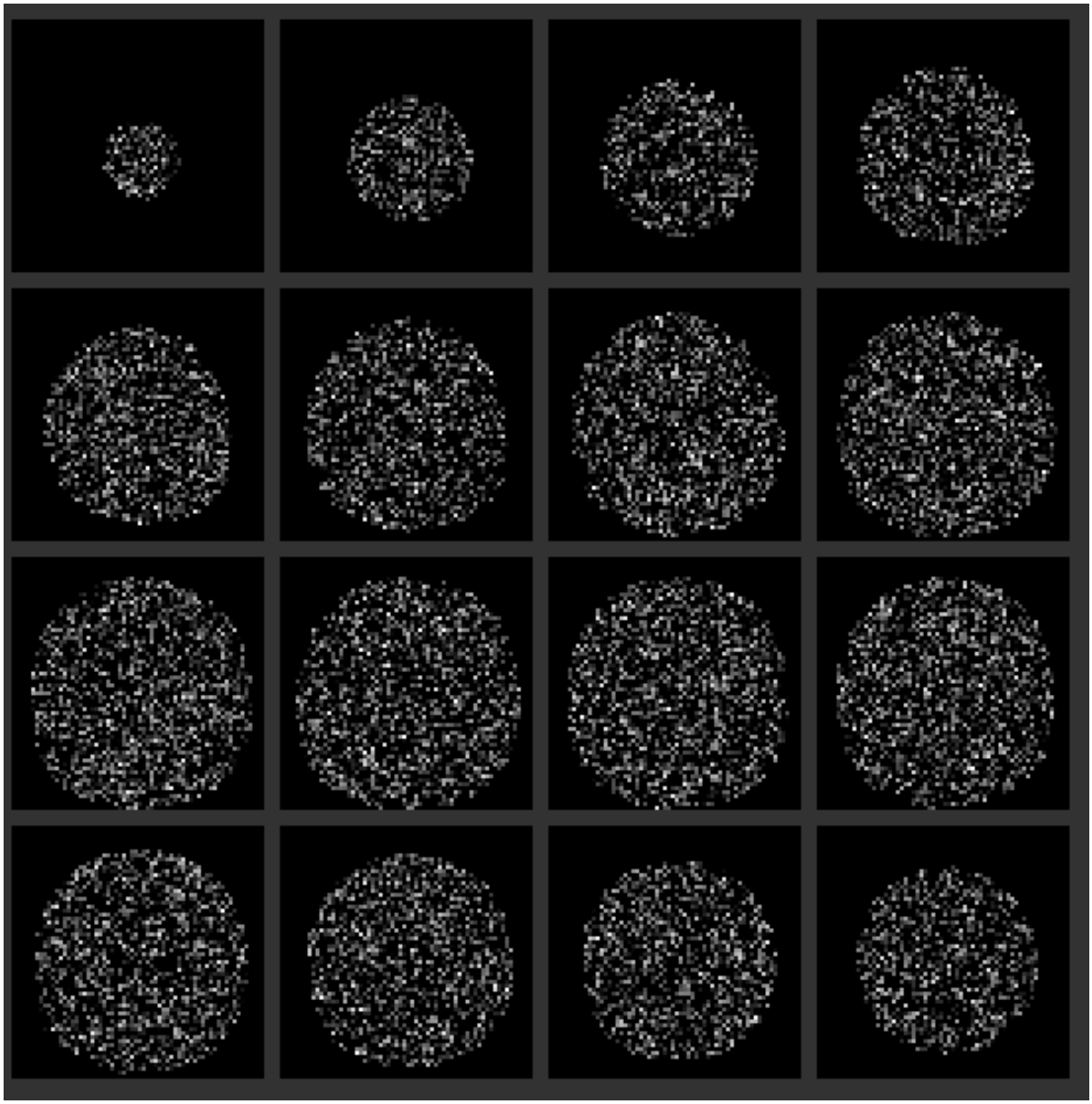

**Figure 27: Difference map of MRI signal to noise ratio with bender on and off. The average percentage difference in MRI signal to noise ratio with the bender on and off is 0.402 +/- 0.001%. The difference map shows no spatial patterns, indicating that no interference is present from the bender.**

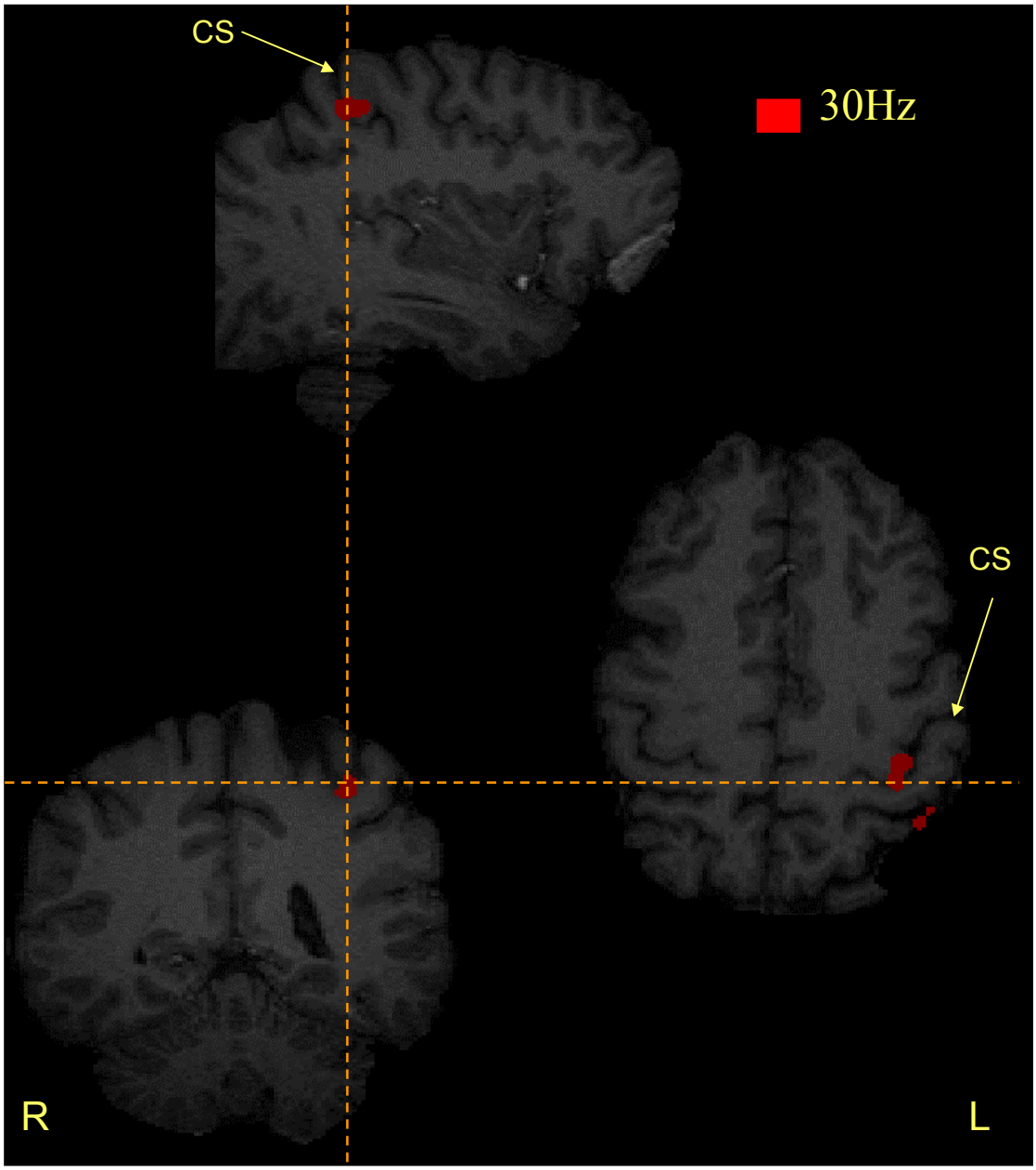


**Figure 28a: FMRI activation in SI and posterior parietal cortices contralateral to the site of a 30Hz stimulus applied on the right index fingertip of a subject. Right: coronal slice, left: transverse slice. Crosshairs show slicing plane. CS: central sulcus.**

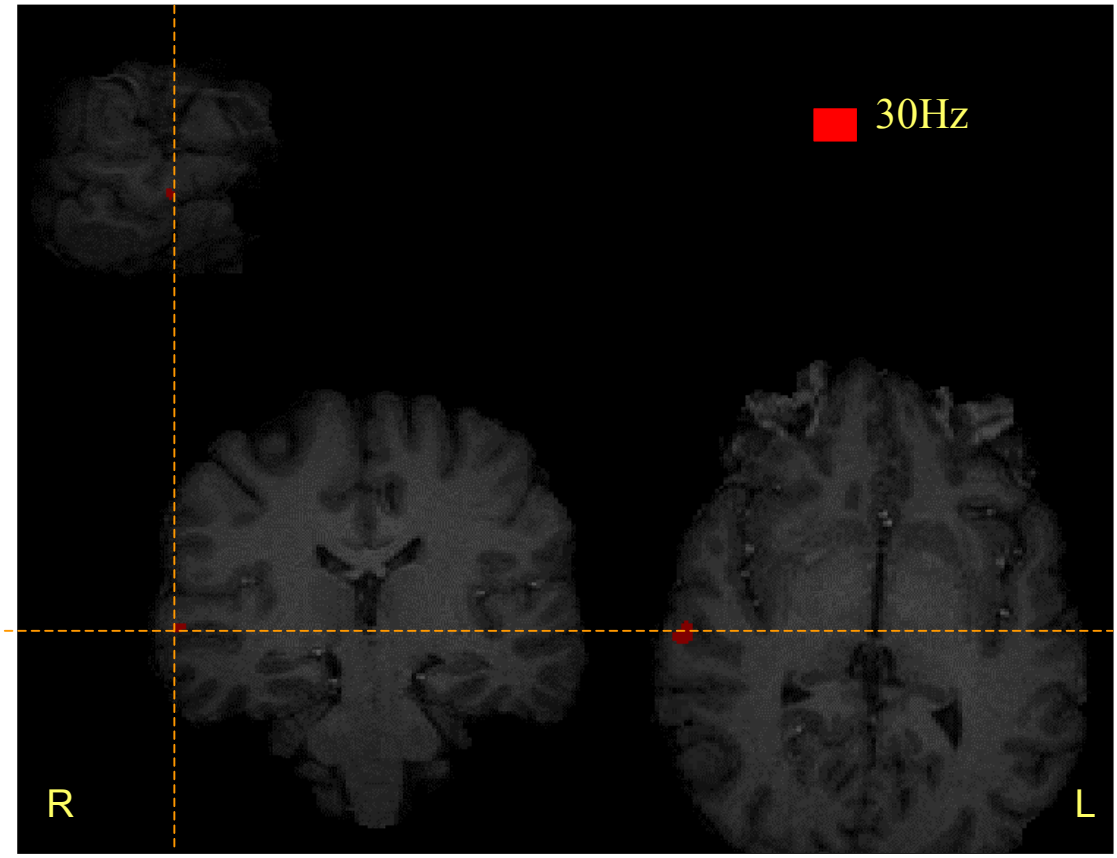


**Figure 28b: FMRI activation in SII ipsilateral to the site of a 30Hz stimulus applied to the right fingertip of the same subject as in Figure 28a. Right: coronal slice, left: transverse slice. Crosshairs show slicing plane.**

***Discussion***

The device described in this chapter fills the need for a vibrotactile stimulator that is stable, has good dynamic range, and has little to no noise. The piezoelectric bender has the advantages of an electromagnetic device in that it delivers a controlled, precise stimulus with a very low-distortion sinusoidal shape (Figure 26) with the benefit of being noise-free in a high magnetic field environment. Using an optical DT allows for the amount of skin displacement to be measured accurately in a high field environment.

Several air-puff and piston-driven devices have been experimented with for MR use (Gelnar et al 1998), but these devices lack the precise control and ability to provide a consistent sinusoidal stimulus of known amplitude and frequency. At least two other MR-compatible piezoelectric vibration devices have been developed. The first, the piezoelectric stimulator of Harrington a nd Downs, consists of a large circular wafer (Harrington and Downs, 2001). While the wafer is artifact-free and the frequency readily controlled, there is no way of accurately controlling or measuring the displacement. The wafer must be held between the subject's index finger, middle finger, and thumb – this does not allow for selective stimulation of a single digit or other skin site, nor is the site of stimulation reliably held constant through the course of the experiment. The device delivers a large stimulus in terms of area, and suffers from the effects of harmonics. The second device, that of Maldjian et al delivers a focused, 8-mm stimulus with good frequency control and can be repositioned on any skin site (Maldjian et al, 1999),. However, the Maldjian device does not include a method for measuring skin displacement .

The vibrotactile stimulator described in this chapter has a relatively noise-free stimulus; however, the noise level in the DT signal at the probe end corresponds to about

10μm displacement peak-to-peak. To accommodate for this noise, the DT needs to be calibrated using a high-amplitude burst before every experiment. The signal from the calibration burst is filtered to extract the stimulus frequency and reject the noise. This is done by performing a Fourier transform and summing the amplitudes of the component at the stimulus frequency plus the components at adjacent frequencies.

The bender's displacement/voltage characteristic is also affected by the stiffness of the skin, which means that the DT must be re-calibrated every time it is repositioned. However, calibration is done automatically and takes only about 3s. The bender element has a linear displacement/voltage characteristic at any given frequency within the range of the driving device, as specified by the manufacturer. Tests of the bender on a range of flexible surfaces have shown that this is true to a good approximation.

Modifications continue to be made to the existing vibrotactile stimulator model to improve its versatility and performance. The present amplifier has been replaced with a high-voltage DC amplifier, allowing us to investigate low frequencies down to DC. The prototype DC amplifier has been used intensively for over 12 months without failure. A modified version of the displacement transducer is in development which should display a noise level approximately an order of magnitude less than the existing model.

Non-metallic materials such as acrylic and ceramic are also being tested for the bender casing. The use of a nonmetallic casing will allow vibrotactile stimuli to be applied closer to the magnetic bore, for example on the subject's face or neck, without causing magnetic field distortion. A preliminary study has been conducted using an acrylic casing, and no detectable noise or distortion was present in the MR images (unpublished observations).

A dual-channel stimulator has already been built using the same principles. The dual channel stimulator comprises two independently controlled benders, each with a separate frequency and amplitude control. The dual-channel stimulator has been used in experiments where two different skin sites were stimulated independently (McGlone et al, 2002).

### *Conclusions*

An MRI compatible vibrotactile stimulator has been developed using a piezoelectric bender with a stable I/O characteristic over a range of frequencies, from DC to several hundred Hz, capable of eliciting the percepts of pressure, "flutter" and vibration. This stimulator has been used in two different MRI scanners to successfully demonstrate activation in human primary and secondary somatosensory cortices in response to vibration of the fingertips and bases. In all cases, no noise or interference was present from the stimulator.

***References***

Bolanowski SJ, Gescheider GA, Verillo RT, and Checkosky CM. (1988) Four channels mediate the mechanical aspects of touch. J Acoust Soc Am 84: 1680-1694.

Chubbuck, J.G. and US Patent 3, 432 (1970) Transducer, transducer system, and transducer suspension spring. Ultrasonics. 8: 260.

Francis ST, Kelly EF, Botwell R, Dunseath WJR, and Folger SE (2000) fMRI of the responses to vibratory stimulation of digit tips. Neuroimage 11: 188-202.

Gelnar PA, Krauss BR, Szeverenyi NM, and Apkarian AV (1998). Fingertip representation in the human somatosensory cortex: an fMRI study. Neuroimage 7: 261-283.

Goble AK and Hollins M (1993) Vibrotactile adaptation enhances amplitude discrimination. J Acoust Soc Am 93: 418-424.

Goble AK and Hollins M (1994) Vibrotactile adaptation enhances frequency discrimination. J Acoust Soc Am 96: 771-780.

Harrington GS and Downs III JH (2001) FMRI mapping of the somatosensory cortex with vibratory stimuli: Is there a dependency on stimulus frequency? Brain Res 897: 188-192

Kelly EF and Folger SE (1999) EEG Evidence of stimulus-directed response dynamics in human somatosensory cortex. Brain Res 815: 326-336.

Logothetis NK, Pauls J, Augath M, Trinath T, and Oeltermann A (2001) Neurophysiological investigation of the basis of the fMRI signal. Nature 412: 150 -157.

Lin W, Kuppusamy K, Haacke EM, and Burton H(1996) Functional MRI in human somatosensory cortex activated by touching textured surfaces. J Magn Reson Imaging 6: 566-572.

Maldjian JA, Gottschalk A, Patel RS, Pincus D, Detre JA, Alsop DC (1999) Mapping of secondary somatosensory cortex activation induced by vibrational stimulation: an fMRI study. Brain Res 824: 291-295.

McGlone F, Kelly EF, Trulsson M, Francis ST, Westling G, and Bowtell R (2002). Functional neuroimaging studies of human somatosensory cortex. Behav Brain Res 135: 147-158.

Mountcastle VB, Talbot WH, Sakata H and Hyvarinen J (1969) Cortical neuronal mechanisms in flutter vibration studied in unanesthetized monkeys. Neuronal periodicity and frequency discrimination. J Neurophysiol 32: 452-484.

Nelson AJ, Staines WR, Graham SJ, and McIlroy WE (2004) Activation in SI and SII: The influence of vibrotactile amplitude during passive and task-relevant stimulation. Cog Brain Res 19:174-184.

Sakai K, Watanabe E, Onodera Y, Itagaki H, Yamamoto E, Koizumi H, and Miyashita Y (1995) Functional mapping of the human somatosensory cortex with echo-planar MRI. Magn Reson Med 33: 736-743.

Tommerdahl M, Delemos KA, Whitsel BL, Favorov OV, and Metz CB (1999a) Response of anterior parietal cortex to cutaneous flutter versus vibration. J Neurophysiol 82: 16-33.

Tommerdahl, M., Whitsel BL, Favorov OV, and Metz CB (1999b) Responses of contralateral SI and SII in cat to same-site cutaneous flutter vs. vibration. J. Neurophysiol. 82: 1982-1992.

Tommerdahl M, Favorov, OV, and Whitsel BL (2005). Effects of high-frequency skin stimulation on SI cortex: Mechanisms and functional implications. Somatosens Motor Res 22: 151-169.

Whitsel BL, Kelly EF, Xu M, Tommerdahl M, and Quibrera M (2001) Frequency-dependent response of SI RA-class neurons to vibrotactile stimulation of the receptive field." Somatosens Mot Res 18: 263-285.

Whitsel BL, Kelly EF, Quibrera M, Tommerdahl M, Li Y, Favorov OV, Xu M, and Metz CB (2003) Time-dependence of SI RA neuron response to cutaneous flutter stimulation. Somatosens Mot Res 20: 45-69.

## 5. Future work

Studies of primate and cat SI cortex have shown that the funneling of the SI response to sustained high frequency skin stimulation is caused by the balance between the RA and PC afferent drives (Whitsel et al 2001, Tommerdahl et al 2005). Tommerdahl and colleagues proposed that the decrease in SI response in caused in part by inhibitory connections from the upper layers of SI, where the axons of the thalamic nuclei dominated by PC afferent input terminate (Tommerdahl et al, 2005). Supporting this hypothesis are the results of psychophysical studies in humans showing that the capacity to spatially localize stimuli improves when stimulus conditions favor an increasing PC: RA ratio (Sherrick et al 1990, LaMotte and Mountcastle 1975).

In Chapter 2 of this manuscript, RA afferent microstimulation at high frequencies could not account for suppression of activation in SI that was seen by Tommerdahl et al (2005). When PC afferents were microstimulated, the results were ambiguous: the SI response was undistinguishable from the SII response in one subject, but in the second subject the SI hemodynamic response was significantly smaller in peak magnitude than the SII response. Repeating the microstimulation study with more PC afferents would help clarify whether the SI hemodynamic response is markedly smaller than the SII response, and confirm that the PC input to SI is not excitatory.

However, microstimulation studies are time consuming and require a great deal of expertise. Furthermore, given the relatively low number of PCs compared to RA and SA afferents, it is very difficult to isolate and stimulate PCs and stabilize them during fMRI

scanning. Instead, the vibrotactile stimulator described in Chapter 4 can be used to replicate the stimulus protocols of Tommerdahl et al (2005) in humans, and fMRI can be used to capture the cortical responses. Under those stimulus conditions, the hemodynamic response in SI should show results that echo those of Tommerdahl et al: as stimuli that engage more PCs are employed, the response in SI becomes "funnelled" to a spatially narrower, but stronger hemodynamic response.

Although the temporal resolution of fMRI (3s for the EPI sequences used in this manuscript) limits the study of cortical dynamics, innovative fMRI analysis methods can be used to map the changes in SI response to a sustained stimulus. Quantifying the pixel-by-pixel time courses of hemodynamic responses in a cluster of activated pixels will map the change in SI response over time. Under stimulus protocols similar to those of Tommerdahl et al (2005), we would be able to identify those pixels in SI that exhibit a sustained hemodynamic response and those that do not. This analysis technique can be applied to SI to see if the pattern of a positive peak response and an inhibitory surround can be detected using fMRI analysis methods.

Recently, ipsilateral cortical input has been shown to modify the contralateral SI response to a sustained flutter stimulus (Tommerdahl et al 2006). The dual channel vibrotactile stimulator described in Chapter 4 can be used to investigate whether the same mechanisms exist in humans. Advances in MR technology, such as the availability of higher magnetic field machines, will allow for higher MR signal strength and better spatial resolution, which will in turn allow for better localization of cortical responses to stimuli.

Several researchers have recently successfully acquired simultaneous or interleaved fMRI and EEG measurements (for review, see Ritter and Villringer 2006). Simultaneous fMRI/EEG measurements leverage the millisecond-level temporal resolution of EEG and the millimeter-level spatial resolution of fMRI to allow for more detailed studies of the role of human somatosensory cortex in stimulus processing. For example, Debener et al (2006) have used fMRI and EEG recordings of the responses to auditory stimuli to investigate the temporal dynamics of information processing within the auditory cortex. The availability of such improved hardware compared with advances in image analysis methods will allow multimodal recordings to be used to further study cortical activity and dynamics.

***References***

Debener S, Usperger M, Siegel M, Engel AK (2006) Single-trial EEG-fMRI reveals the dynamics of cognitive function. Trends Cogn Sci 10:558- 563.

LaMotte HM, Mountcastle VB (1975) Capacities of humans and monkeys to discriminate between vibratory stimuli of different frequency and amplitude: A correlation between neural events and psychophysical measurements. J Neurophysiol 42: 400-419.

Ritter P and Villringer A (2006) Simultaneous EEG-fMRI. Neurosci Biobehav R 30:823-838.

Sherrick CE, Cholewiak RE, and Collins AA (1990) The localization of low- and high-frequency vibrotactile stimuli. J Acoust Soc Am 88: 169-179.

Tommerdahl M, Favorov, OV, and Whitsel BL (2005) Effects of high-frequency skin stimulation on SI cortex: Mechanisms and functional implications. Somatosens Mot Res 22: 151-169.

Tommerdahl M, Simons SB, Chiu JS, Favorov OV, and Whitsel BL (2006) Ipsilateral Input Modifies the Primary Somatosensory Cortex Response to Contralateral Skin Flutter. J Neurosci. 26: 5970-5977.

Whitsel BL, Kelly EF, Xu M, Tommerdahl M, and Quibrera M (2001) Frequency-dependent response of SI RA-class neurons to vibrotactile stimulation of the receptive field." Somatosens Mot Res 18: 263-285.

**Appendix: Background and principles of fMRI analysis**

The theory behind functional MRI postulates that local alterations in neuronal activation induce local changes in metabolism, leading to changes in cerebral blood flow and blood volume (Belliveau et al, 1991). Intrinsic optical imaging (OIS) experiments have verified that there is a tight coupling between neuronal activity and changes in the microcirculation (Frostig et al, 1990). These changes in local cerebral perfusion are reflected in changes in the blood oxygenation levels of nearby capillaries. The physical method by which this change in blood oxygenation level is translated into a measurable MR signal is based on the magnetic properties of hemoglobin. Oxyhemoglobin is a diamagnetic substance: oxyhemoglobin molecules have no unpaired electrons from iron, and thus, do not cause local variations ('susceptibility') in the magnetic field. Deoxyhemoglobin on the other hand is a paramagnetic substance, containing unpaired electrons in its iron atoms. A greater amount of deoxyhemoglobin in blood causes an increase in local magnetic field susceptibility in the surrounding area. Thus, a change in the oxy:deoxyhemoglobin ratio will cause a small local change in MR signal from the corresponding nearby tissue. These local susceptibility changes, or T2* changes, can be measured using Echoplanar Imaging (EPI, Mansfield et al 1977).

Belliveau et al (1991) first measured T2* changes in the human brain using a paramagnetic contrast agent to produce cerebral blood volume maps of the human brain during exposure to alternating bright and dark conditions. Paramagnetic contrast agents are injected into the blood to enhance the magnitude of local susceptibility changes. The

images were acquired using a modified EPI sequence. By overlaying the cerebral blood volume maps onto higher-resolution 'anatomical' MR images, Belliveau et al showed that there was a significant increase of cerebral blood volume in human visual cortex during the bright condition compared to darkness.

Working independently, Ogawa et al (1990) showed that visual stimulation produces a detectable transient increase in intrinsic MR signal intensity. This signal change was detectable without a paramagnetic contrast agent, and measured a 5-20% change at 4T. Ogawa et al observed that these changes occurred predominantly in gray matter, adjacent to blood vessels. They concluded that a local elevation in human brain venous blood oxygenation accompanies an increase in neuronal activity, and coined the term blood-oxygenation level dependent (BOLD) response to describe this phenomenon.

Since then, a wealth of experiments have succeeded the initial papers, and proved that the BOLD response can be detected not only in visual cortex, but in all areas of the brain. In all cases, the BOLD response could be correlated to the presented stimulus in a physiologically meaningful manner. Kwong et al (1992) used gradient echo images to measure changes in blood oxygenation and inversion recovery images to measure changes in blood flow during exposure to periodic photic stimulation. Plots of signal intensity vs. time for areas of interest within the visual cortex, as well as subtraction images for whole brain MRI, showed consistent signal change in the visual cortex that corresponded to stimulus on and off times. In a separate study, Menon et al (1992) used gradient echo images of visual stimulation and generated functional brain maps using the subtraction method. These functional maps were able to distinguish between the visual responses of left hemispheric and right hemispheric stimulation and suggested that the

BOLD phenomenon could be used to noninvasively investigate higher order cortical processes in humans. FMRI results correlated well with previous PET studies in humans (Belliveau et al, 1992).

Investigation of the BOLD phenomenon was extended to cortical areas other than visual cortex. Finger-tapping was shown to evoke a BOLD response in motor and somatosensory cortices that was significantly correlated to the stimulus (Bandettini et al, 1993). Kurth et al (1998) used non-painful electrical stimulation on digits 2 and 5 to show that fMRI could be used to assess the somatotopy of cortical representation of the hand. Other vibrotactile stimulation experiments (Gelnar et al 1998, Francis et al 2000) have used fMRI to confirm somatotopy in the cortical representation of the hand in human SI.

Gradient Echo EPI is particularly susceptible to artifacts from nearby draining veins; exactly how much of the measured BOLD signal arises from gray matter and how much from adjacent veins is difficult to determine. Frahm et al (1993) first recognized that although stimulus-related changes in fMRI signals do reflect associated cortical changes in blood flow and oxygenation (Buxton and Frank 1992), the signal changes are also strongly dependent on MRI image acquisition and experimental parameters. Since 'activation' is defined as any signal change that is statistically related to stimulus on and off times, confounding factors may include draining veins, stimulus-correlated motion artifacts, experimental conditions and signal analysis techniques.

Frahm et al suggested several steps to minimize draining vein contributions to fMRI images (Frahm et al, 1994). On the image acquisition side, they suggested using low flip-angle imaging sequences as well as spatial presaturation scans. On the

experimental design side, periodic or boxcar stimulation paradigms were suggested. The biggest factor in mistakenly identifying draining vein contributions as part of 'activation', was the use of subtraction images to identify areas of activation. Frahm et al (1994) suggested the use of correlational analysis methods rather than subtraction methods, for more accurate identification of pertinent areas of activation. Indeed, in the ten years since the publication of that paper, correlational analysis using statistical parametric mapping (SPM, Friston et al 1995) methods has prevailed as the most widely utilized and accepted fMRI analysis method.

Functional MRI experimental paradigms frequently employ the boxcar experimental design, which consists of repeated blocks of the stimulus alternating with rest periods or a control stimulus. An example of the simple boxcar design is a vibrotactile stimulation experiment consisting of twenty blocks of 16s stimulation followed by 16s rest. The rest periods in boxcar design experiments are typically no shorter than 12s, in order to allow the hemodynamic response function to return to baseline. Two or more stimuli can also be presented within a single boxcar experimental design. An example of an experimental design employing two stimuli consists of stimulating two different skin sites, e.g. digit tip and digit base, in random order, with each stimulus period followed by a rest period long enough to allow the hemodynamic response function to return to baseline.

Event-related designs consist of single events, such as presentation of an image of a famous face. Events are typically repeated every 8-12s. The distinction between block (epoch) design experiments and event-related experiments is somewhat arbitrary; an 'event' is defined as a short presentation of a stimulus, whereas a 'block' is defined as a

long, repeated presentation of a stimulus. The theoretical treatment for both types of experiments is identical mathematically; however, the event-related option affords more flexibility in modeling the data.

The most widely used fMRI analysis method is that of Friston et al, who developed a statistical parametric mapping (SPM) based approach for detecting which areas of the brain exhibit a signal change that correlates significantly with the stimulus (Friston et al, 1995). SPM consists of two main steps: the general linear model (GLM) is first applied to each voxel independently, and the resultant parameter estimates are then thresholded using random field theory to correct for multiple comparisons. The voxels that are significantly correlated with the GLM ("activation maps") are overlaid onto anatomical MRI images to provide more precise localization of the areas of activation. In order to conform to the statistical assumptions made by SPM, two key preprocessing steps must be performed. These are motion correction and spatial smoothing.

The GLM treats each data point, or voxel in the case of fMRI, as a linear, time-invariant time series. For this approach to hold true, all voxels must occupy the same space in the time series; therefore motion correction is an essential preprocessing step in fMRI analysis. The most commonly used motion correction algorithm is Automated Image Registration, AIR (Woods et al 1998a, b), which uses a rigid-body, 6-parameter interpolation algorithm. Smoothing the data is important for three reasons: smoothing improves the signal-to-noise ratio of the underlying fMRI images; smoothing imposes a normal distribution according to the Central Limit Theorem and thus ensures validity of inferences based on parametric tests; and smoothing ensures that the error terms represent an underlying Gaussian field with smoothness greater than voxel size, as assumed in

Gaussian Random Field theory. By the matched filter theorem, the optimum smoothing kernel corresponds to the size of the effect anticipated.

The GLM consists of a 'best fit' linear regression for each voxel in the image and is formulated as $Y=X\beta+\varepsilon$, where Y is the input matrix containing the observed data over time, X is the design matrix containing the model to which the data is fitted, $\beta$ is the term describing the best fit, and $\varepsilon$ is the error term. Each column of the design matrix corresponds to some effect or explanatory variable that may influence the result, such as stimulus on and off times. Part of the design matrix usually involves convolution of the explanatory variable with a 'typical' hemodynamic response function (HRF). SPM provides options for the user to choose either the canonical HRF as defined by Boynton et al (1996), or a set of basis functions that could best describe the variations of the HRF in space and time. The basis function set recommended by Friston et al (1995) is the canonical HRF and its derivatives with respect to latency and dispersion, which are the key parameters that determine its form. Confounding parameters, such as motion parameters, can also be modeled in the design matrix to yield a better fit to the observed data.

The resultant matrix of parameter estimates, $\beta$, is then thresholded using Gaussian Random Fields theory, to correct for multiple comparisons since neighboring fMRI voxels are not independent. GRF is preferred over the Bonferroni correction, because the Bonferroni correction assumes that each voxel is independent, and results in a multiple comparison correction that is too stringent (Friston et al, 1996). The GRF results in a number of resels corresponding to the degree of smoothness of the data. The Euler Characteristic (Worsley 1996) is derived from the number of resels, and this in turn gives

rise to the Z threshold. This results in a statistical map containing error, or probability values for each voxel within the image, according to Student's T distribution. The user then provides a specified T value (default, uncorrected $p<0.001$ or corrected $p<0.05$) at which to threshold the data. The pixels that survive the thresholding are then said to be statistically significant at the specified p value.

The main limitation of SPM derives from it being a hypothesis testing approach rather than a true estimation approach. Because the exact relationship between neuronal activity and the BOLD effect is still not characterized, SPM is based on a 'best fit' approach. Currently, SPM allows for a number of options for modeling the shape of the data including boxcar functions, sinusoidal functions, and gamma functions. The preferred model is the canonical hemodynamic response function of Boynton et al (1996) and its temporal derivatives; however, the hemodynamic response function may vary from subject to subject, and even varies within locations in the same brain. Usage of the temporal derivatives helps to incorporate local variations of the hemodynamic response function onset time into the GLM.

The thresholding approach employed by SPM does not give an estimate of the shape of the signal; however, the time course of the hemodynamic response can be extracted for a particular voxel or group of voxels using SPM's user interface. SPM works based on fMRI signal intensity alone; it cannot differentiate between draining vein contribution and gray matter contribution. Usage of low flip-angle, gradient echo sequences has been shown to minimize draining vein contribution to the fMRI signal.

Because of the flexibility of SPM, the user has almost complete control over how the data is manipulated. Using Matlab programming and options within SPM's user

interface itself, one can expand the standard analysis techniques to investigate different aspects of the hemodynamic response such as latency and dispersion. SPM analysis can also be modified to look at aspects of signal change over time. For example, the issue of how the cortex processes sensory information can be investigated by comparing cortical areas with an early hemodynamic response, to cortical areas with a later hemodynamic response. Cortical dynamics can be indirectly investigated by using SPM to look at changes in areas of activation over a prolonged stimulus time. The specific SPM techniques used in data analysis are discussed in the methods section of each chapter.

***References***

Bandettini PA, Wong EC, Hinks RS, Tikofsky RS, and Hyde JS (1992) Time course EPI of human brain-function during task activation. Magn Reson Med 25: 390- 397.

Belliveau JW, Kennedy DN, McKinstry RC, Buchbinder BR, Weisskoff RM, Cohen MS, Vevea JM, Brady TJ, and Rosen BR (1991) Functional mapping of the human visual cortex by magnetic resonance imaging. Science 254: 716-719.

Belliveau JW, Kwong KK, et al. (1992) Magnetic resonance imaging mapping of brain function: human visual cortex. Invest Radiol 27: S59-S65.

Boynton GM, Engel SA, Glover GH, and Heeger DJ. (1996) Linear systems analysis of functional magnetic resonance imaging in human V1. J Neurosci 16: 4207- 4221.

Buxton RB and Frank LR (1992) A model for the coupling between cerebral blood flow and oxygen metabolism during neural stimulation. J Cerebr Blood F Met 17: 64-72.

Frahm J, Merboldt K-D, Hanicke W, Kleinschmidt A, and Boecker H (1994). Brain or Vein -- Oxygenation or Flow? On signal physiology in functional MRI of human brain activation. NMR Biomed 7: 45-53.

Francis ST, Kelly EF, Botwell R, Dunseath WJR., Folger SE (2000) fMRI of the responses to vibratory stimulation of digit tips. Neuroimage 11: 188-202.

Friston KJ, Holmes AP, Worsley KJ, Poline JB, Frith C, and Frackowiak RSJ (1995) Statistical Parametric Maps in Functional Imaging: A General Linear Approach. Hum Brain Mapp 2:189-210.

Friston KJ, Holmes AP, Poline JB, Price CJ (1996) Detecting activations in PET and fMRI: levels of inference and power. Neuroimage 4: 223-235.

Frostig RD, Lieke EE, T'so DY, and Grinvald A (1990) Cortical functional architecture and local coupling between neuronal activity and the microcirculation revealed by in vivo high-resolution optical imaging of intrinsic signals. PNAS 87: 6082-6086.

Gelnar PA, Krauss BR, Szeverenyi NM, and Apkarian AV (1998) Fingertip representation in the human somatosensory cortex: an fMRI study. Neuroimage 7: 261-283.

Kurth RK, Villringer K, Mackert B-M, Schwiemann J, Braun J, Curio G, Villringer A, and Wolf K-J (1998) fMRI assessment of somatotopy in human Brodmann area 3b by electrical finger stimulation. Neuroreport 9: 207-212.

Kwong KK, Belliveau JK, et al. (1992) Dynamic magnetic resonance imaging of human brain activity during primary sensory stimulation. PNAS 89: 5675-5679.

Mansfield P (1977) Multi-planar image formation using NMR spin echoes, J Phys C, 10:L55-L58.

Menon RS, Ogawa S, Kim S-G, Ellerman JM, Merkle H, Tank DW, and Ugurbil K (1992) Functional Brain mapping using magnetic resonance imaging: signal changes accompanying visual stimulation. Invest Radiol 27: S47-S53.

Ogawa S, Lee T-M, Nayak AS, and Paul G (1990) Oxygenation-sensitive contrast in magnetic resonance image of rodent brain at high magnetic fields. Magn Reson Med 14: 68-78.

Woods, RP, Grafton ST, Holmes CJ, Cherry SR, and Mazziotta JC (1998a) Automated Image Registration: I. General methods and intrasubject, intramodality validation. J Comput Assist Tomogr 22: 139- 152.

Woods, RP, Grafton ST, Holmes CJ, Cherry SR, and Mazziotta JC (1998b) Automated Image Registration: II. Intersubject validation of linear and nonlinear models. J Comput Assist Tomogr 22: 153- 165.

Worsley KJ, Marrett S, Neelin P, Vandal AC, Friston KJ, and Evans AC (1996) A unified statistical approach for determining significant signals in images of cerebral activation. Hum Brain Mapp, 4: 58-73.